THERMAL ANALYSIS OF RECEIVERS FOR SOLAR CONCENTRATORS AND OPTIMIZATION PROCEDURE FOR POWER PRODUCTION

A THESIS

Presented to

The Faculty of the Division of Graduate Studies

By

Prakash Rao Damshala

In Partial Fulfillment

Of The Requirements for the Degree

Doctor of Philosophy in the School of Mechanical Engineering

Georgia Institute of Technology

May 1978

THERMAL ANALYSIS OF RECEIVERS FOR SOLAR CONCENTRATORS

AND OPTIMIZATION PROCEDURE FOR POWER PRODUCTION

Approved:

J. Richard Williams, Chairman

Prasanna Kadaba

Robert Evans

Jay Schlag

S. V. Hanagud

Date approved by Chairman 8/9/78

ACKNOWLEDGMENTS

I would like to thank my co-advisor, Dr. J. R. Williams, for giving me the opportunity to work on this problem of his funded research project. His follow-up of this thesis for its completion is very much appreciated.

I am also very grateful to my other co-advisor, Dr. P. V. Kadaba, who shaped this thesis.

I am very grateful to my other thesis committee members, Drs. R. B. Evans, S. Hanagud and J. H. Schlag for valuable suggestions and constructive criticisms.

This thesis would not have been completed without the help of Drs. A. Larson, T. Jackson, and S. P. Kezios.

I would like to thank my parents for their patience and encouragement to finish this thesis.

I also wish to thank Mrs. Jane Lutz for correcting numerous typing errors.

TABLE OF CONTENTS

TABLE OF CONTENTS (continued)

LIST OF TABLES

LIST OF ILLUSTRATIONS

LIST OF ILLUSTRATIONS (continued)

LIST OF ILLUSTRATION (continued)

SUMMARY

This thesis deals with the thermal analysis of receivers for linear solar concentrators and the concentrator system optimization procedure for power production. The particular linear concentrator used for this study is the 540 ft^2 prototype faceted fixed mirror concentrator at Georgia Tech, which utilizes the fixed mirror-moving receiver concept as proposed by John Russell [1].*

The thermal analysis of the collector utilizing an evacuated receiver manufactured by Corning Glass Co. is described which predicts the thermal efficiency of the receiver and exit temperature of the collector fluid. Therminol 66 is the heat transfer fluid. A linear mathematical equation is obtained for the thermal efficiency of this receiver for arbitrary values of solar intensity, inlet temperature and ambient temperature.

A solar/fossil power plant of 100MW has been designed to illustrate the procedure for optimizing the system for the least cost of unit power produced. A Rankine cycle using toluene as the working fluid is coupled to the collector circuit through a counterflow heat exchanger. Pertinent component models and heat balance equations are included in the simulation. The concentrator, collector and Rankine systems are coupled and a procedure is outlined to optimize the entire solar concentrator system for power production. A simple optimization technique is employed on

* The numbers in square brackets refer to the references listed in bibliography.

100 MW plant located in Atlanta. The results of this analysis indicates that the power can be generated at a cost of 5.0¢/KWh, provided the concentrator cost does not exceed $2 per square foot. The present selling cost of power from Georgia Power Company is 3.0¢/KWh. This selling cost includes the power generation and distribution cost as well as their profits.

NOMENCLATURE

Latin Letter Symbols

a_1, a_2, a_3 and a_4 = constants defined in Chapter VII

A_c = concentrator area

A_r = receiver area

B_1 = overall width of the concentrator

B_2 = space in between two rows of concentrators

C_1 and C_2 = constants are defined in Chapter VII

C_p = specific heat at constant pressure

D = diameter of the copper tubes

D_e = diameter of glass envelope

f = friction factor

E = frictional power per unit area of heat transfer surface

H_T = solar flux incident on unit area of glass envelope

h_{p-c} = heat transfer coefficient (due to molecular conduction) between plate and glass envelope

h_{c-s} = radiational heat transfer coefficient between glass envelope and surroundings

$h_{r,c-s}$ = radiational heat transfer coefficient between glass envelope and plate

h_4 = enthalpy of vaporized Rankine fluid at temperature T_4

h_4' = enthalpy of Rankine fluid at temperature T_4

h_c = enthalpy of Rankine fluid at temperature T_C

i_{ann} = annual interest rate

I = solar insolation incident on receiver = $x_c q_{in}$

K = thermal conductivity of absorber plate

K_a = thermal conductivity of air

L = length of the heat exchanger

$\dot{m}$ = mass flow rate

$\dot{m}_1$ = mass flow rate of the collector fluid

$\dot{m}_2$ = mass flow rate of Rankine fluid

N_{nu} = Nusselt number

N_{pn} = Prandtle number

N_{re} = Reynolds number

N_{st} = Stanton number

P = pressure of air inside the glass envelope

ΔP = pressure drop of the collector fluid

Q = total solar flux falling on the row of heat exchangers

q^+ = heat flux at the root of the tube per unit length of tube as shown in Fig. 4

q_{in} = solar flux (beam component as measured by pyrheliometer) falling on concentrator per unit area

q^- = heat flux at the root of the tube per unit length of tube as shown in Fig. 4

q_u = heat gained by the collector fluid over unit length of the tube

r_1 = hydraulic radius

S = heat absorbed by plate per unit area

$t^{\cdot}$ = mean distance between glass envelope and plate

$T_a = T_\infty$ = ambient temperatures

T_{bi} = temperature of plate over ith tube assumed uniform

T_c = Rankine fluid temperature at condenser

T_e = exit collector fluid temperature

T_g = mean glass temperature

T_i = inlet collector fluid temperature

T_p = mean plate temperature

U_e = total heat transfer coefficient between the fluid in pipe headers and surroundings or between the absorber plate and the surroundings

U_m = mean velocity of fluid inside the copper tubes

U_t = total heat transfer coefficient between plate and surroundings

V_o = volume flow rate of fluid

W = distance between the centers of the tubes

X_c = fraction of solar flux falling on unit area of concentrator that reaches receiver

Greek Letter Symbols

Ψ_i = non-dimensional plate temperature

ξ_i = non-dimensional length variable

Θ = angle between the solar flux plane and the normal to concentrator aperture plane

Θ_i = temperature excess over the tube surface

δ = thickness of plate

τ_g = transmittance of glass envelope (visible range)

α_p = absorptivity of plate (visible range)

ε_1 = effectiveness of heat exchanger

ε_2 = effectiveness of evaporator

ε_g = emissivity of glass (infrared)

ε_p = emissivity of plate (infrared)

η = y/L

η_2 = Rankine cycle efficiency

η_c = concentrator efficiency

η_o = overall thermal efficiency

η_r = thermal efficiency of the solar receiver

α = thermal accommodation coefficient or solar altitude

ρ = density of fluid

ρ_c = reflectivity of the concentrator glass mirrors

μ = viscosity of fluid

ω = hour angle

CHAPTER I

INTRODUCTION

Although the first use of solar energy dates back as early as 212 B. C., solar energy has become a subject of intense research since 1970 due to the rise in the cost of fossil fuels. The essential component of solar/thermal systems is the heat exchanger that absorbs solar flux and heats a fluid running through it. Many types of flat plate collectors are already in use all over the world to heat water. Temperatures up to 200°F can be obtained through the use of such flat plate collectors [2]. The flat plate collectors are less expensive, easier to maintain, and simpler than concentrating reflector type collectors. However, temperatures higher than 200°F cannot be obtained by simple flat plate collectors.

According to reference [3], residential and commercial space heating and colling accounts for 20% of all U. S. energy consumption. Industrial process heat accounts for 28% of which 80% is at temperatures less than 500°F. About 60% of all the process heat is used to produce steam. Thus, it is evident that energy at high temperatures can only be obtained by the use of focusing collectors since flat plate collectors have an upper limit of approximately 200°F. If focusing collectors can collect solar energy at high temperatures and the cost of such collectors is comparable to that of conventional sources of energy, then solar energy may be viable. The purpose of this investigation is to convert solar energy into electricity at the least possible cost.

The essential difference between a flat plate collector and a focusing collector lies in the intensity of the radiation flux received at the absorber surface. Also, a non-uniform heat flux exists on the absorber surface unlike the uniform flux on the flat plate collector. Rollins [1] obtained non-uniform heat fluxes at the focal plane of the fixed mirror concentrator at different positions of the sun.

All the focusing collectors absorb only the beam component of the radiation and the diffuse component is lost at the receiver surface. In order to absorb the beam component, the concentrator or the heat exchanger must have the capability of tracking the sun. This requires additional mechanisms. Because of the necessity of tracking and optical concentration, focusing collector costs increase sharply over that of flat plate collectors. However, a very wide range of temperatures (from 200°F to 6000°F) can be obtained using focusing collectors. The higher the concentration ratio of the reflectors, the higher will be the temperatures obtained at the focal plane.

Because the optimization and development of the heat exchanger for the focusing collector is a purpose of this investigation, the research reported here addresses itself to the analysis of the heat exchanger, its component parts, and other physical and geometrical parameters.

The main part of the receiver is the tube in which the working fluid absorbs heat. A highly corrosive resistant and inexpensive material which is readily available and which can be easily shaped (forged/machined/cast) to any geometry is desirable. A galvanized sheet metal tube was selected for the air heat exchangers. A small diameter

copper tube embedded in a copper plate (see Figure 5, p. 26) was selected for the Corning Glass heat exchanger used for liquids.

A selective black coating having high absorption characteristics at wavelengths less than 2.5 microns and low emission characteristics at longer wavelengths is desirable. Such a coating when applied over a receiver surface absorbs energy at shorter wavelengths while preseving the low emissivity of the substrate at larger wavelengths. Kokoropoulos, Salam and Daniels [4] have noted that a selectively absorbing coating should be of a thickness equal to or greater than the short wavelengths to be absorbed and less than 1/10 of the larger wavelengths for which low emissivity is desired.

A 1200°F flame proof VHT coating (SP-102 black) was used in the air heat exchanger because it is very inexpensive. Black chrome and chrome nickel coatings have been developed at the NASA Lewis Research Center [5]. A black chrome coating was used for the Corning glass heat exchanger.

Air properties and its thermal characteristics are well known. So experiments were conducted using air as a working fluid. Using water as a working fluid requires a pressurized system, so Therminol 66 (a product of Monsanto Co.) was used as a working fluid with the Corning glass heat exchanger. Therminol 66 does not have high vapor pressures at high temperatures which is the case with water. It is also very stable at higher temperatures, non-corrosive, and can be used for the temperature range of 25°-650°F [6].

Insulation was used to reduce the heat losses from the air heat exchange tubes. These losses were expected to be high at the higher

tube temperatures, therefore, an insulation that could stand high temperatures and retain a low value of thermal conductivity was desirable. The thermal conductivity of such an insulation should be less than that of air. In the initial experiments ordinary fiberglass insulation proved to be a failure since it charred at high temperatures. Finally, Fiberfrax (Lo-Con blanket type) insulation of Carborundum (A_2lo_3, SiO_2) was used. It is easy to shape and can be used at temperatures up to 2000°F. For the Corning glass heat exchanger analysis, no insualtion was considered since the tubes were in a vacuum.

The single strength glass cover, used initially to cover the air tube exchanger, proved unsatisfactory because of the high temperatures and finally Pyrex glass was selected. In the Corning glass heat exchanger, the glass envelope is made up of Pyrex glass.

In certain simple concentrators like v-trough collectors tracking is done manually, but for the fixed mirror concentrator it is done by a automatic tracking device. This device essentially consists of two black coated strips pasted on a drum. It has a slit in between them to receive the incoming solar flux. The solar cells are located directly beneath these strips. When the incoming solar flux is not normal to the plane of the strips it falls on one of the rows of solar cells that in turn activates a small electric motor. The motion of this electric motor is transmitted to the receiver through a four-bar mechanism until the receiver is at the focal plane of this reflected solar flux. When this position is achieved, the incident solat flux falls normal to the pair of black coated strips and the slot in between them. At this position the solar flux will not fall on any solar cells thus keeping the electric motor shut down.

CHAPTER II

AUGMENTATION TECHNIQUES

The literature previously cited deals mainly with heat exchangers for focusing solar collectors that are yet to take a practical form for daily operation. The following literature pertains to the different techniques employed to augment the heat transfer to the working fluid from the heated tube surface.

Watkinson, Miletti and Tarasoff [8] made heat transfer and pressure drop measurements on integral inner fin tubes of several designs in turbulent water flow. Based on inside tube diameter and nominal area, heat transfer was enhanced over smooth tube values up to 170% at constant Reynold's number and up to 80% at constant pumping power. They observed that fin spiraling improved performance under both constant flow and constant pumping power conditions. It is expected that similar heat transfer enhancement will be observed in the proposed solar heat exchanger when an integral inner finned tube is used in place of smooth tube.

Webb and Eckert [9] developed equations to define the performance advantage of roughened tubes in heat exchanger design, relative to the smooth tubes of equal diameter. Three rough tube applications are presented: 1) to obtain increased heat exchange capacity; 2) to reduce the friction power; and 3) to permit a reduction of heat transfer surface area. A heat exchanger design procedure and generalized heat transfer and friction co-relations are developed for the case of "repeated rib"

roughness. It is again expected that similar heat transfer enhancement and/or other above mentioned results will be observed in the proposed solar heat exchanger when a repeated rib roughened tube replaces the smooth tube.

O. H. Klepp [10] obtained 22% better heat transfer coefficients for the tubes containing twisted tapes for the same pumping power. Tape twists (measured as the ratio of the tube length per 180 tape twist to the tube diameter) varied from 2.38 to 8.05; Reynolds moduli ranged from 20,000 to 380,000; and wall-to-gas-absolute temperature ratios from (1.0 to 2.1).

However any liquid heat transfer fluid is always a better heat transfer medium than gases because of the higher thermal conductivity value compared to that of gases.

General Considerations of Heat Exchanger Design

The cost of mechanical energy is generally four to ten times as much as its equivalent in heat in most thermal power systems. This is true because of the low thermal efficiencies and high capital costs of the power plants. In heat exchangers mechanical energy is required to move the fluid through them. For low density fluids such as gases, the friction-power expenditure to move the fluid is as great as the heat energy transferred, thus friction power has a dominant influence in the basic design of solar heat exchangers.

The heat transfer rate per unit of receiver surface area can be increased by increasing the fluid-flow velocity, this rate varies as something less than first power of the velocity. The friction-power

expenditure is also increased with flow velocity, usually as much as the cube of the velocity and never less than the square. This behavior influences the selection of the characteristics of different types of heat exchangers by putting limitations of low mass-velocities for gas-flow heat exchangers in which the friction power is high. The thermal conductivities of gases are generally low. This fact together with low mass-velocities causes the heat transfer rates per unit surface area to be very low. Thus large surface areas are provided for gas-flow heat exchangers. One method of providing an extra heat transfer area is by means of internal fins.

The heat transfer coefficient, can be evaluated for some particular set of fluid properties [7] from

$$h = \frac{C_p \mu}{(N_{pr})^{2/3}} \frac{1}{4r_h} (N_{st} N_{pr}^{2/3}) N_{re}$$

The friction power expended per unit of surface area can be readily evaluated as a function of the Reynold's number, the friction factor, and the specified fluid properties from

$$E = \frac{1}{2g} \frac{\mu^3}{\rho^2} \left(\frac{1}{4r_h}\right)^3 f[(N_{re})^3]$$

Choice of fluid is design is done by obtaining a high value for $\frac{h}{E}$, all other things being equal. The other considerations that play important roles in design are volume, weights, operational and initial costs of the whole unit.

A high performance surface is one which has high heat flux per unit of the friction power expenditure. A compact surface has small flow passages and the convection conductance h of such a surface is inversely proportional to the hydraulic diameter of the passage. Thus compact surfaces tend, by their very nature, to have high conductances.

It does not appear to be possible to establish a generally applicable selection criterion for the use of augmentative techniques due to large number of factors which enter into the ultimate decision. Most of the considerations revolve around economics: development costs, initial cost, operating cost, maintenance cost, etc. There are other factors also such as reliability and safety.

CHAPTER III

INTRODUCTION TO AIR AND LIQUID HEAT EXCHANGERS

This portion of the research deals with the development of a computerized parametric study of heat exchangers for a linear cylindrical solar concentrator. The evaluation includes the consideration of engineering and economic aspects. Generally the term heat exchanger refers to the device in which a fluid absorbs heat from another fluid at a higher temperature. The heat collector considered here is a special type of heat exchanger that allows a fluid flowing through it to absorb the heat from concentrated solar radiation falling on the blackened surface of the tube wall. Figure 1, shows a solar air heat exchanger.

It is seen from Figure 1 that only a portion of the heat exchanger tube is exposed to the concentrated solar flux, and the remaining portion is insulated to prevent heat losses. As a result of impinging solar flux on the tube, its temperature increases and it loses heat to the environment by thermal radiation and convection from the surface not covered by insulation. In addition, there will be minor heat losses from the surface of the tube covered with insulation. The magnitude of this heat loss depends upon the thermal conductivity and the thickness of insulation material. The heat exchanger tube shown in Figure 1 is enclosed in a galvanized steel pipe to protect it from moisture and weather. In addition, the two stainless steel deflectors containing a transparent cover is attached to the pipe as shown in Figure 2. The transparent cover reduces convection heat losses from the exposed surface of the

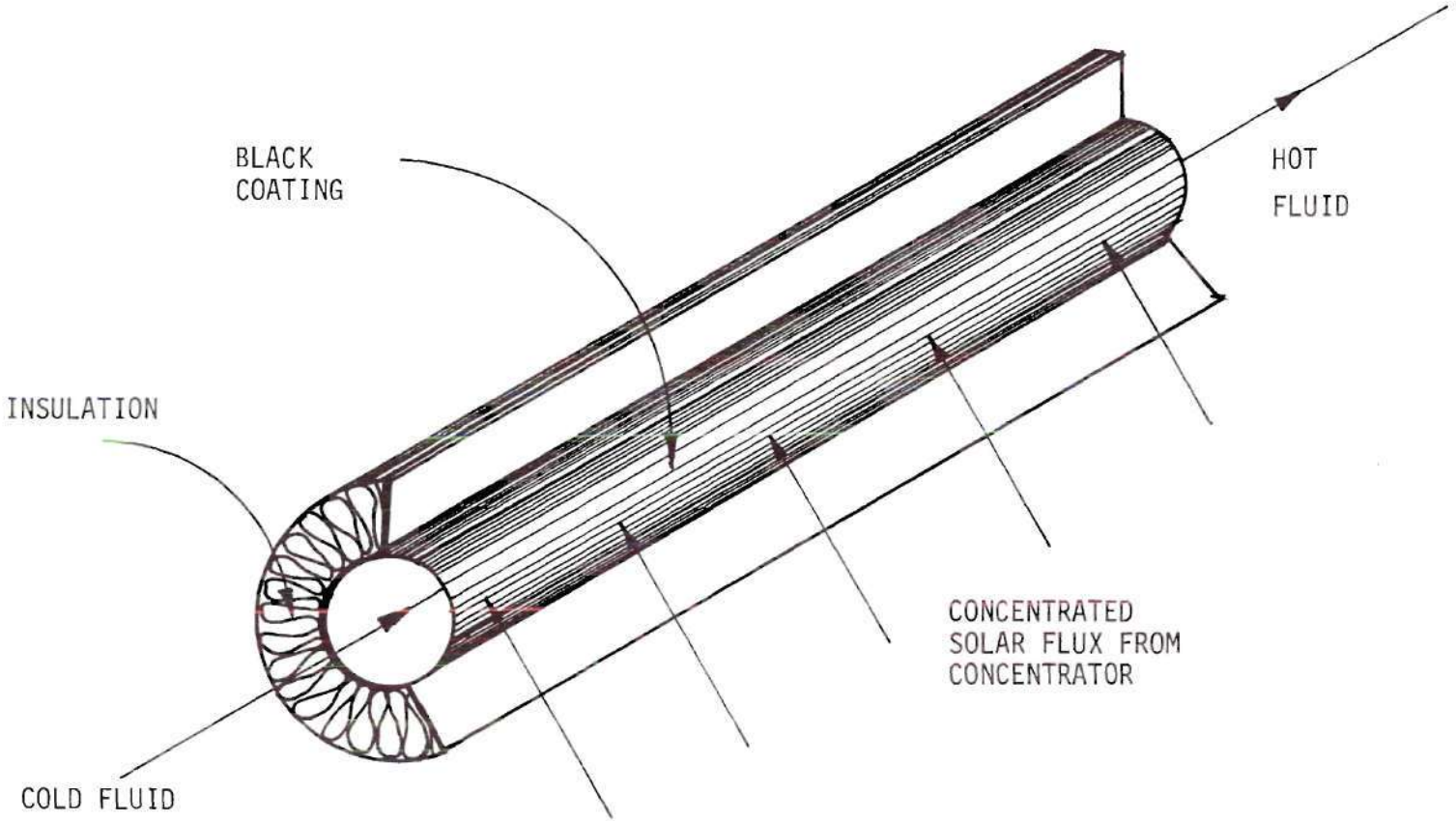

Figure 1. Heat Exchanger Elements

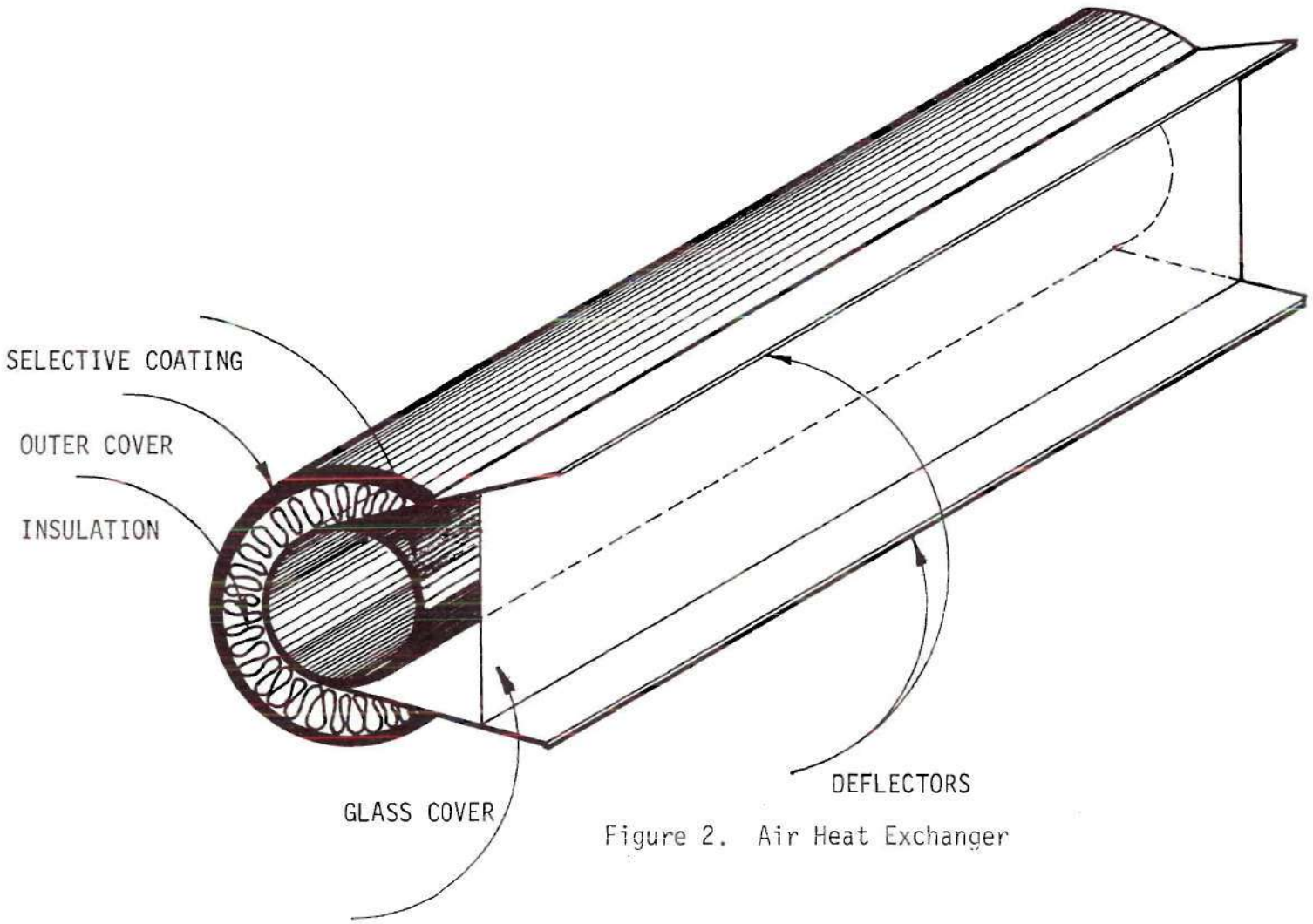

Figure 2. Air Heat Exchanger

tube. The radiation losses from the absorber surface can be reduced by applying a selective coating to the exposed surface of the tube. The selective coating is such that its $\frac{\alpha}{\varepsilon}$ value is high in the desired range of wavelengths.

The pressure drop of the fluid flowing through the tube depends on the roughness of the inside surface of the tube, the geometry (circular or non-circular), and other obstacles such as fins. Increasing the inside surface of the tube by means of fins increases the heat transfer to the fluid (due to fin effect) at the expense of increased pressure drop.

The air heat exchanger shown in Figure 2 is a simple circular tube with no internal lines. Initial experiments [11] were conducted with the simple type of heat exchangers for a linear focusing concentrator of a length 7' - 6" having an aperture of 6' - 7". This concentrator is a Fixed Faceted Mirror Concentrator (FFMC) with 28 facets geometrically aligned on cylindrical surface. The heat exchanger is placed in the focal plane of this concentrator as shown in Figure 3. As the altitude of the sun changes during its travel from east to west in the southern horizon the focal plane of the concentrator moves along a circle from west to east. An automatic tracking mechanism is attached to the concentrator to keep the receiver in the focal plane during the day.

The deflectors are made of highly reflective stainless steel material and the glass cover is pyrex. These features are shown in Figure 4. The exposed surface of the absorber tube is blackened with triple x-brown stove polish. The insulating material is a fiberfrax (Lo con type) material composed of Al_2O_3 and SiO_2 having a thermal

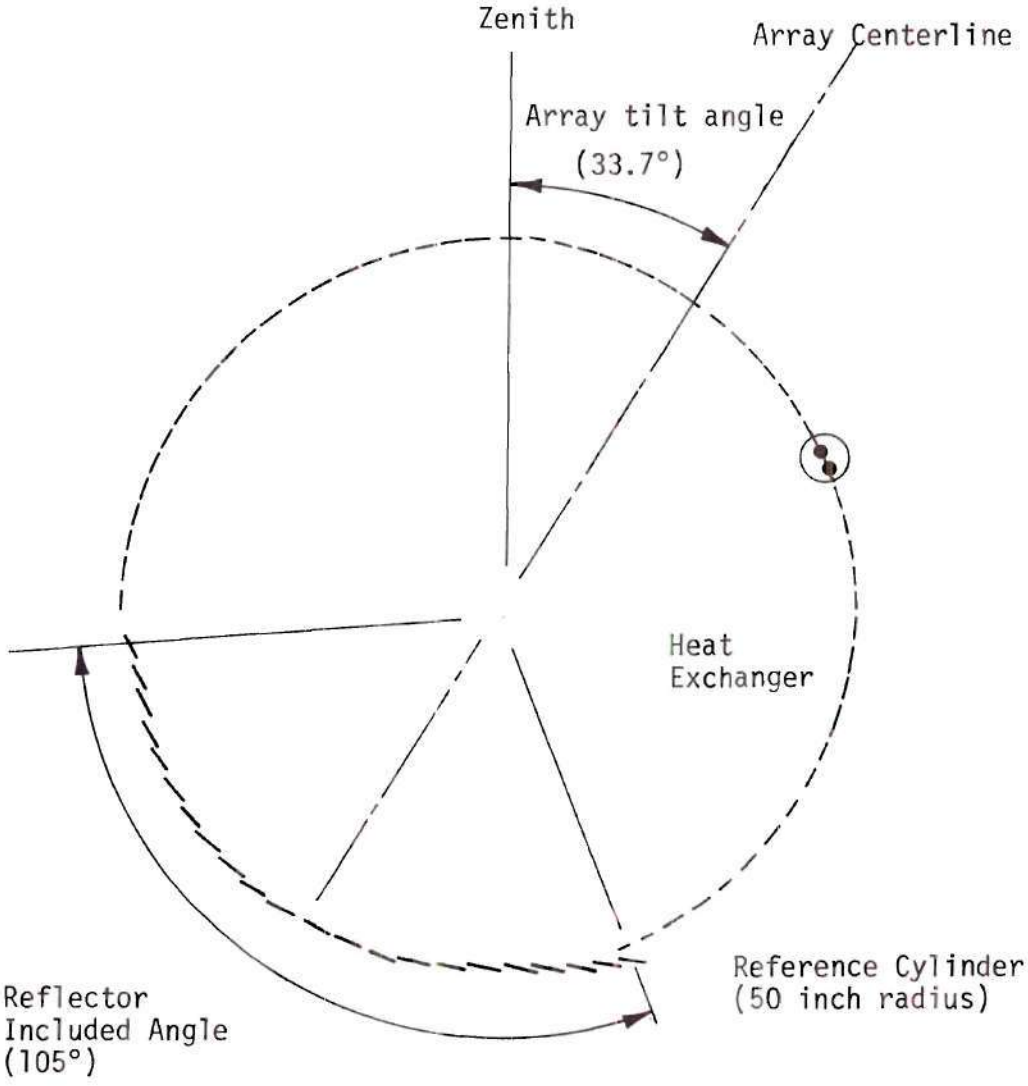

Figure 3. Concentrator Geometry

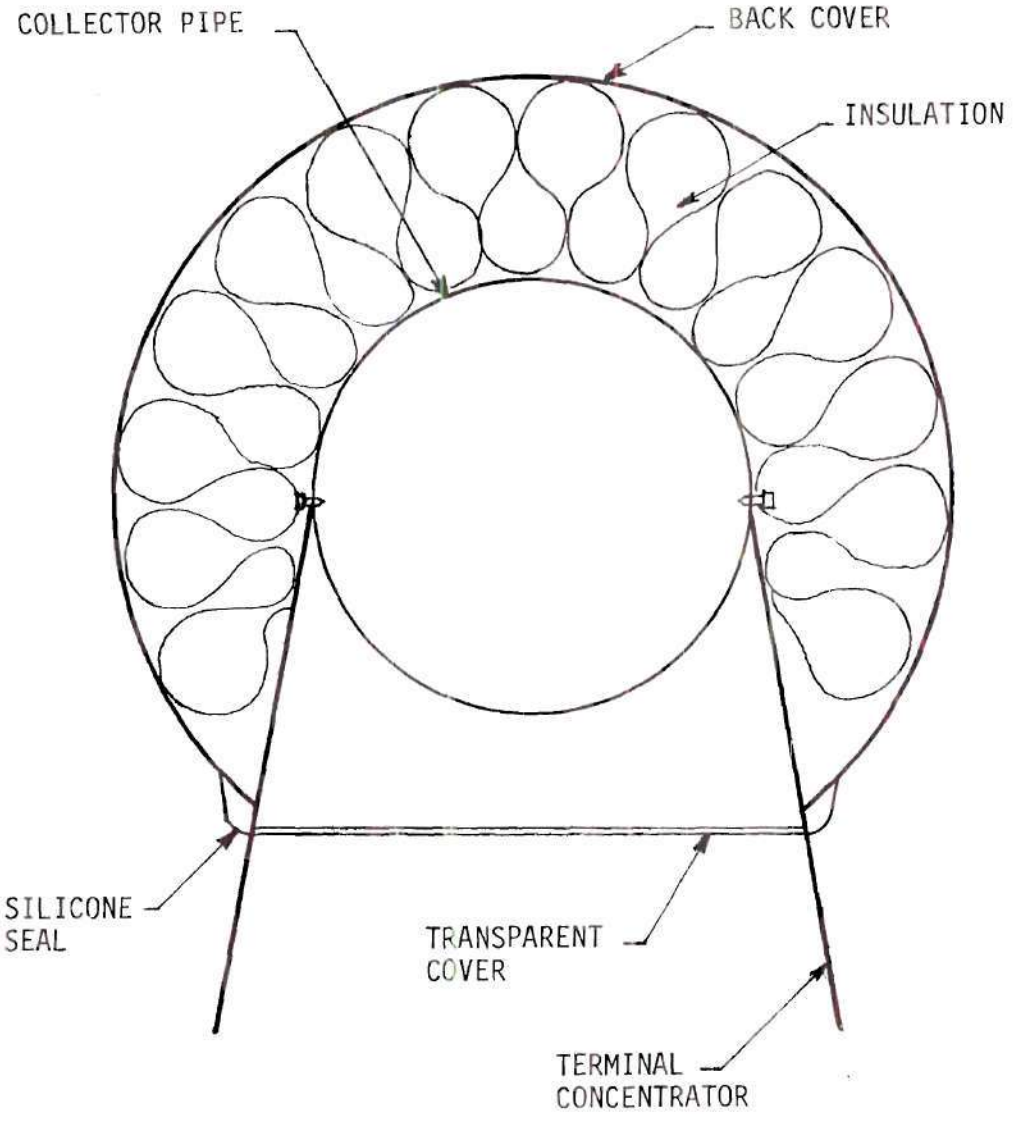

Figure 4. Cross Sectional View of Heat Exchanger

conductivity of 0.38 BTU/hr ft F° and lastly the tube is galvanized iron. From the preliminary experiments on this air heat exchanger, it has been found (2) that the temperature of the pipe is nonuniform around the circumference and along the tube wall. The collection efficiency is very low and ranges from 10% to 25%. The maximum surface temperature obtained in air heat exchanger is at low flow rates. Based on these pessimistic results, modifications in the construction of the collector to improve collector efficiency appear desirable. Tubes with internal fins or twisted tapes are some of the alternatives that were considered. However, since the frictional power losses in the tube of the air heat exchanger were already very high, the experiments with internal fins were not considered to be favorable.

Hot air has a wide range of applications such as in chemical industries, agricultural processes and many other processes. However, before considering the use of hot air for such application the severity of the pumping power requirement of the air flow through the receiver, the processing equipment, connecting pipes, bends and dampers should be seriously considered. Heating air in receivers directly from solar energy is always preferred, provided it is economically comparable to other alternative forms of energy. The reflectance of the present glass slat mirrors is of the order of 0.92 compared to 0.76 at the time of taking readings with air heat exchangers. This increase in reflectivity of mirrors suggests further improvement in concentrator efficiency. Air heat exchangers having small air flow rates will have less pumping power losses but are capable of delivering air at high temperature. It is expected that a sharp decrease in material cost accompanied with sharp

increase in their quality might enable air heat exchangers to provide hot air economically.

Liquids, becuase of their high heat capacity, are a better medium to transfer heat than gases and their frictional power losses are generally very low. Consequently, a new type of heat exchanger (manufactured by Corning Glass Co.) was selected (Figure 5) along with a heat transfer fluid such as Therminal 66. Analysis of this configuration has shown that this choice of heat exchanger improved the collection efficiency to 40% keeping the frictional power losses to a very low value.

The pumping power losses in air heat exchangers is many times more than that in liquid heat exchangers, the chief reason being the volume flow rate of air is roughly 1800 times that in liquid system (see Table 7) with the mass flow rate being the same for both cases. Assuming one mechanical power unit is roughly equal to four thermal units, then all of the heat collected in air heat exchanger would be just sufficient to overcome the frictional power loss. The mechanical shaft power obtained from receiver-rankine cycle system due to liquid heat exchanger usage is predicted to be around 9.41% of the incident flux. This power output is dependent on the highest Rankine fluid temperature, which in turn depends on the mean fluid temperature in solar collectors (liquid heat exchangers). The upperbound on the maximum collector fluid temperature is its decomposition temperature and also the corresponding vapor pressures produced at these temperatures. At present Therminol 66 manufactured by Monsanto Co. is best suited and also Dowtherm A fluid that can be used where the concentrator

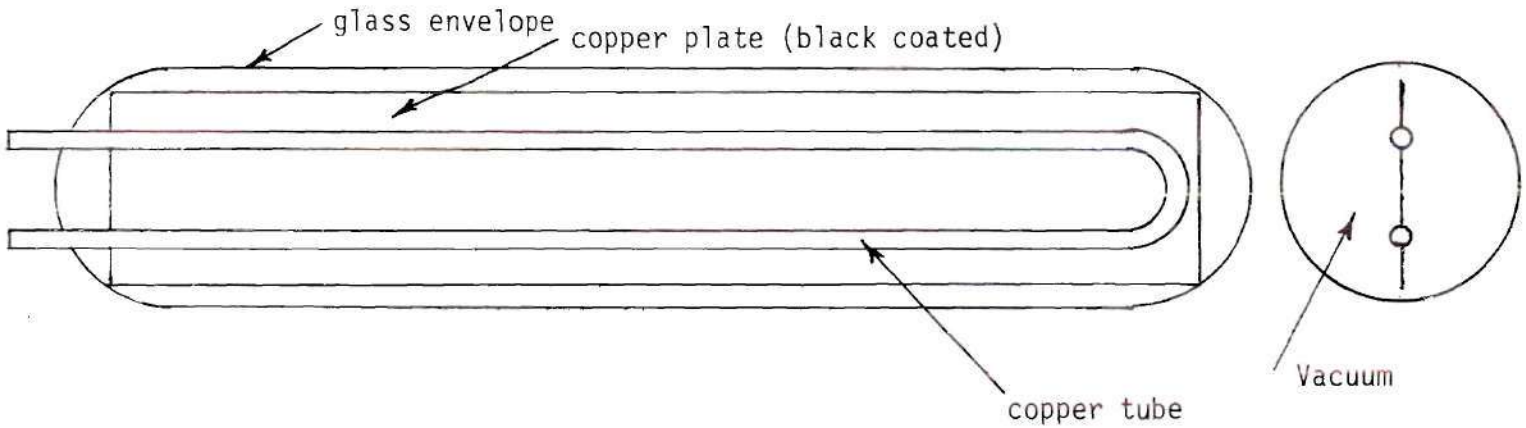

Figure 5. Heat Exchanger (Corning Glass Co.)

ratio or when solar fluxes are low.

The important characteristic properties of the collector fluid are that:

1. It should be a high-performance heat transfer fluid.
2. It is chemically stable at high temperatures.
3. It's vapor pressures at high temperatures be small.
4. It's inexpensive, inflammable, non-corrosive, non-toxic and easy to handle.

It is hoped that a heat-transfer fluid with above properties when marketed will have strong economic and engineering impact in solar industry. Therminol 66 satisfies most of the above requirements but it is expensive.

CHAPTER IV

LITERATURE REVIEW

The development of heat exchangers for focusing collectors is in its infancy. No optimum heat exchanger configuration has been developed and no rigorous thermal analysis has been done to establish the thermal characteristics of such a heat exchanger. Although theoretical considerations have been suggested for the development of a heat exchanger for focusing solar collectors, no experimental results on an actual operation of such an heat exchanger are available.

M. H. Cobble [12] gave theoretical analyses of three types of heat exchangers (flat plate, circular plate, and cylindrical) and obtained expressions for the temperature fields and exit temperatures. However, the models he employed are only theoretical. G. O. G. Lof, D. A. Fester and J. A. Duffie [13] optimized the focusing collector through a detailed study of the energy balances for a parabolic cylindrical reflector with tubular receivers of three diameters. They observed that the thermal losses from the heat exchanger increase with receiver wall temperature and their magnitude are higher that the useful heat energy gain of the working fluid. In their paper emphasis is given to the size of the heat exchanger tube at the focal plane and also on the reflector parameters but no detailed thermal analysis of the heat exchanger is given. Lof and Duffie [14] developed a set of general graphical relationships for establishing the receiver reflector

area ratio which will provide the maximum useful heat delivery from a focusing collector.

Lumsdaine [15] obtained a summary of the receiver efficiencies in terms of concentrator parameters for receivers of different geometries. Simplified lumped analysis expressions are derived for these heat exchangers and the results compare very well with more complicated distributive analysis results. These analyses are very theoretical in nature and overlooked the practical constructional and other details of the heat exchangers.

Pope and Schimmel [16] have analyzed the effects of variations in concentration, absorptance, and emittance of the receiver, silvering of the envelope, and system geometry on the performance of linear focused collectors. Convective and radiative transport between the receiver to the envelope and from the envelope to the environment are modeled. Their study indicates that collector extraction efficiencies of 40 to 60 percent can be obtained. This analysis is also somewhat idealistic from the consideration of a realistic configuration for the heat exchanger. It may not be possible to employ such a heat exchanger effectively for continuous operation.

Palmer and Kuo [17] developed a more efficient heat exchanger in which solar flux concentrated by a focusing mirror enters a high temperature glass pipe through a narrow window. The pipe contains a thin slab of graphite that absorbs the radiation and converts it to thermal energy. This energy at high temperature is absorbed by flowing helium gas which is then fed into the turbine of a closed-cycle system.

Even though this is the most recent development in utilizing focusing solar heat exchangers, it lacks analytical approaches for predicting the effects of variations of pertinent parameters on the performance of the heat exchanger utilizing the gaseous medium.

A research group at Itek Optical Systems Division [18] performed a breadboard simulation test on a 1 m^2 focusing solar collector system. An analytical model was developed and experiments were performed by passing an electric current through a rod surrounded by insulation. The test results showed a close agreement between theoretical and experimental values of efficiencies. This report emphasizes solar power generation and economic considerations of other components of plant rather than on optimization of the heat exchanger for the focusing collector, at different load demands.

The heat exchanger for the solar concentrator is meant to be used eventually for the production of electric power and for solar cooling. The optimum inlet and outlet fluid conditions of the heat exchanger depend on the end use and the system arrangement. S. L. Sargent and W. P. Teagen [19] showed how solar powered organic Rankine cycle engines can be used for cooling and refrigeration effects. Daryl Pigmore and R. Barber [20] have developed a demonstration package supplying residential cooling and/or electricity via a solar heated Rankine cycle. The Rankine cycle efficiency data as obtained by them are used in this thesis for optimization of the receiver of a space power plant.

A. M. Lindsey [47] investigated the performance of a segmented plane solar energy concentrator of area 25 $ft.^2$. The basic

principle of concentration is same as that proposed by Russel [1, 23] in his srudies on central station solar power plant. The original idea dates back to the work of Gunter [48]. In this concentrator the plane mirror segments are rotated in order to keep the reflected solar flux image on a common linear receiver. The tracking is accomplished by equally rotating all segments by an amount proportional to the seasonal changes in the sun's position. He found that the concentrator can be fabricated economically and it concentrates efficiently. In his testing of this concentrator with various receiver configurations, unevacuated acrylic tube system is found to be superior in performance, and Lindsey suggests that an evacuated receiver tube enclosed in a glass envelope (having inlet and outlet of the collector fluid tube at the same end) would be ideal in minimizing the thermal losses.

In the fixed mirror concentrator of this project the mirror slats are fixed but the receiver of light weight is rotated along a reference circle to be in focal plane of reflected concentrated light. J. R. Williams and B. Rollins [1] have obtained the solar flux distribution at the focal plane of a fixed mirror concentrator of 56 sq. ft. area. The axis of this concentrator was oriented in N-S direction. A prototype fixed mirror concentrator of 540 sq. ft. area with its oriented E-W axis is installed at Georgia Institute of Technology and a receiver system for this concentrator system is currently being studied.

S. I. Abdel - Khalik [21] obtained heat removal data for a flat-plate solar collector with a serpentine tube. The collector was of the sheet and tube design and the tube bound to the absorbing plate

in a serpentine fashion. Equations describing the variation of fluid temperature in the different segments of the serpentine tubes are derived. These equations are then used to determine the heat removal factor for the collector. This heat removal factor can be used to determine the collector efficiency as well as the exit temperature of the fluid. The computation of these parameters involve numerous trial and error procedures specially for fluids whose properties are highly dependent on temperature. The absorber plate of this collector is identical to that of the Corning glass tube heat exchanger (receiver) except for the flat glass cover. The results of this paper can be utilized in the analysis of the present receiver.

Lof and Tyboul [22] have performed a detailed study of cost optimization for dwellings heated and cooled by solar energy. The annual capital cost of equipment and the annual cost of the auxiliary fuel are added to obtain the total annual cost of the solar systems. The optimum solar collector area is determined corresponding to the minimum total annual cost of the solar systems. Their optimization technique is very simple and useful for analysis of flat plate collector systems where the cost of collectors and other equipment are readily available. If the costs of different components of solar concentrator systems were well established, a similar approach for optimization could be done.

CHAPTER V

CONCENTRATOR PERFORMANCE

With the present technology, high temperatures can be obtained by use of solar energy only through the use of concentrators. Since large concentrating surfaces are subject to high wind loadings, it is often advantageous to fix the reflecting surface in a stationary supporting structure and steer a much smaller heat exchanger so that it remains in the focal region of the concentrator at all times. If this concentrator can be built at a very cheap labor cost and also by using inexpensive flat reflecting elements it will minimize the cost. Russel [23] invented a Faceted Fixed Mirror Concentrator (FFMC) that has no off-axis aberration and focuses sunlight sharply regardless of the incident direction of the beam radiation. This fixed mirror concentrator (Figure 6) is composed of long, narrow flat reflecting elements arranged on a concave cylindrical surface. The angle of each of these reflecting facets is fixed so that the focal distance is twice the radius of the cylindrical surface for the flux normal to the concentrator aperature. The geometrical angles of each element are tabulated in Table 1. The focus line of these facets lies on the reference cylindrical surface, parallel to the fixed mirrors, regardless of incident sunlight angle (See Fig. 7). Such a concept permits supporting the heat collector at the center of the reference cylinder. This greatly simplifies the positioning of the heat exchanger which

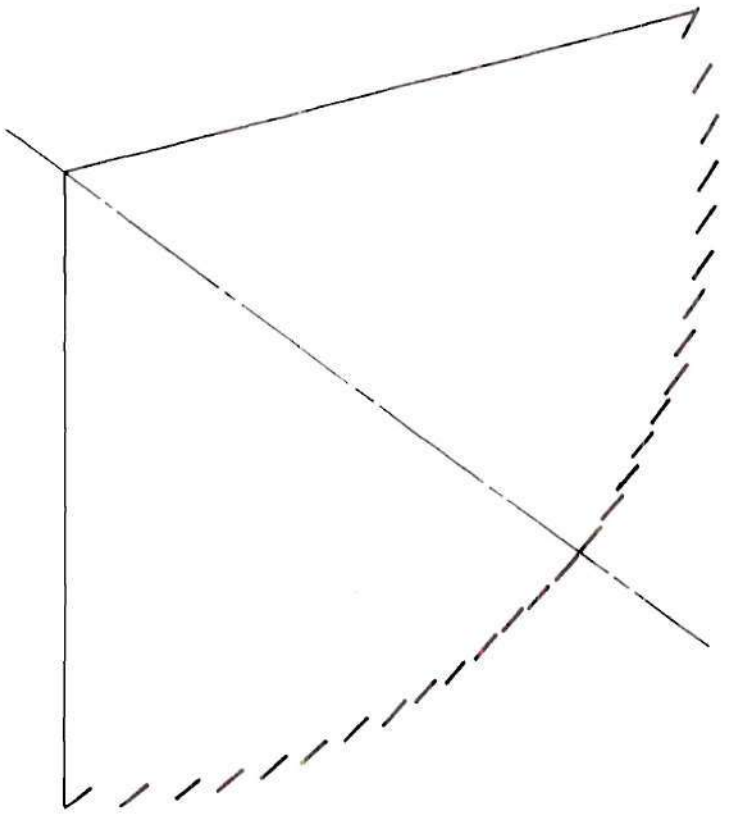

Figure 6. The Angular Positions of Slats

Table 1. Solar Reflector Coordinates

Slat No.	X-Axis	Y-Axis	Theta	Mirror Angle
0	1.4500	-49.9790	-1.661	.415278
1	4.3499	-49.8104	-4.991	1.24774
2	7.2492	-49.4717	-8.336	2.0841
3	10.1473	-48.9595	-11.709	2.92733
4	13.0435	-48.2687	-15.122	3.78043
5	15.9372	-47.3920	-18.587	4.64675
6	18.8277	-46.3197	-22.120	5.5301
7	21.7142	-45.0388	-25.740	6.43493
8	24.5959	-43.5321	-29.467	7.36669
9	27.4720	-41.7767	-33.329	8.33215
10	30.3414	-39.7417	-37.360	9.34012
11	33.2029	-37.3840	-41.610	10.4025
12	36.0553	-34.6413	-46.146	11.5365
13	38.8967	-31.4173	-51.072	12.7679

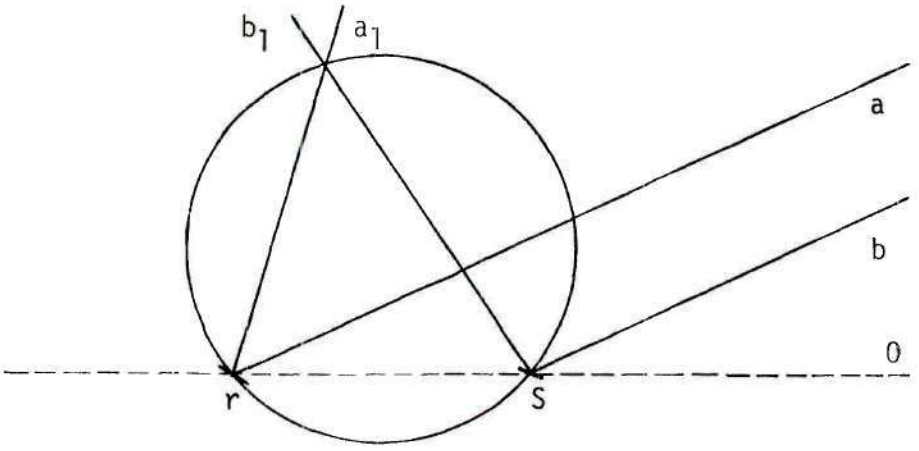

Figure 7. Intersection of Two Parallel Rays

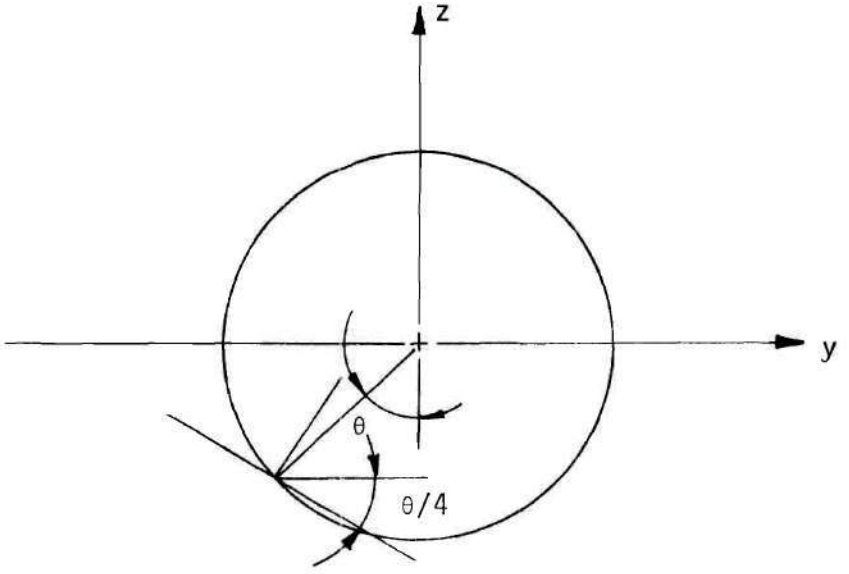

Figure 8. Specifications of Angular Position of Slats (Taken from Ref. [17]).

can be done by a simple four-bar mechanism. The solar heat flux falling on the heat exchanger tube q, can then be determined. Let q_{in} be the solar flux falling on a normal surface, that is, as measured by pyroheliometer.

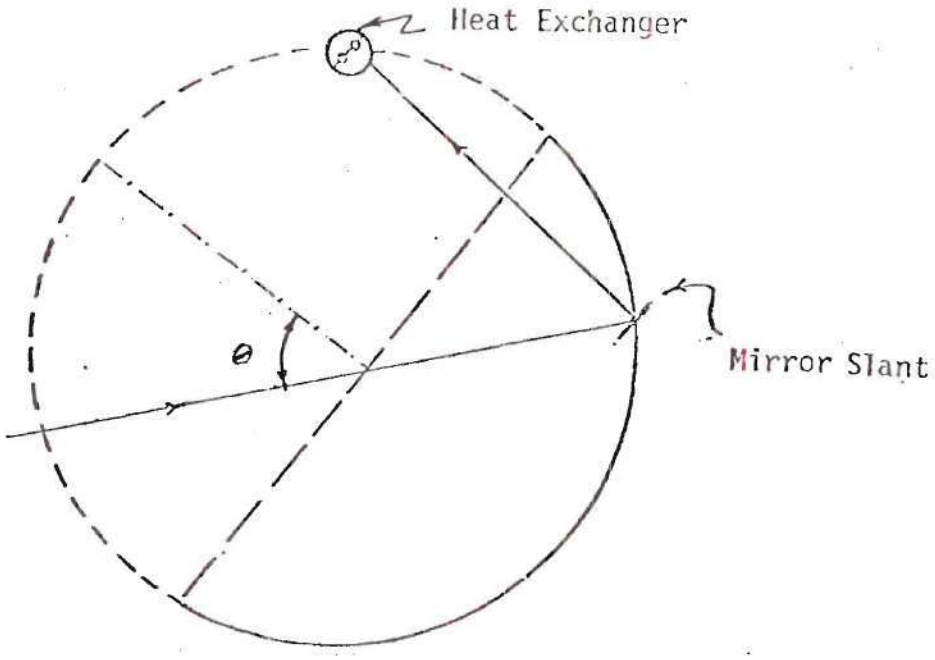

Figure 9. Angle of Incidence

The geometric relationship between a plane of any particular orientation relative to the earth at any time (whether that plane is fixed or moving relative to the earth) and the incoming beam solar radiation, that is the position of the sun relative to that plane, can be described in terms of several angles. These angles and relationships between them [24] are: (see Figure 10)

ϕ = latitude angle (north position)

δ = declination angle (i.e., the angular position of the sun at solar noon with respect to the plane of the equator) (north position)

S = the angle of tilt from the horizontal (i.e., the slope of the plane)

γ = The surface azimuth angle, that is, the deviation of the normal to the surface from the local meridian, the zero point being due south, east positive, and west negative.

ω = hour angle, solar noon being zero, and each hour equaling 15° of longitude with mornings positive and afternoons negative (e.g., ω = 15 for 11:00, and ω = 37.5 for 14:30)

θ = the angle of incidence of beam radiation, the angle being measured between the beam and normal to the plane.

The declination , can be found from the approximate equation of Cooper [25]

$$\delta = 23.45 \text{ Sin } (360\ [\frac{284+n}{365}]) \qquad (1)$$

where n is the day of the year.

The relation between Θ and the other angles is given by

$$\begin{aligned}\text{Cos } \Theta = {} & \text{Sin } \delta \text{ Sin } \phi \text{ Cos s- Sin } \delta \text{ Cos } \phi \text{ Sin s Cos } \gamma \\ & + \text{Cos } \delta \text{ Cos } \phi \text{ Cos s Cos } \omega \\ & + \text{Cos } \delta \text{ Sin } \phi \text{ Sin s Cos } \gamma \text{ Cos } \omega \\ & + \text{Cos } \delta \text{ Sin s Sin } \gamma \text{ Sin } \omega\end{aligned} \qquad (2)$$

Solar time = standard time + E + 4 $(L_{st} - L_{loc})$

Standard time = Eastern Daylight Time - 1

Where E = the equation of time in minutes from Figure 11.

L_{st} = standard meridian for the local time zone

Standard meridians for continental U. S. Time zones are:

Eastern, 75°w; Central, 90°w; Mountain, 105°w; and Pacific, 120°w.

The solar flux falling on the heat exchanger tube can be found by

$$q = q_{in}\ A_c\ \rho_c\ \text{Cos } \Theta\ (1-K_e)\ /A_r \qquad (3)$$

or $q = q_{in}\ A_c\ \text{Cos } \Theta\ n_c/A_r$, where concentrator efficiency $n_c = \rho_c\ (1-K_e)$

where Ke = factor that accounts for the edge and shadow losses. These shadow losses are largely dependent on the solar angle component above southern horizon (see Figure 12) and this angle in turn depends on the time of the day and also the day of the year (see Figure 13).

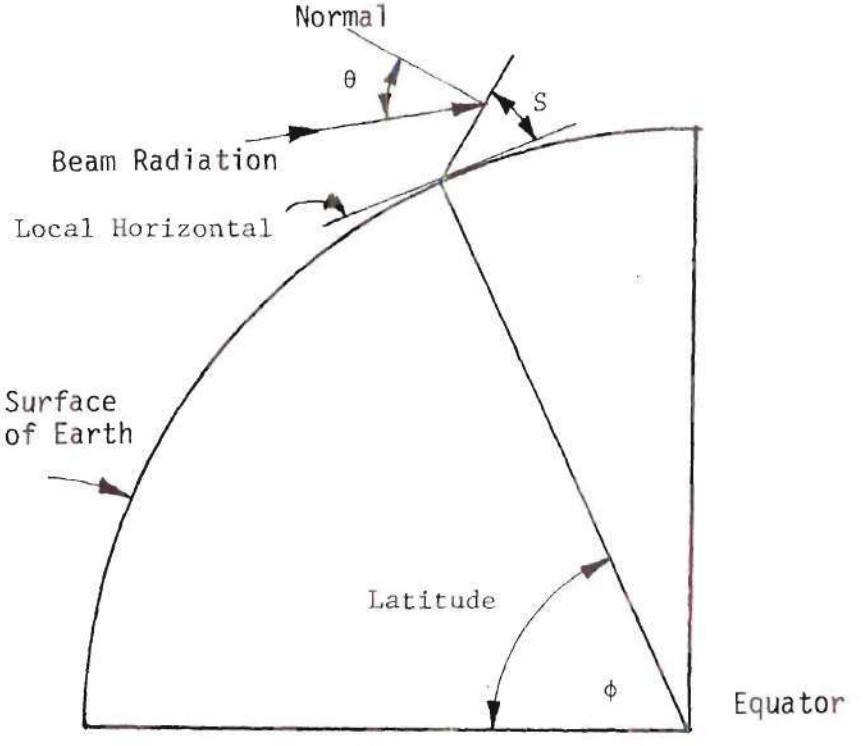

Figure 10. Definition of Different Angles

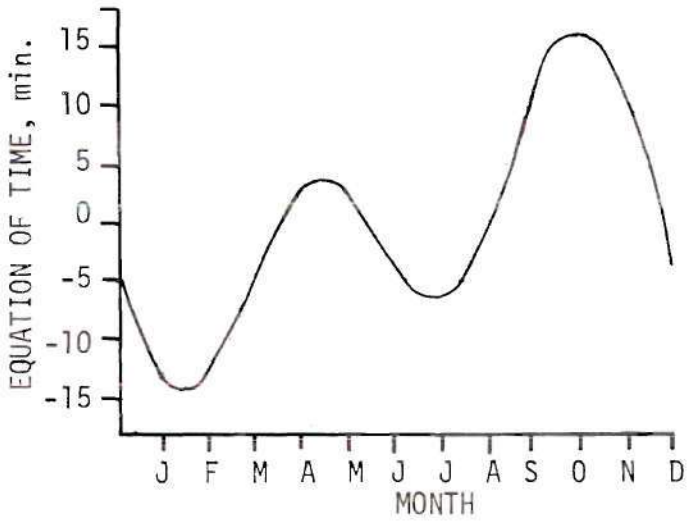

Figure 11. The Equation of Time, E., In Minutes, as a Function of Time of Year. From Ref. [3]

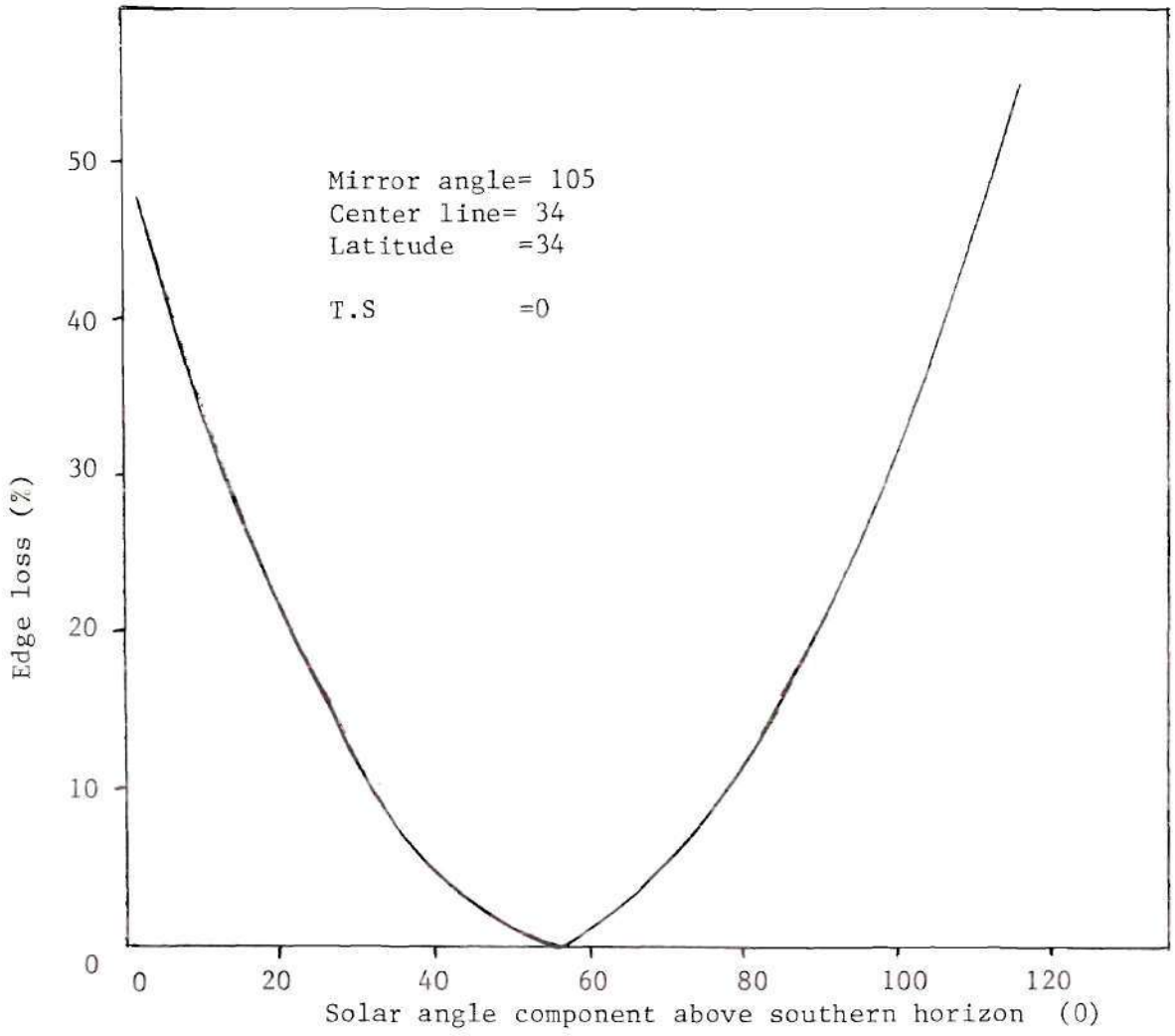

Figure 12. Variation of Edge Losses

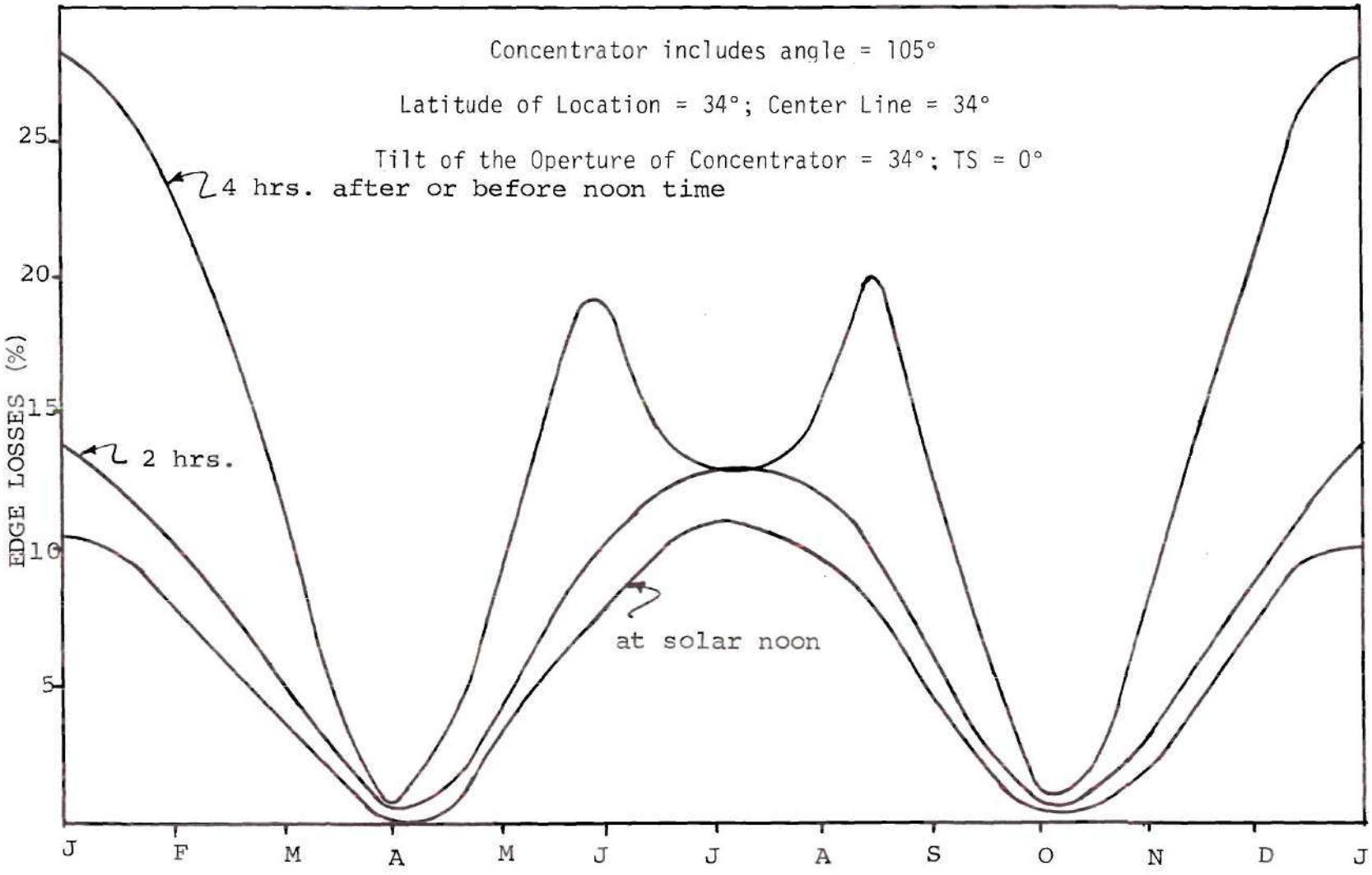

Figure 13. Hourly Edge Loss Variation Over the Year

Russel [26] discussed in detail about the numerical computation of these edge losses. He also presented graphically the edge losses for the two cases: $\theta_{in} = 90°$ and $\theta_{in} = 120°$. From these two curves, a curve is extrapolated (Figure 13) to represent the edge losses for the following parameters of the present solar concentrator. (See Figure 6)

Mirror angle $\theta_{in} = 105°$

Center line angle = 34°

Latitude angle $\phi = 34°$

Tangential slat angle = 0°

According to Russel [1] the concentrator of this geometry is selected to have the minimum edge losses and maximum concentration for a given unit length along the E-W axis of concentrator.

Generally for a long concentrator, with its axis parallel to the east west axis, edge losses do not exceed 10%. Unfortunately the reflection losses will be as high as 25%. The end losses as illustrated in (Figure 15) are negligible for a relatively a long concentrator. The numerical computation of these minor losses involves very complicated relationships and therefore were abandoned in view of the heavy emphasis placed on receivers and on the thermal analyses of other components. A further discussion on concentrator losses are discussed in Chapter VII.

The heat flux at the focal plane was measured experimentally by using Hy-Cal Pyroheliometer. (See Figure 18). It has a range of 0-25 solar constants. The three lead wires coming out of its base were connected to the chart recorder to obtain the output in millivolts.

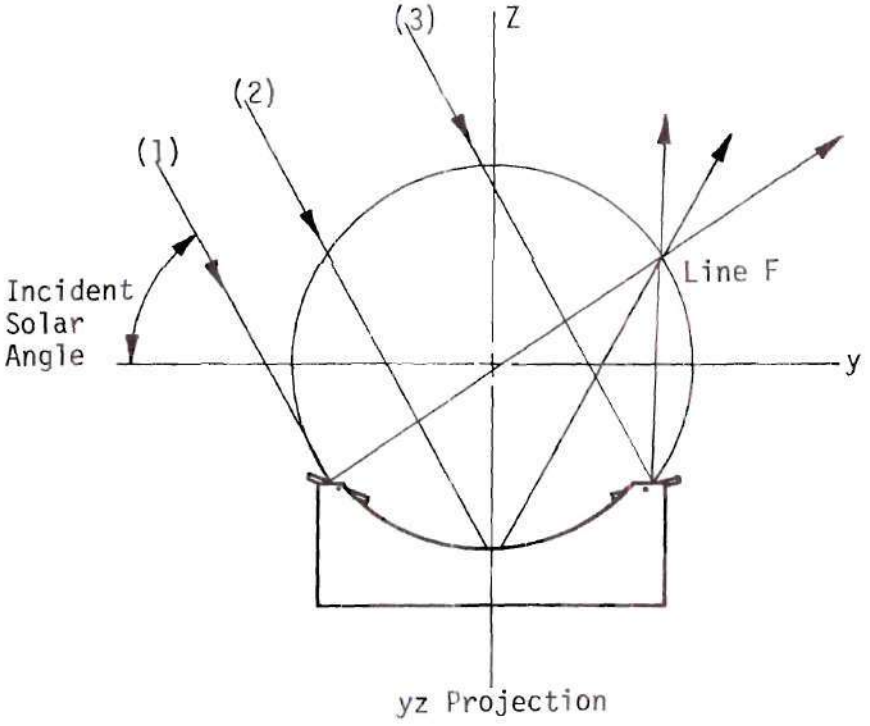

Figure 14. Focal line position on reference circle.

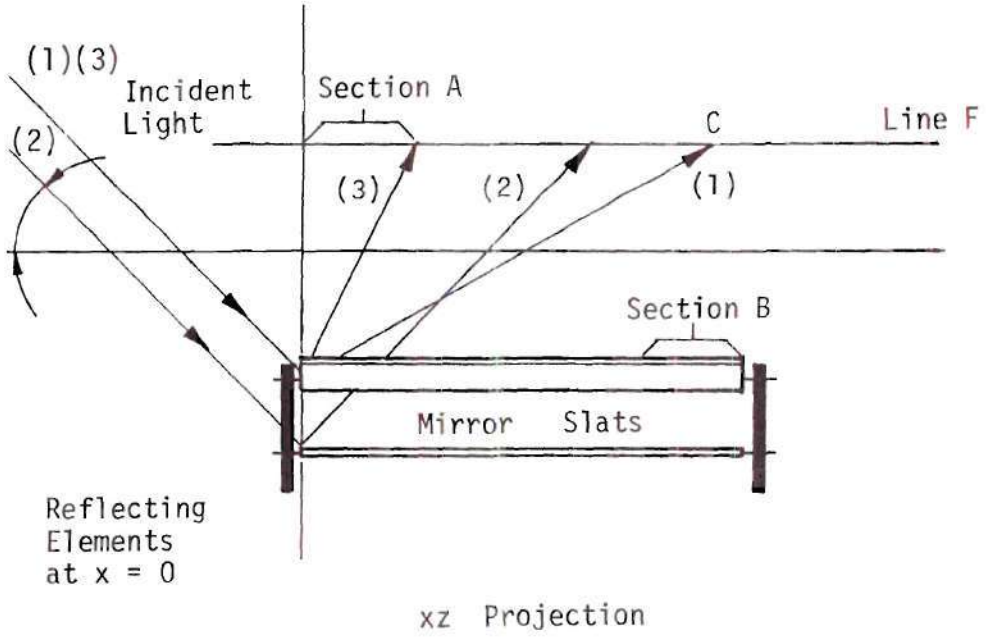

Figure 15. Reflecting Path Lengths

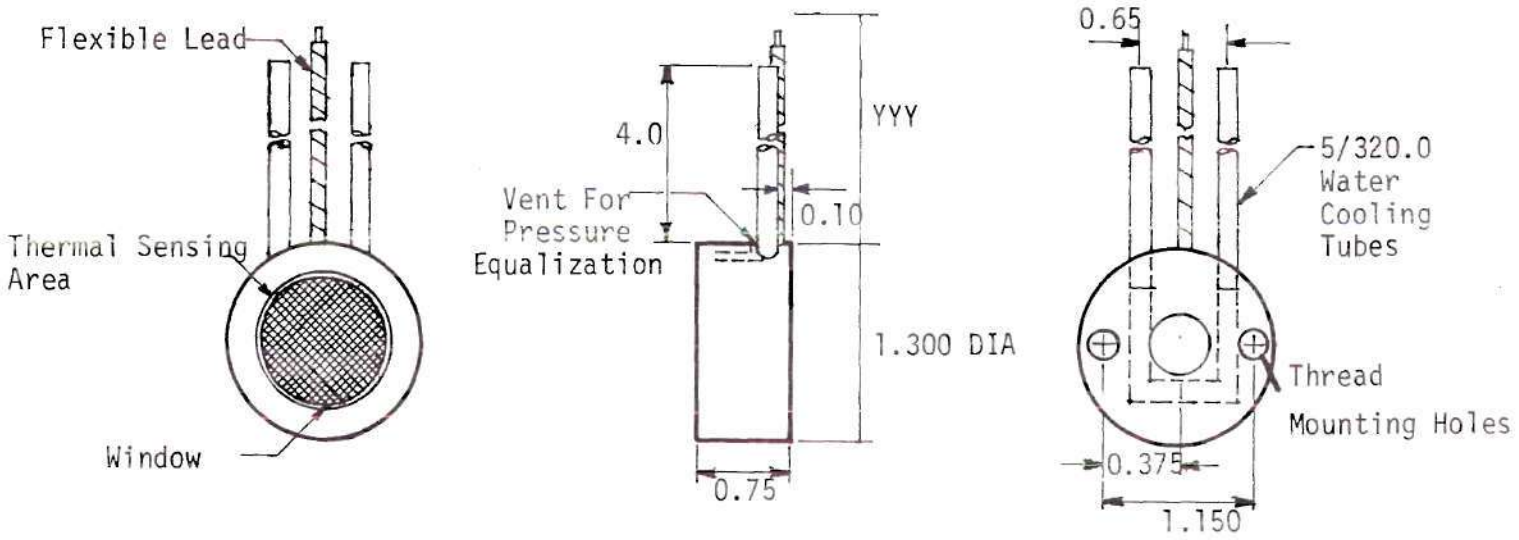

Figure 16. Hytherm Pyroheliometer

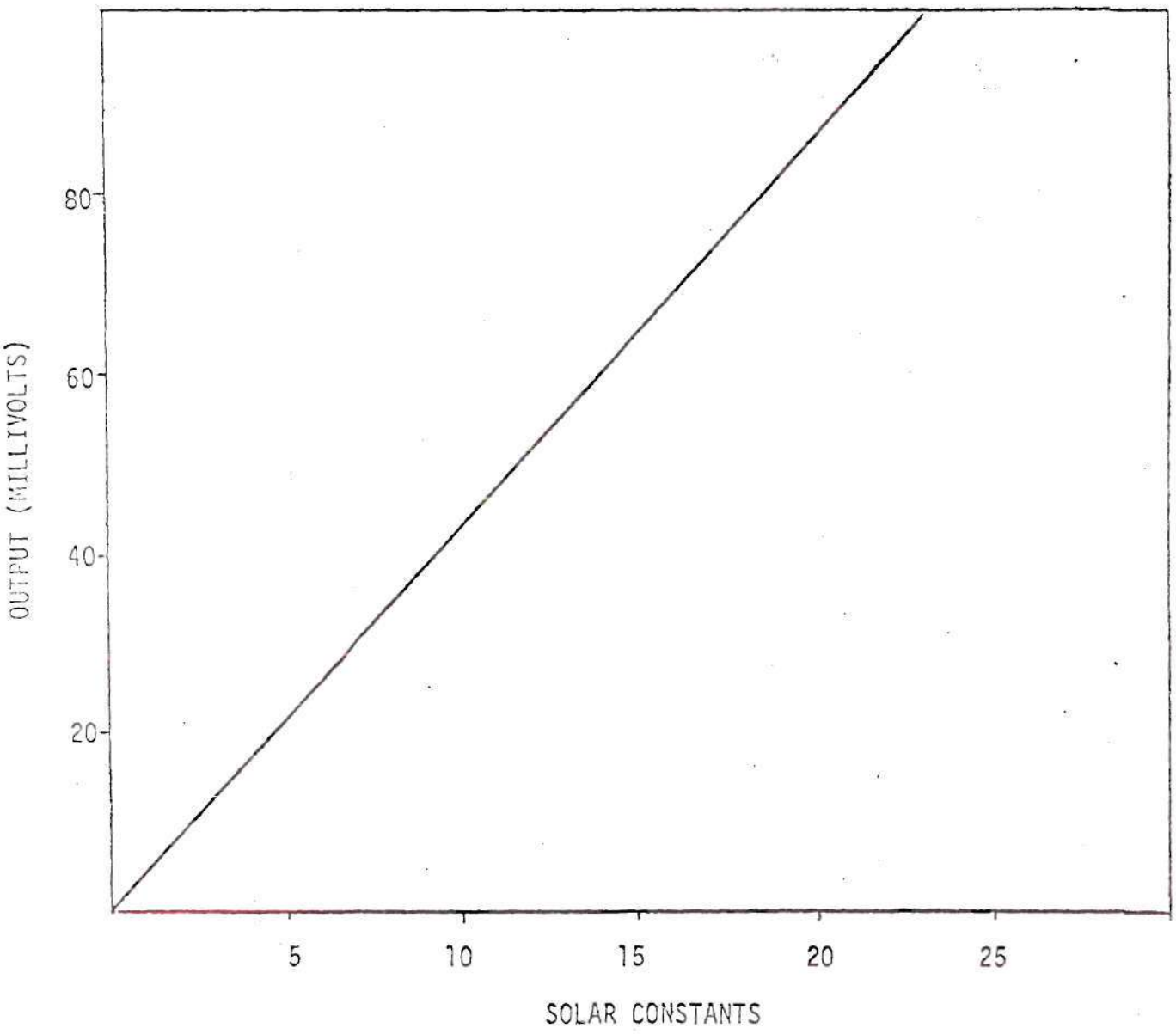

Figure 17. Calibration of Hy-cal Pyroheliometer

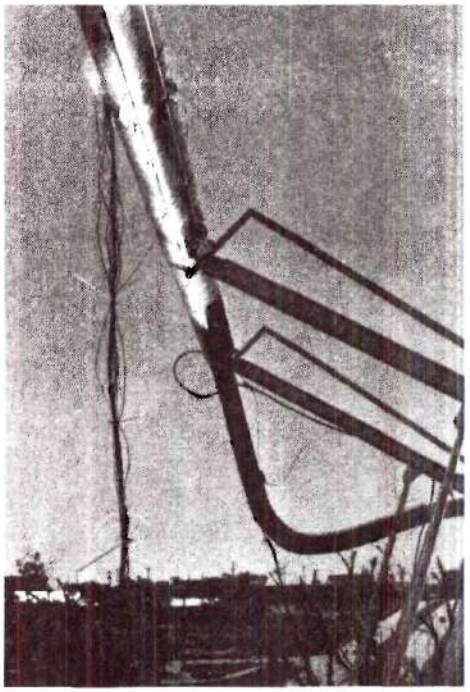

Figure 18a.
Receiver in Focal Plane

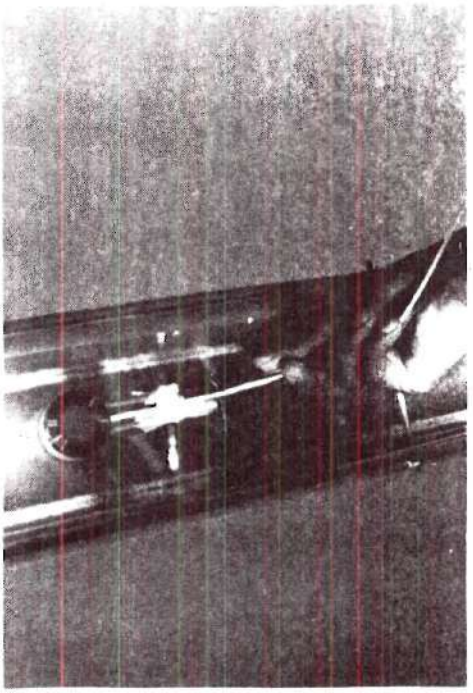

Figure 18b.
Measurement of Solar Intensity

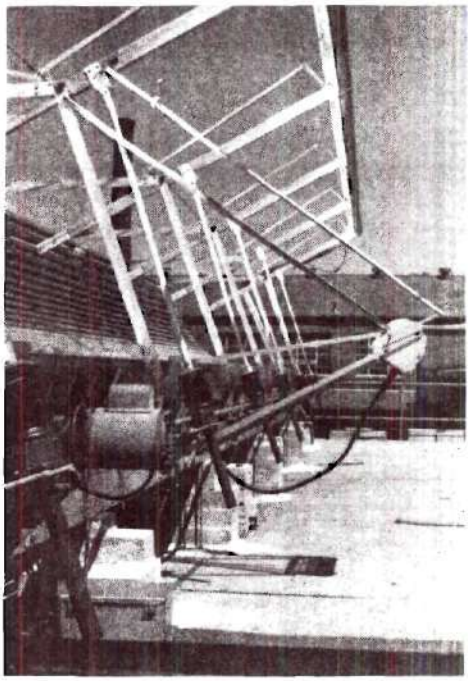

Figure 18c.
Tracking Device

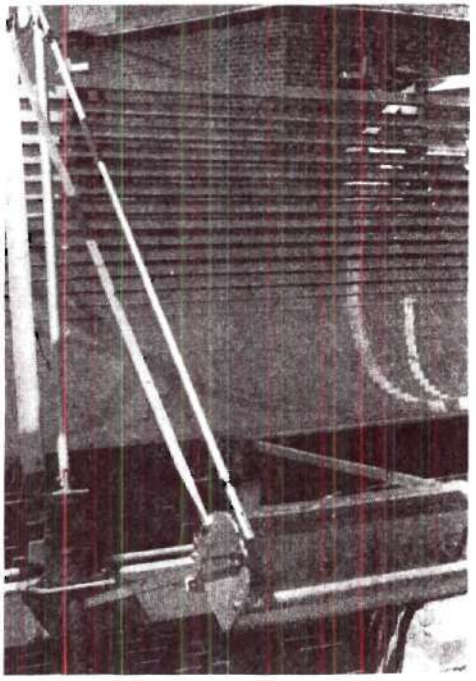

Figure 18d.
Tracking Device

The pyroheliometer readings were taken at equal intervals across the focal plane and the net actual solar flux falling on the heat exchanger was determined. The ratios of the actual solar energy falling on the heat exchanger over that on the reflector of the same length would give the concentrator efficiency. Table 2 indicates the measured values of solar flux at the focal plane and the corresponding concentrator efficiencies.

Such low values of concentrator efficiencies are due to misalignment of slats due to which the concentrated solar flux deviates from the focal plane as shown in Figure 18a. The sun tracking system consisting of four bar mechanism as shown in Figures 18c and 18d might have also caused some deviation of the concentrated flux.

Table 2. Experimental Results of Concentrator Efficiency

Run No.	Date	Time EDT Local	Solar Flux Falling on Reflector BTU/hr	Solar Flux Measured at Focal Plane BTU/hr	Concentrator Efficiency %
1	4-8-76	4:08 PM EST	5522	2994.3	57.34
2	4-8-76	4:15 PM "	5154.5	2816	54.63
3	5-12-76	11:27 AM "	7909.6	3986.4	50.4
4	5-12-76	11:29 AM "	8001.8	4328.97	54.1
5	5-12-76	11:30 AM "	8055.4	3625.0	45.0
6	5-12-76	11:35 AM "	8324	5318	63.9
7	5-12-76	11:36 AM "	8501.4	5439	64.0
8	5-17-76	11:24 AM "	8867	5131	57.9
9	5-17-76	11:29 AM "	8980	5084.3	56.6

Note: Number of slats = 28

Included angle of concentrator = 105°

Tilt of the concentrator = 34°

Average Efficiency = 55.985%

CHAPTER VI

SYSTEM SIMULATION PROCEDURE FOR OPTIMIZATION

Thermal Analysis of Corning Glass Receiver

In this chapter a mathematical model is presented for the thermal analysis of receivers. The fixed mirror concentrator consists essentially of a large number of slats along the circumference of a reference circle. The width of the reflected rays at the focal plane is slightly larger than the width of a slat. Thus the width or the diameter of the receiver collector is slightly larger than this width in order to avoid low interception factors. Numerous papers have been published on performance of such solar collectors. They vary from extremely simple analysis of Meinels [27] to the more refined analysis of D. O. Lee, W. P. Schimmel, Jr. [35] and of Edenburn [29]. Lee and Edenburn both considered a black coated circular cylindrical tube collector enclosed in an evacuated glass envelope. Labor and the capital cost prohibit the reduction of slat width to extremely low values. The solar receivers considered in this paper is shown in Figure 20 and it is manufactured by Corning Glass Company.

The solar receiver consists of a black chrome coated absorber plate with copper tubes embedded in it in a U-tube arrangement. The absorber plate is enclosed in an evacuated glass envelope. This collector is mathematically modelled as a flat plate collector having glass covers on either side. Khalik [21] considered a flat plate collector with N-number of tubes embedded on to a plate in a serpentine

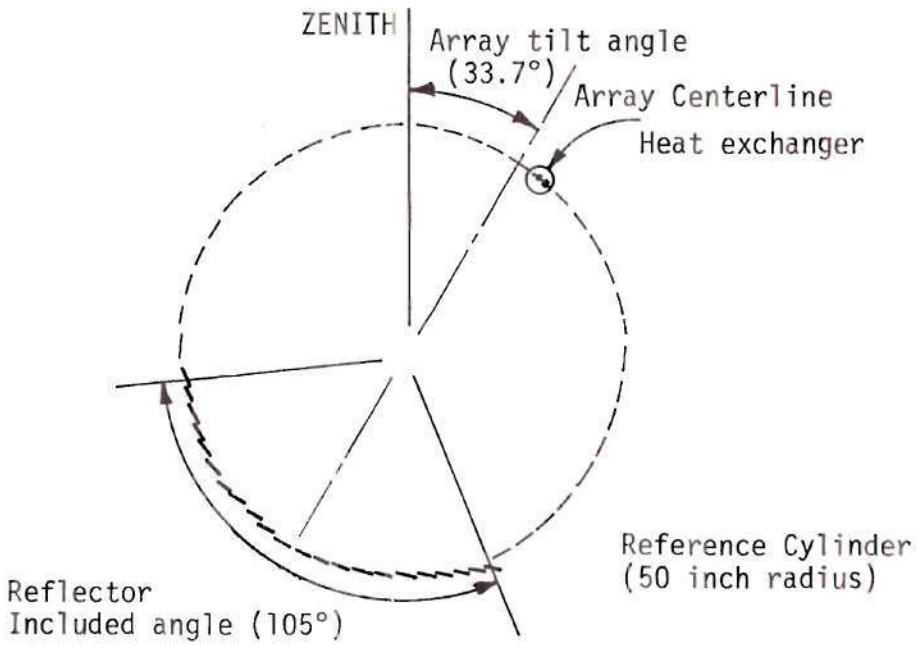

Figure 19. Concentrator Geometry

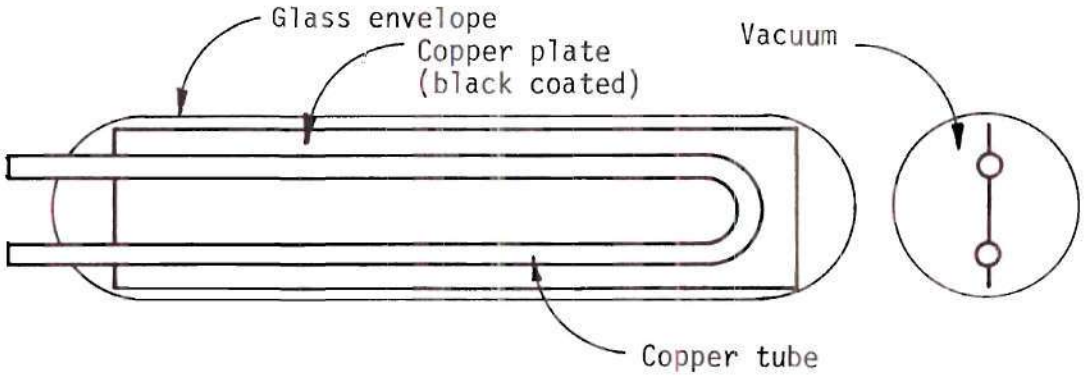

Figure 20. Heat Exchanger (Corning Glass Co.)

fashion. He obtained mathematical expressions for heat removal factors. In his analysis the value of U_L, the overall heat transfer coefficient, is treated as an experimentally measured input variable. However, this parameter depends on the type of glass envelope, absorber plate, and ambient temperature. In the present analysis, the radiation and conduction (based on kinetic theory models) losses from absorber plate to glass envelope and also the convection and radiational losses from glass envelope to environment are considered in computing the value of U_L. The mathematical analysis for temperature distribution of the absorber plate and that of the fluid are as obtained by Khalik [21] and are used in this analysis for obtaining mean plate temperature, glass temperature, and exit temperature of the fluid. Collector fluid after being heated by the solar flux is passed through a conventional counterflow heat exchanger in which fluid (Toluene) for Rankine power plant is vaporized. The vaporized fluid passes through a turbine to produce shaft power. The Rankine efficiency primarily depends on the maximum fluid temperature, as shown by the results of Prigmore and Barber [20]. Properties of Benzene were readily available in reference [30]. Benzene is selected as Rankine fluid (only for the simple plant without storage) as it was also found to be a suitable candidate fluid for solar Rankine cycles [31]. The complete properties of Toleune could not be obtained to use that fluid for this analysis. However, Toleune is considered for this optimization of a 100 MW power plant. For this optimization analysis complete properties of Toleune is not required.

Section A: Thermal Analysis of Receivers

Thermal analysis of the receiver is carried out by treating each of the three regions of the absorber plate (shown in Fig. 22) as fins. As fins generally absorb or loose heat at the base edge and loose or absorb heat energy on the fin surface, the temperature distribution for such fin surfaces are already developed for various boundary conditions at the leading edge of the fin surfaces. The molecular heat conduction in the space between the absorber plate and glass envelope as shown in Figure 5 is taken into account and can be evaluated approximately if the receiver is considered to be in the shape as shown in Figure 21. First the fin equations are solved for each regime and the plate temperature distribution is obtained in terms of the temperatures of the tube surfaces, which in turn is related to incoming solar flux through energy balance. After applying the energy balance equation of convective heat transfer between the collector fluid and the tube surface, the expression for the exit fluid temperature is evolved. Analysis is begun with an initial guess of average plate temperature and a simple relaxation technique is applied for the convergence of the solution.

The analysis is similar to that of Khalik [21] and it is based on the following assumptions:

1. The incident concentrated solar flux falls normal to the glass envelope. Reflection losses due to grazing angles are minimized.

2. The temperature of the glass envelope is considered to be uniform.
3. The reflectivity and absorptivity effects of glass envelope are negligible.
4. The absorber plate is located at a distance of $\frac{2D_e}{3\pi}$ from the assumed flat glass envelope cover on either side of the plate as shown in Fig. 22. This assumption is made to simplify the analysis for evaluating the molecular heat conduction in the space between absorber plate and glass envelope.
5. There is no temperature gradient through the thickness of the absorber plate.
6. The heat losses from the edges of the absorber plate along its length are zero since it is not in contact with glass envelope.
7. Longitudial conduction both in the absorber plate and glass envelope in the direction of flow is neglected.
8. All thermal processes are taking place at steady state conditions. The governing equations for the temperature distribution of absorber plate and also that of working fluid are written as shown below. The complete solution to these equations can be found in Appendix. The standard fin equation frequently seen in many text books is derived from the energy balance on a differential fin element of width dx and of unit length as shown in Fig. 22.

heat conducted to the adjacent element ℓ + heat loss from the surface

= heat absorbed by the plate

$$(-K\,\tilde{\delta}\,\frac{\partial T_i}{\partial x^2}\,dx) + U_L\,(T_i - T_a)\,dx = S\,dx$$

where S is the solar energy absorbed per unit area, i.e.,

$$S = H_T\,\tau_g\,\alpha_p$$

and T is the temperature of the fin.

After simplification the equation becomes,

$$\frac{\partial T_i}{\partial x^2} - \frac{U_L}{K\delta}\,(T_i - T_a - S/UL) = 0$$

However the given problem consists of three regions that can be treated as fins as shown in Figure 22. In order to have one governing differential equation for all these three regions, and also to prescribe simple and homogeneous boundary conditions, the following normalized parameters are defined:

$$\psi_i = \frac{(T_i - T_a - S/U_L)}{(T_{bi} - T_a - S/U_L)}$$

and

$$\xi_i = \frac{X - [(i - 1)\,W + (W + D)/2]}{(W - D)}$$

The substitution of these two variables in the above equation will result:

$$\frac{\partial^2 \psi_i}{\partial \xi_i^2} - n^2 \psi i = 0 \quad (i = 0, 1, 2) \tag{4}$$

where

$$n^2 = U_L (w - D)^2 / K\delta$$

The above notation and part of the solution to the equation (4) is taken from Khalik's work reference [21]. The term n^2 is a nondimensional fin parameter. The boundary conditions to the equation (4) can be written as follows:

Physical	Similar
For region i = 0	
@ $x = 0$, $\frac{\partial T_i}{\partial x} = 0$	@ $\xi_i = \frac{1}{2}$; $\frac{d\psi_i}{d\xi_i} = 0$
@ $x = \frac{W-D}{2}$, $T_i = T_{b_1}$	@ $\xi_i = 1$; $\psi_1 = \frac{\Theta_i + 1}{\Theta_i}$
For region i = 1	
@ $x = \frac{W + D}{2}$; $T_i = T_{b_1}$	@ $\xi_i = 0$; $\psi_i = 1$
@ $x = \frac{3w - D}{2}$; $T_i = T_{b_2}$	@ $\xi_i = 1$; $\psi_i = \frac{\Theta_i + 1}{\Theta_i}$
For region i = 2	
@ $x = \frac{3W + D}{2}$; $T_i = T_{b_2}$	@ $\xi_i = 1$; $\psi_i = 1$
@ $x = 2W$, $\frac{\partial T_i}{\partial x} = 0$	@ $\xi_i = \frac{1}{2}$; $\frac{d\psi_i}{d\xi_i} = 0$

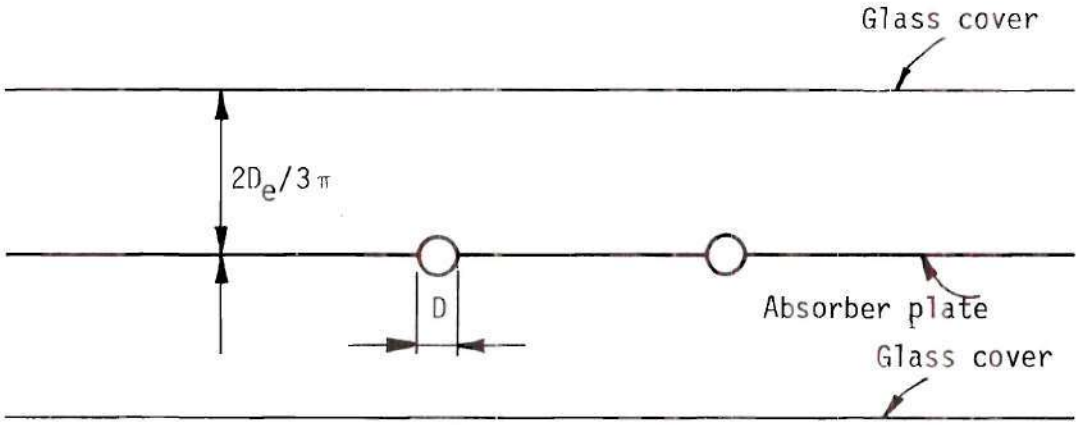

Figure 21. Receiver Tube in Flat Plate Form.

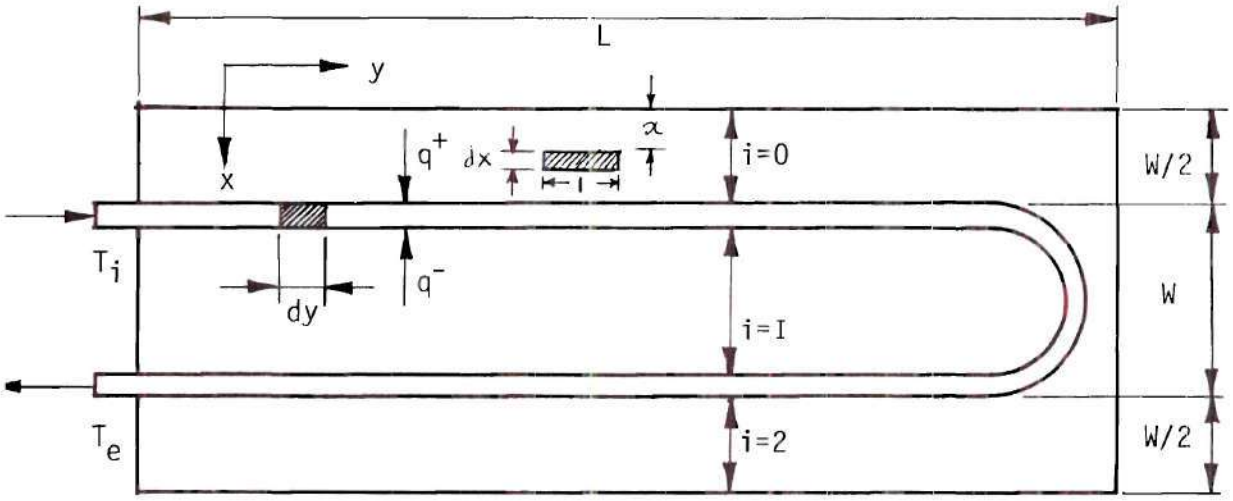

Figure 22. Thermal Analysis of Absorber Plate.

It is to be noted that the variable $\S_i$ as defined above, make equation 4 to be valid for all the three regions.

Temperature Distribution of Fluid

The heat gained by the differential fluid element is equal to the product of the mass flow rate, specific heat and the rise in temperature of differential fluid element

$$\frac{d\phi i}{d\eta} + (-1)^i \, L \, \frac{q_{ui}}{mCp} = 0$$

where $\phi_i = \dfrac{\Theta_{fi}}{\Theta_{fi}\big|_{n=0}}$; $\Theta_{fi} = T_{fi} - T_a - (S/U_L)$ (8)

$\eta = y/L$

Applying the balance of energy on a differential fluid element as shown in Figure 22

$$q_{ui} - q_i - D \, U_i \, \Theta_i \tag{9}$$

$$q_i = q_i^{+} + q_i^{-} \tag{10}$$

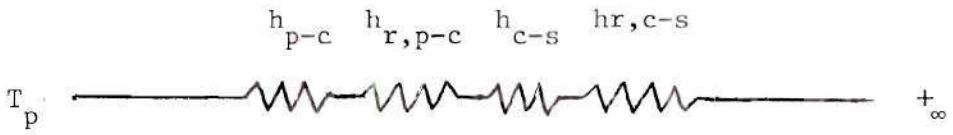

Figure 23. Thermal Analysis Circuit for Evaluation of U_L.

The above thermal circuit is for one side of the absorber plate, thus for two sides the heat loss co-efficient is given by

$$U_L = \frac{2}{(h_{p-c} + h_{r,p-c})^{-1} + (h_{c-s} + h_{r,c-s})^{-1}} \tag{11}$$

where the convective heat transfer coefficient between absorber plate and the glass cover in evacuated place is given by

$$h_{p-c} = K_a \frac{(1-C_2)}{t} \text{ from ref. [32]} \tag{12}$$

$$C_2 = \frac{2C_1}{1 + 2C_1} \tag{13}$$

$$C_1 = \frac{2-\alpha}{\alpha} \frac{2\gamma}{\gamma+1} \frac{\lambda}{Pr_a} \frac{1}{t} \tag{14}$$

$$\lambda = 8.46 \times 10^{-7} \frac{(T_p + T_g)}{2P} \tag{15}$$

The radiative heat transfer coefficient between the absorber plate and glass cover is given by:

$$h_{r,p-c} = \sigma \frac{(T_p^{\sim} + T_g^{\sim})(T_p + T_g)}{\left(\frac{1}{\varepsilon_p} + \frac{1}{\varepsilon_g} - 1\right)} \tag{16}$$

The radiative and convective coefficient between the glass envelope and outdoor environment are given by: Ref. [29]

$$h_{r,c-s} = \sigma \varepsilon_g (T_g^{\sim} + T_s^{\sim})(T_g + T_s) \tag{17}$$

$$h_{c-s} = \frac{K_a \; C \; N_{Rea}^{M}}{D_e} \qquad \text{Ref [29]} \tag{18}$$

where M and C are constants that depend upon the Reynold's number of air. The overall heat transfer coefficient between the plate and the surrounding is given by:

$$U_t = \frac{1}{(h_{p-c} + h_{r,p-c})^{-1} + (h_{c-s} + h_{r,c-s})^{-1}} \tag{19}$$

The equilibrium glass temperature

$$T_g = T_p - U_t \; (T_p - T_a) \; / \; (h_{p-c} + h_{r,p-c}) \tag{20}$$

If the flow of fluid is laminar and fully developed Ref [33]

$$N_{Nu} = 4.36 \quad (N_{Nu} < 2300) \tag{21}$$

and for turbulent flow: Ref. [33]

$$N_{Nu} = 0.023 \; (N_{Re})^{0.8} \; (N_{Pr})^{1/3} \quad (N_{Re} > 2300) \tag{22}$$

Similarly the Darcy friction factor for laminar flow is Ref [34]

$$f = \frac{64}{N_{Re}} \qquad (N_{Re} < 2100) \tag{23}$$

and for turbulent flow is:

$$f = \frac{0.316}{(N_{Re})^{0.25}} \quad (N_{Re} > 2100) \tag{24}$$

Here the Daney-Weisback friction factor is defined by the equation:

$$\frac{\Delta P}{\rho} = f \frac{L}{D} \frac{U_m^2}{2 g_c} \tag{25}$$

The exit temperature of the fluid is given by:

$$T_e = T_\infty + (S/U_L) + (T_i - T_\infty - S/U_L)\ \phi_2 \Big|_{n=o} \tag{26}$$

and frictional power loss = ΔP Vo (27)

The solution to the above system of equations is iterative. Initially approximate values are chosen for the mean temperature of the plate and that for the glass in order to compute the value of U_L. With this value of U_L and the given operational parameter like T_i, H_T and T_a the mean temperature of the plate is computed. The above computation is repeated until the values of U_L, T_g and T_p of the entire receiver tube converge. A simple relaxation technique is employed for the convergence. The output variables, thermal efficiency of solar receiver and the exit fluid temperatures serve as input variables to the Rankine cycle. A computer program has been written to compute the optimum mean temperature of the collector fluid that produces maximum shaft power for a given solar insolation and ambient conditions for a system with no storage tank. The complete solution to the governing equations are presented in appendix B and C. Flow chart and the computer program for the thermal analysis of receivers are enclosed in appendix C and D.

The following parameters have been fixed for this study of optimization:

Emissimity of absorber plate	ε_p = 0.1
Absorptivity of absorber plate	α_p = 0.9
Linear aperture lengths of concentrator	= 6' 7"
Length of the heat exchanger tube	L = 7' 0"
Diameter of glass envelope	= 4"
Diameter of copper tubes	= 5/16"
Width of copper plate	= 3.45"
Transmittance of glass envelope	= 0.92
Concentrator slat width	= 2.90"
Concentrator included angle	= 105°
Effectiveness of the heat exchanger	= 0.85
The pressure inside the receiver tube	= 0.0021168 psf
Heat Transfer Fluid:	Therminol '66

Therminol 66 fluid is selected for this analysis since it has a high boiling point = 660°F at atmospheric pressure, whereas the water at the same temperature will have about 3200 psi. Such high pressures require thick walled tubes that increases the overall weight of the receiver. Selection of Therminol 66 is thus justified.

Section B: Sample Calculations - Receiver Efficiency

Writing eqn (1) Chapter VI for the declination

$$\delta = 23.45 \text{ Sin } [360 \ (\frac{284 + n}{365})] \tag{1}$$

and

$$\begin{aligned} \text{Cos } \Theta = {} & \text{Sin } \delta \text{ Sin } \phi \text{ Cos S} - \text{Sin } \delta \text{ Cos } \phi \text{ Sin s Cos } \gamma \\ & + \text{Cos } \delta \text{ Cos } \phi \text{ Cos s Cos } \omega \\ & + \text{Cos } \delta \text{ Sin } \phi \text{ Sin s Cos } \gamma \text{ Cos } \omega \\ & + \text{Cos } \delta \text{ Sin s Sin } \gamma \text{ Sin } \omega \end{aligned} \tag{2}$$

$$q = q_{in} A_c \rho_c \text{ Cos } \Theta \ (K_e)/ A_r \tag{3}$$

The above three equations are from Chapter VI.

The equation (3) can be re-written as

$$q = q_{in} KA_c/A_r$$

where $$K = \rho_c \text{ Cos } \Theta \ (K_e)/A_r$$

Θ = angle of incident ray with the normal to the concentrator aperture (found from eqn 1 & 2)

K_e = Edge loss found from figure 14

ρ_c = Concentrator reflectance (0.76)

In this particular sample calculation the following data is assumed. These values are realistic and assumed to represent actual data during a year. Computer calculations are done using these data.

q_{in} = The heat flux as recorded by Pyroheliometer = 300

K = 0.6 for Jan 15 or July 15 at one hour from solar noon.

Inlet temperature of fluid T_i = 300° F., 760° R

Flow rate = 0.5 gpm

Ambient Temperature = 70° F.

Heat Transfer co-efficient to surrounding h_{c-s} = 1.5

Pressure inside the envelope P = 0.002168 psf

Initial guess of plate temperature = 800° R.

Substituting these data into equations (4) through (25), the following results are obtained:

Actual mean temperature of plate (through the solution of equation 4) = 842.9° R.

Glass temperature of envelope T_e = 558.1° R.

Reynolds No. = 3839

Prandtle No. = 20.56

Nusselt No. = 56.19 (from eqn 22)

Heat transfer co-efficient between fluid and the tube wall

h_f = 143.0 B/hr fl^2 F°

Exit Temp. of fluid (obtained from equation 26)

T_e = 809.8° R.

The co-efficient of Heat loss from plate (obtained from equation (11)) U_L = 0.4411 B/hr ft^2 F°

The heat gained by the working fluid is obtained from

$$Q_u = \int_{T_i}^{T_f} V \rho (T) C_p(T) dT$$

where V = volume flow rate

Q_u = 5448.9 B/hr for 7' 0" length of receiver.

The Receiver efficiency is found from

$$\eta_r = \frac{Qu}{q A_r}$$

The receiver efficiency for this sample calculation is found to be

$$\eta_r = 65.24\%$$

This value checks with Figure 27. Thus, the receiver efficiency η_r, and the exit fluid temperature T_e are found from this analysis. In the analysis similar computation is repeated for different values of q_{in}, T_i, h_c, T_w, and in the flow rate. In all these computations the same equations from (4) to (27) were used. The flow chart and the computer program enclosed in Appendix should illustrate the computational procedure in more details.

A Few Brief Comments On Graphical Results Of Analysis

The graphical results are obtained through the solution of equation (4) and (8) i.e., from equation (26). The efficiency of the receiver is found from:

$$\eta_r = \int_{T_i}^{T_f} m(T)\ Cp(T)\ dT/qA_r \qquad (28)$$

The efficiency of the receiver is computed for various operating conditions. The range of the various parameters that affect the value of efficiency are as follows:

Heat Flux:	60 - 180 BTU/hr ft^2	(at the concentrator aperture)
Flow rate:	0.2 - 5 gpm	
Inlet Fluid Temperature:	100° F - 600° F	
Ambient Temperature:	0° F - 100° F	
Wind speed:	0 - 15 mph	
Diameter of tube:	3/16" - 8/16"	

The values of the overall heat transfer co-efficient U_L ranged from 0.21 to 0.81 at plate temperatures from 200° F to 650° F respectively.

Effect of Heat Flux: Figure 24 indicates that at higher heat fluxes for a given flow rate, the efficiency is high due to better heat extraction. The efficiency is found to be constant at flow rates higher than about 0.5 gpm. This is due to the fact that the temperature rise of the fluid is small which causes plate temperature to be uniform.

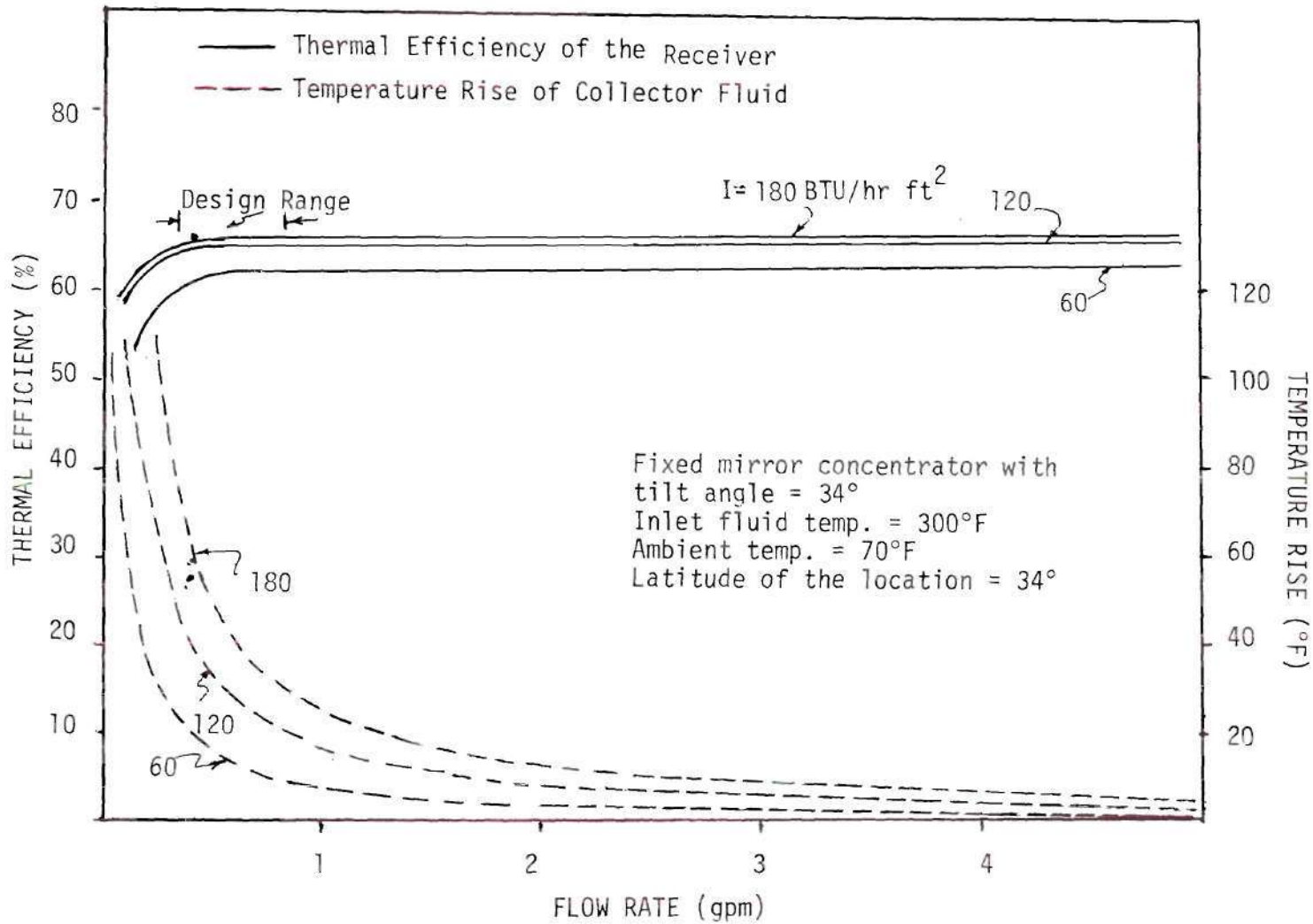

Figure 24. Variation of Receiver Efficiency With Flow Rate and Solar Flux.

Apparently, the optimum flow rate is about 0.5 gpm where the temperature rise of the fluid is reasonably high and this value is maximum for the given arymptotic efficiency values.

Effect of Inlet Fluid Temperature: Figure 25 shows the variation of the receiver efficiency with inlet fluid temperature. Initially the efficiency decreases with the increase of T_i. This is expected due to higher thermal losses from a higher mean plate temperature. However, from T_i = 200° F the efficiency increases due to increase in T_i. This is due to turbulent conditions that exist at this temperature. The viscosity of the Therminol fluid decreases drastically at higher temperature thus making it a turbulent flow at a higher temperature from a laminar flow at lower temperature for a given mass flow rate. Naturally heat extraction is better in turbulent flow and this accounts for the increase in efficiency for inlet fluid temperature range of 200° - 200° F. This decrease in efficiency is due to the higher plate temperature.

Effect of Working Fluid: As indicated in Figure 26, the air appears to be a poor choice, due to large pumping power requirements. However, the receiver efficiency are almost same for all the fluids at higher flow rates. At lower flow rates the efficiency of water exceeds that of Therminol 66 or air and it is due to its higher thermal conductivity value.

Effect of Wind Speed and Ambient Temperature: Figure 28 shows that efficiency of receiver is insensitive to the variation of wind speed or ambient temperature. It is because the resistance offered by surroundings is negligible to that of vacuum conditions inside the

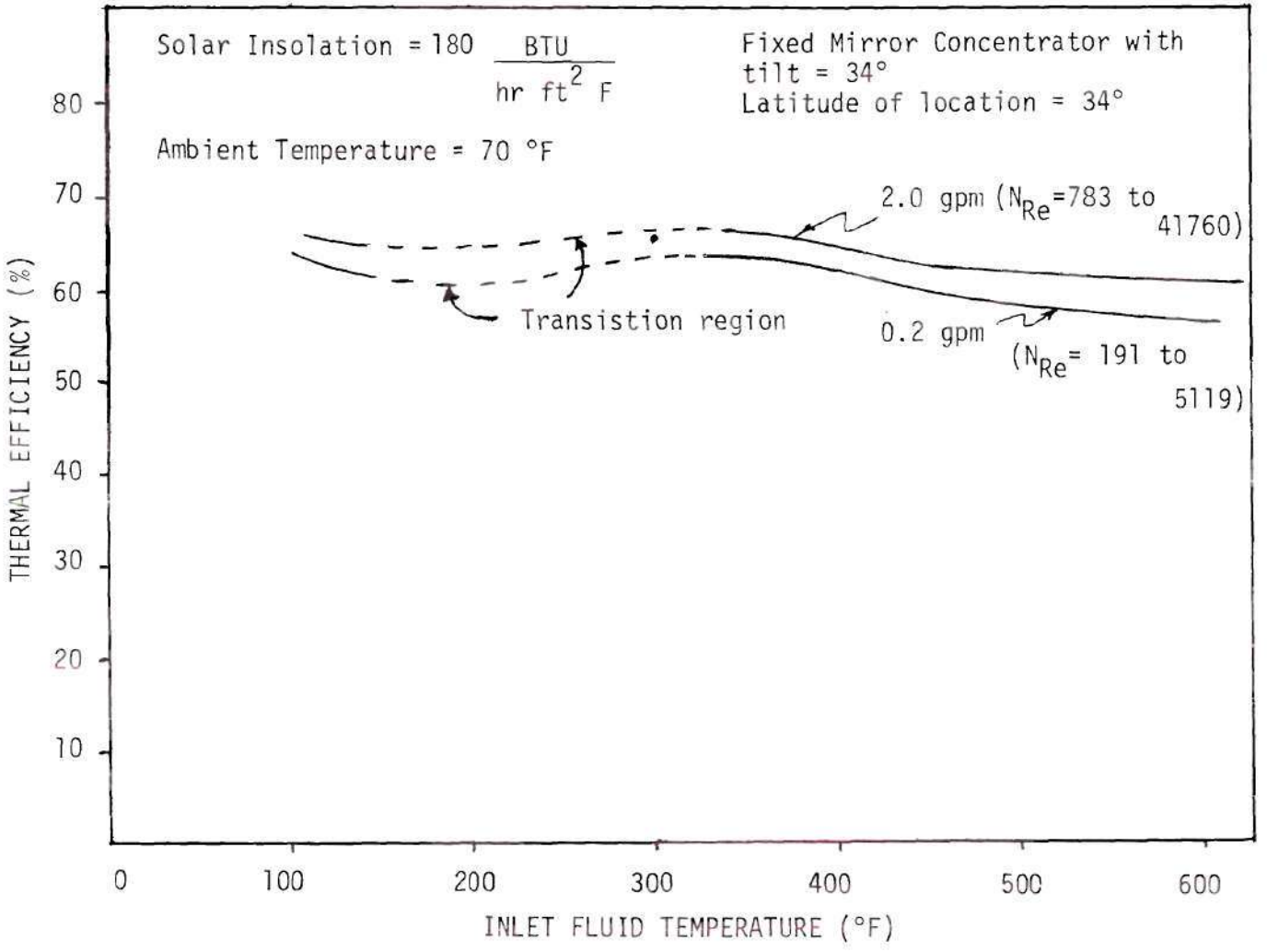

Figure 25. Variation of Receiver Efficiency With Flow Rate and Inlet Fluid Temp.

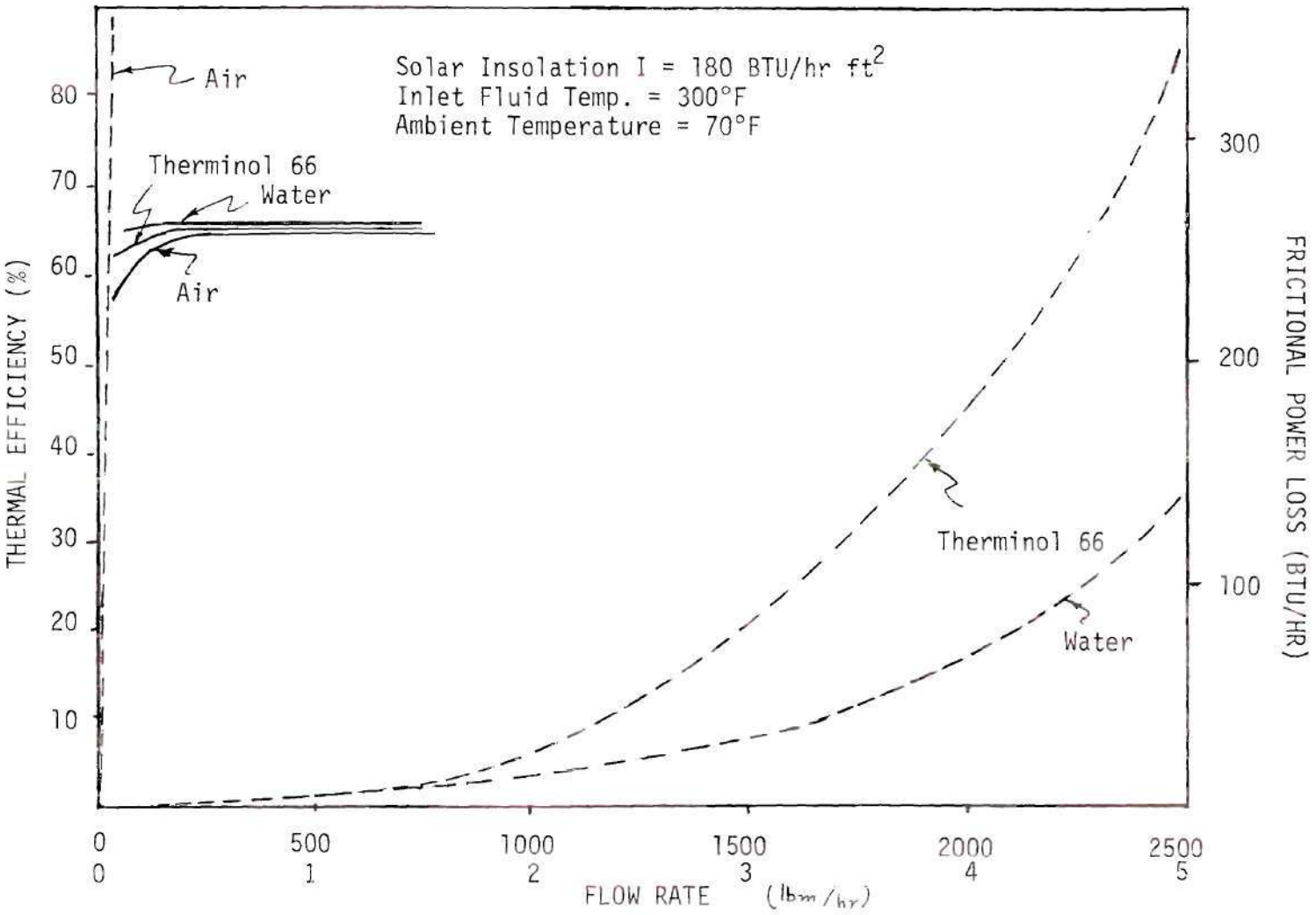

Figure 26. Effect of Collecter Fluid on Receiver Efficiency.

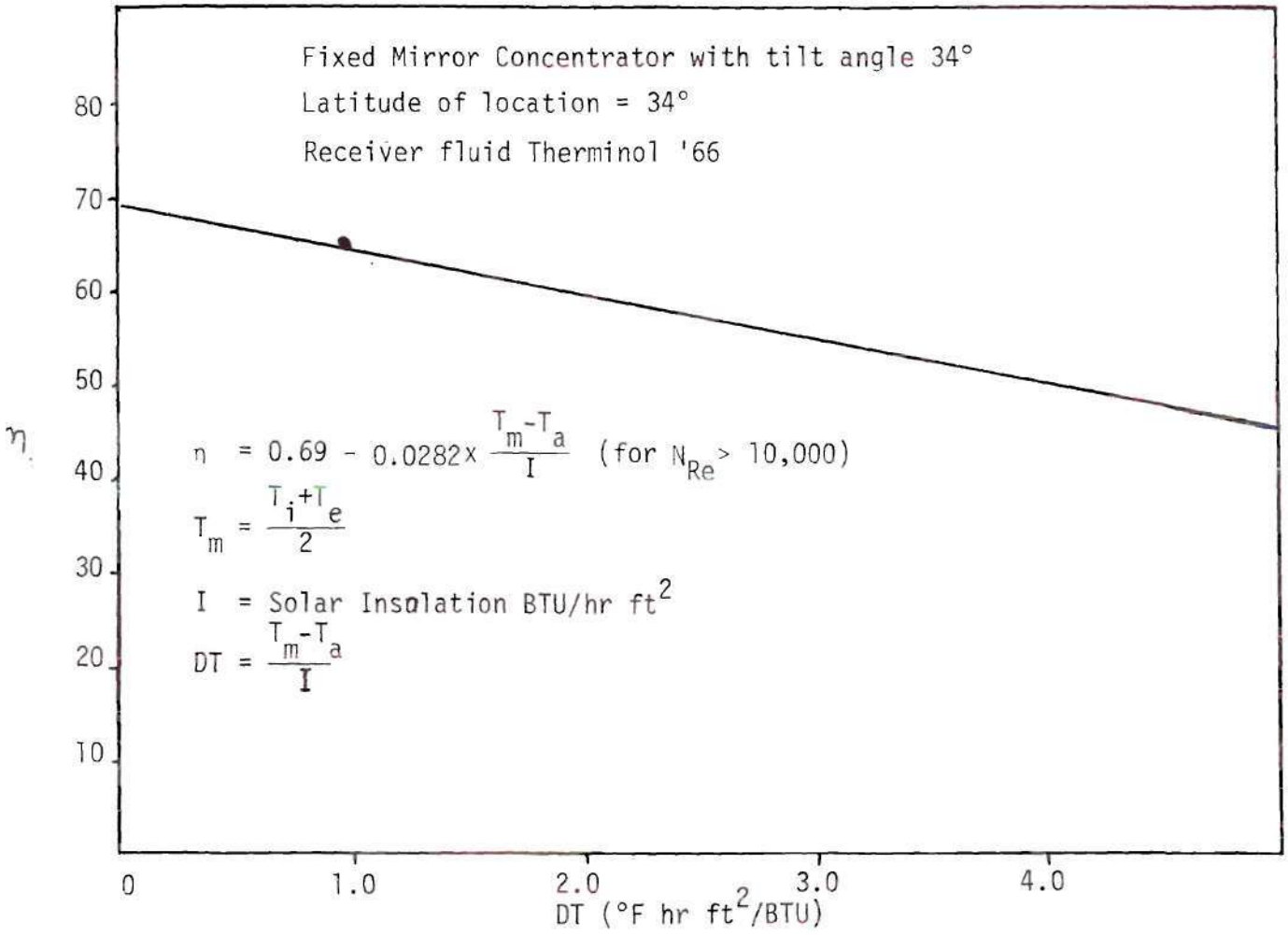

Figure 27. Receiver Component Model Equation.

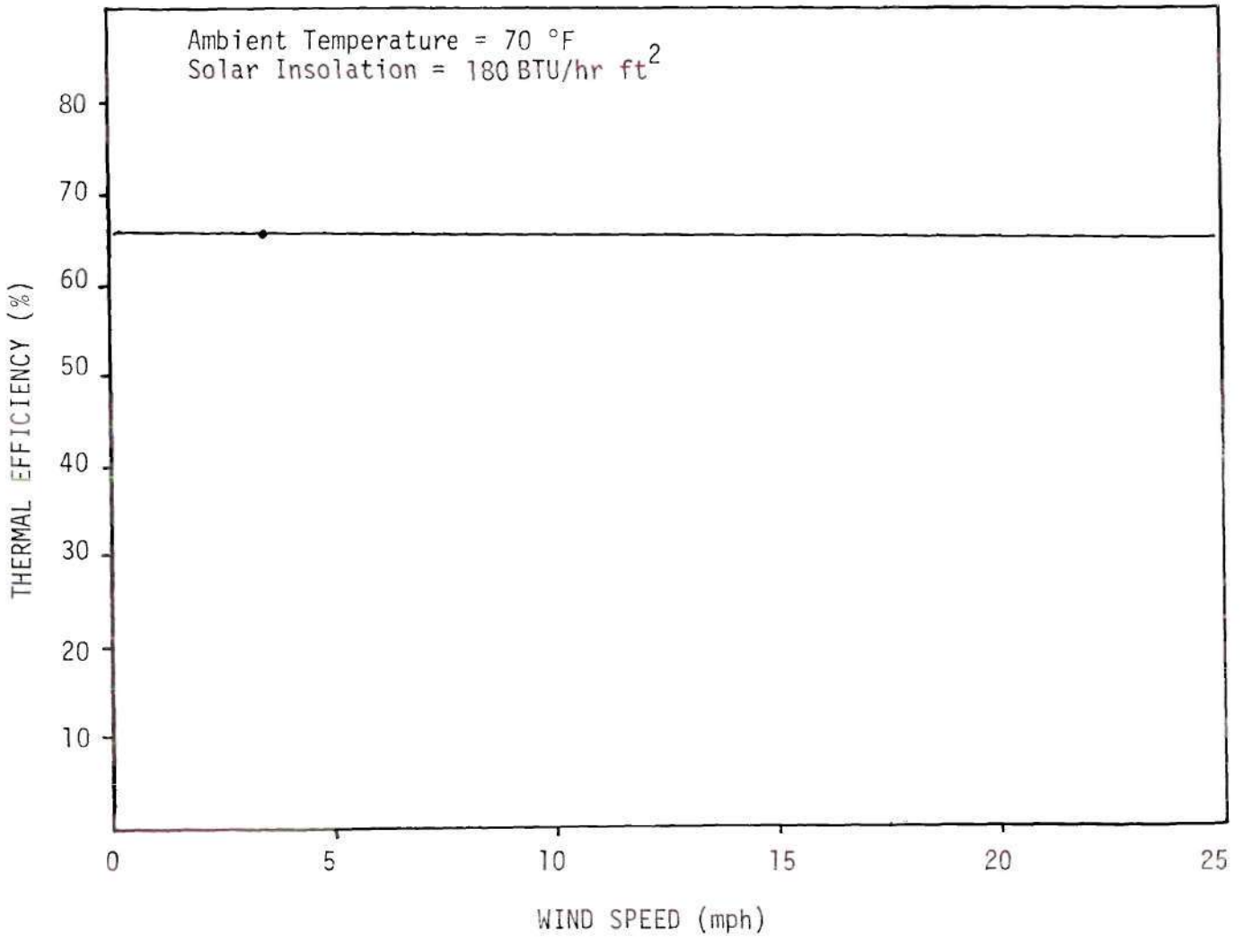

Figure 28. Effect of Wind Speed on Receiver Efficiency.

receiver tube. Only radiational losses are dominant in the receiver tube.

Enviromental Conditions	Absorber Plate Temperature	Glass Temperature
Wind speed zero mph	843° R	592° R
Wind speed 15 mph	842° R	535° R
Ambient Temperature 0° F	843° R	495° R
Ambient Temperature 100° F	843° R	585° F

Effect of Mean Fluid Temperature per Unit Flux: Figure 27 indicates the receiver efficiency variation with excess of mean fluid temperature over ambient temperature per unit-flux. This is a very important result of the analysis as it represents the summary of the entire analysis on a single line except the pumping power requirements on the effect of working fluid. The variation of the three variables namely, the flow rate, the inlet fluid temperature (both are accounted in T_m) and the solar flux I, and their effect on η_r is represented on a single line. Essentially the plate temperature of the receiver determines the thermal losses and therefore, the efficiency of the receiver, However, the plate temperature depends upon three variables, the solar flux, flow rate and the inlet fluid temperature

$$\eta = 0.69 - 0.0282 \frac{T_m - T_a}{I} \qquad (29)$$

This equation is represented on Figure 27 is developed from Figure 27 and is specially suitable for system simulation analysis of the concentrator system. Since the thermal losses from the receiver absorber

plate depends on fourth power of plate temperature. The computer results of Appendix F indicate that the curve in Figure 27 has a slight downward curvature at higher values of DT; however, the values of DT higher than 5 are out of practical design range and only the linear portion of this curve is significant within the scope of this thesis.

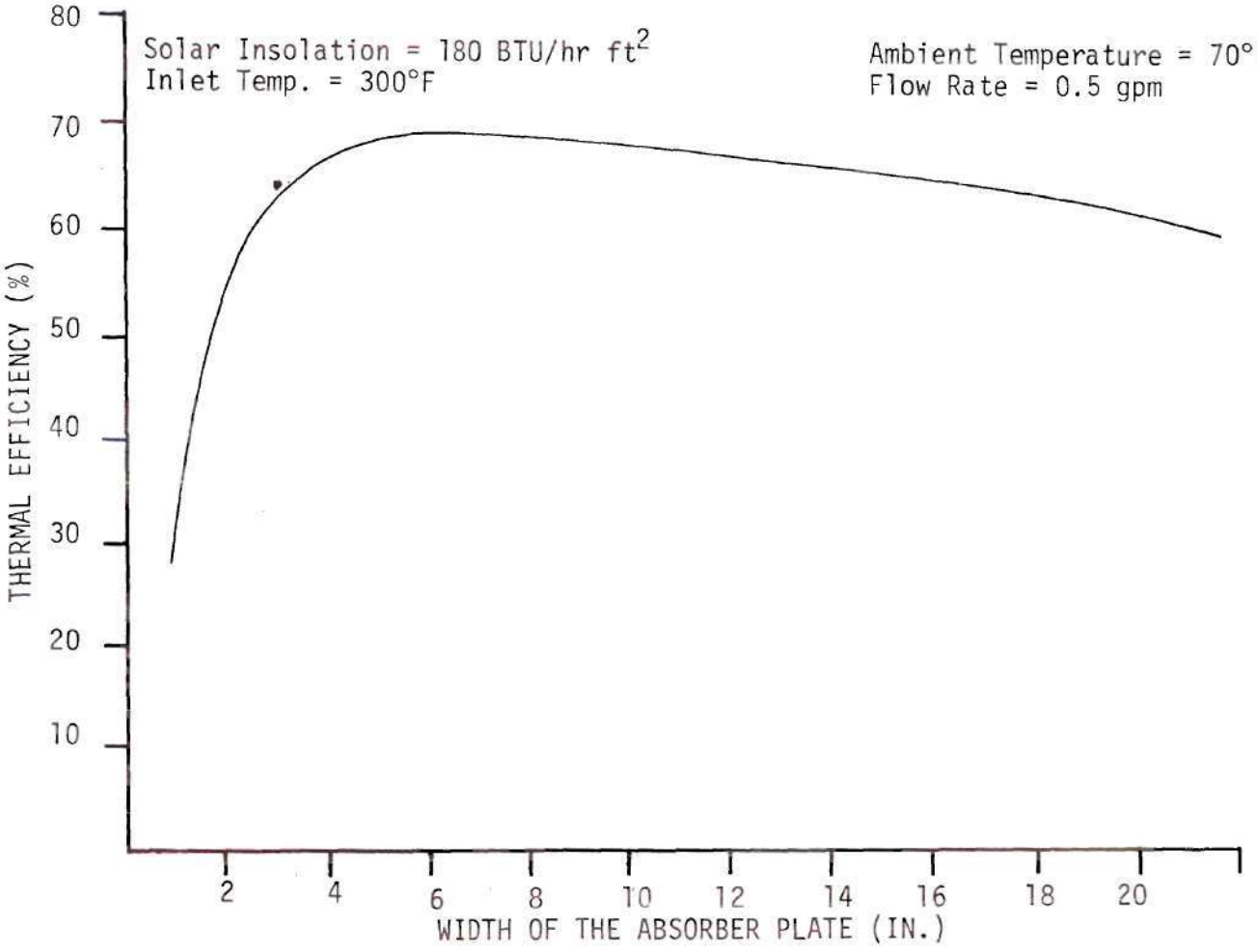

Figure 29. Effect of Absorber Plate Width on Receiver Efficiency

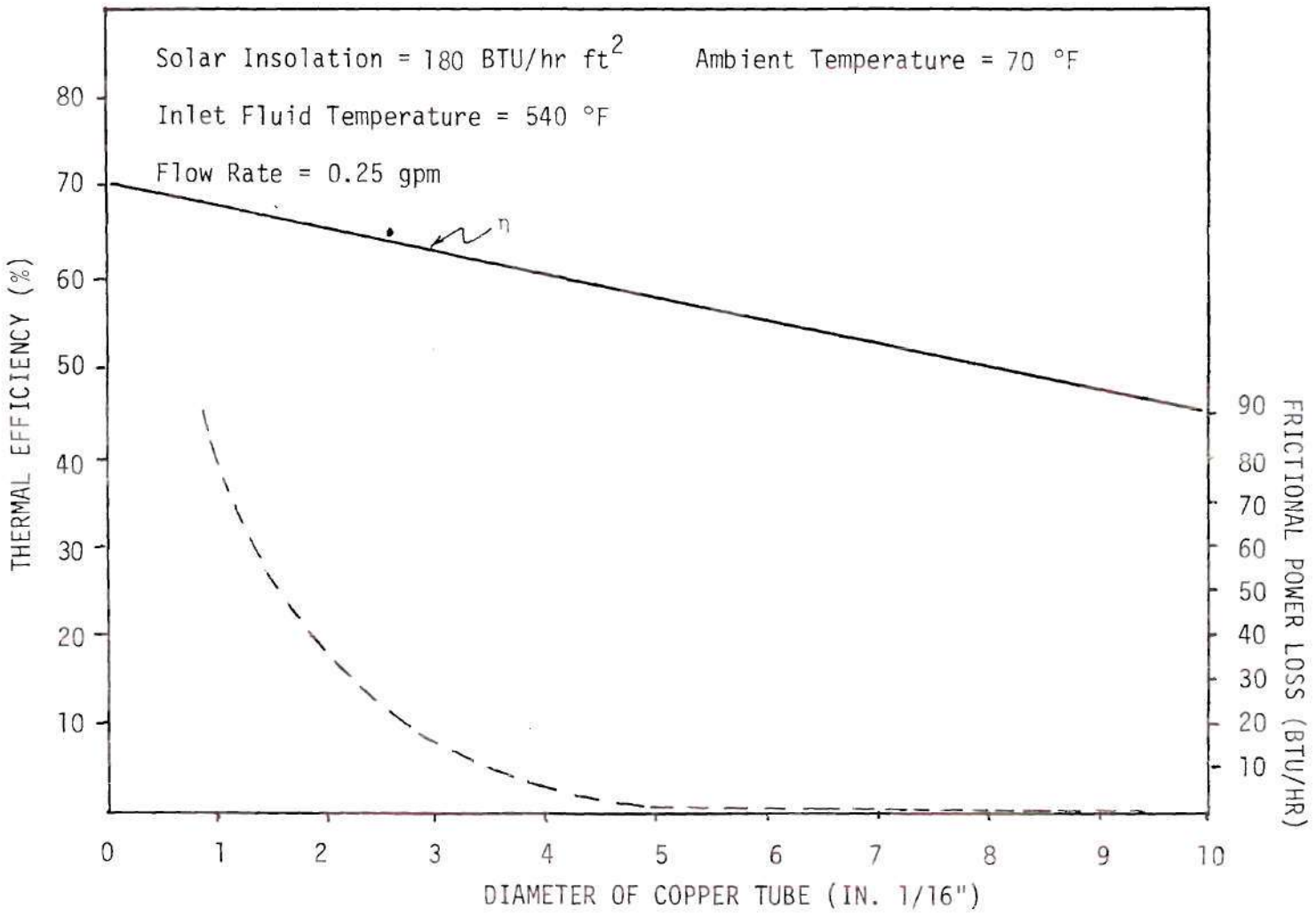

Figure 30. Variation of Receiver Efficiency with Diameter of Copper Tube.

Section C: Optimization of a Simple Space Power Plant without Storage

A power plant without storage on the ground cannot produce power continuously and even during daytime when sunshine is available it will not produce constant power for a given concentrator area. The simple power plant shown in Figure 31 can provide a constant power only under a constant solar intensity at the focal plane of the receiver. This requires that the concentrator is at a fixed orientation with sun. These arrangements are suitable for space power plants where the solar flux is available for the entire 24 hours a day. Even in normal solar power plants with storage facilities, the plant may work in this mode (as shown in Figure 31) for a period of time when the storage tanks are full at the maximum temperatures and the solar flux is constant at the focal plane during that period.

The purpose of this optimization analysis is to determine the optimum mean temperature of the collector fluid that produces maximum shaft power by the turbine. A high collector fluid temperature is not permissible at low solar fluxes in order to have positive collection efficiencies. But the turbine efficiency is directly proportional to the inlet temperature of the rankine fluid. Thus the mean temperature of the collector fluid becomes critical at low solar fluxes and this mean temperature can be controlled by the mass flow rate of the rankine fluid. In this section of the analysis, an expression is derived for the mass flow rate of the rankine fluid in terms of solar flux, the maximum allowable rankine fluid temperature and the mass flow rate of collector fluid.

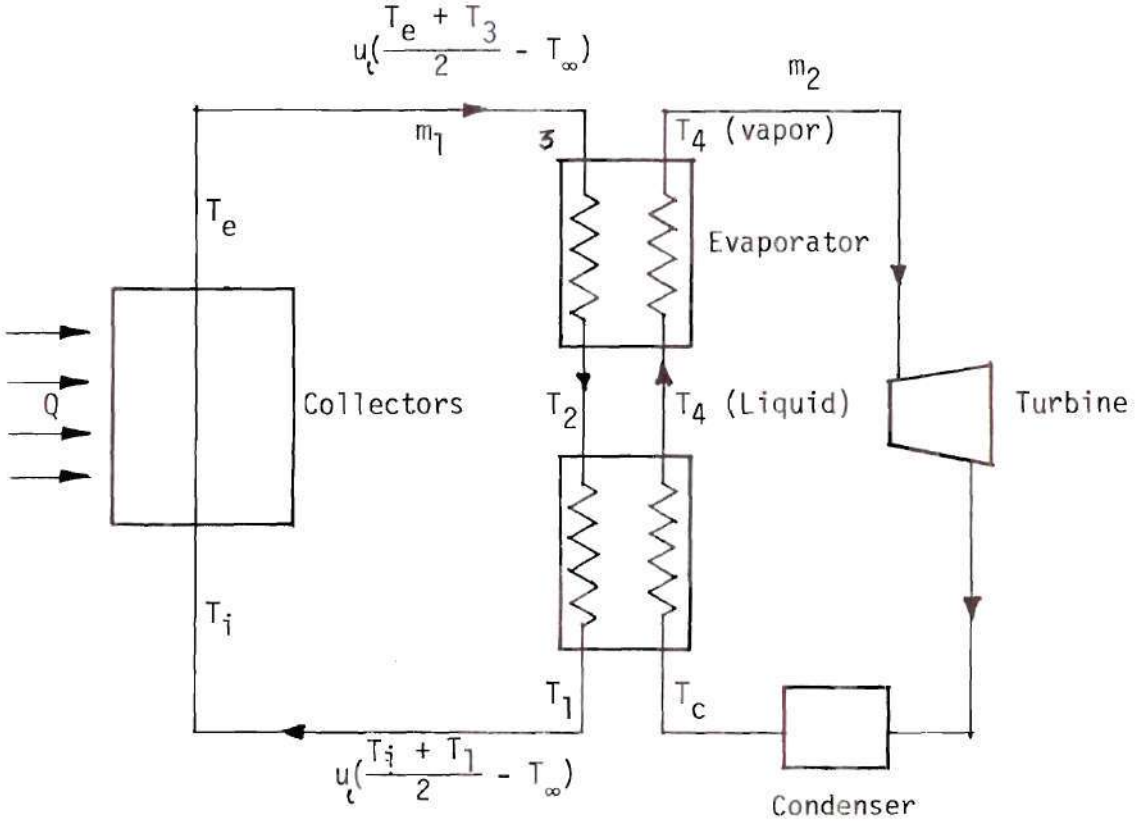

Figure 31. Thermal Network of Solar Power System

The following assumptions are made in this analysis.

1. The heat capacitance effects of all the devices are neglected. Steady state conditions exist all the time. This condition does not apply to the stoichastic variation of ground solar intensity,
2. The evaporator is of counterflow type having an effectiveness of unity for the special case discussed in this analysis. This assumption is justified only at high value of number of transfer units, ref [7] which is ideal but not too unrealistic,
3. The rankine fluid is Benzene and the turbine characteristics are such that it's efficiency depends strongly on the inlet fluid temperature. The relationship between the thermal efficiency of the rankine system and the inlet fluid temperature is taken from ref [20] (of R-114) in absence of the pertinent data for Benzene. This assumption is justified in obtaining approximate values.

Balance Equations for Optimization of a Systems Without Storage

For the Solar Collector:

$$\dot{m}_1 c_1 (T_e - T_i) = Q N_t \tag{30}$$

For the boiler section:

$$\dot{m}_1 c_1 (T_3 - T_2) = \dot{m}_2 (h_4 - h_4') = \varepsilon_2 \dot{m}_1 c_1 (T_3 - T_4) \tag{31}$$

Where c_1 and c_2 are specific heats of fluids for the preheater that brings the fluid up to saturation condition

$$\dot{m}_1 c_1 (T_2 - T_1) = \dot{m}_2 c_2 (T_4 - T_c) = \varepsilon_1 \dot{m}_2 c_2 (T_2 - T_c) \tag{32}$$

The piping losses between collector and the boiler is

$$\dot{m}_1 c_1 (T_1 - T_i) = U_\ell \left(\frac{T_i + T_1}{2} - T_\infty \right) \tag{33}$$

and for the return section to the collector

$$\dot{m}_1 c_1 (T_e - T_3) = U_\ell \left(\frac{T_e + T_3}{2} - T_\infty \right) \tag{34}$$

Let $\dot{m}_1 c_1 = x_1$ and $\dot{m}_2 c_2 = x_2$.

From the above four equations* the Rankine fluid flow rate m_2 is given by

$$\dot{m}_2 = \frac{-\beta \pm \sqrt{\beta^2 - 4 \alpha E}}{2E} \tag{35}$$

where

$$E = \{\varepsilon_1 c_2 (h_4 - h_c) (1 - \varepsilon_2)\} \tag{36}$$

$$\beta = [\{(h_4 - h_c) \{x_1 (a^{\sim} - 1) + x_1 \varepsilon_2\} - x_1 \varepsilon_1 c_2 B (1 - \varepsilon_2) + c_2 \varepsilon_1 \varepsilon_2 T_4 - x_1 (1 - a^{\sim}) \varepsilon_1 c_2 T_c] \tag{37}$$

*See Appendix C for the solution of this system of equations.

$$e = -(x_1 A + c) \tag{38}$$

where

$$A = (1 - a^{\sim}) \{a Q\eta i + abx_1 + bx_1 + \varepsilon_2 T_4 x_1\} \tag{39}$$

$$B = \frac{aQ\eta_1}{x_1} + ab + b \tag{40}$$

$$C = x_i \{x_1(a^{\sim} - 1) + x_1 \varepsilon_2\} B \tag{41}$$

$$a = \frac{\dot{m}_1 c_1 + \frac{U_\ell}{2}}{\dot{m}_1 c_1 - \frac{U_\ell}{2}} \tag{42}$$

$$b = U_\ell T_\infty / (\dot{m} c_1 - U_\ell / 2) \tag{43}$$

ε_1 is the effectiveness of heat exchangers

ε_2 is the effectiveness of evaporator

u_ℓ is the overall heat transfer coefficient of pipe insulating material and

ℓ is the length of each pipe header.

Special Case

If ε_2 = the effectiveness of the evaporator = 1.0 then the expression for $\dot{m}_2$ reduces to

$$\dot{m}_2 = \frac{x_1^{\sim}(1 - a^{\sim}) T_4 + (bx_1^{\sim} + ax_1 Q\eta_1 + ab)}{x_1 a^{\sim}(h_4 - h_c) - x_1(1 - a^{\sim}) \varepsilon_1 c_2 T_c + c_2 \varepsilon_1 T_4} \tag{44}$$

Rankine power output is given by (shaft power)

$$q_u = \eta_2 \dot{m}_2 (h_4 - h_c) \tag{45}$$

where η_2 = Rankine cycle efficiency

For Series Arrangement

$$\eta_2 = \frac{x_1^{\alpha'}(1 - a)T_4 + (bx_1^{\alpha'} + ax_1 Q\eta_1)}{x_1\, a(h_4 - h_c) + x_1(1 - a)\,\varepsilon_1 c_2 (T_4 - T_c)} \tag{47}$$

$$U_\ell = \frac{1}{2\pi r_3 h} + \frac{\ln (r_2/r_1)}{2\pi k_1} + \frac{\ln (r_3/r_2)}{2\pi k_2}$$

where k_1 and k_2 = thermal conductivity of insulating materials.

h = coefficient of heat transfer of the environment.

The overall efficiency vs. the mean fluid temperature curves shown in Figure 32 indicate that the receiver arrangement in series utilize higher temperatures more efficiently than the parallel flow arrangement. These curves indicate the optimum mean collector fluid temperatures for any given solar insolation to produce maximum power. In the optimization model a constant effectiveness value is assumed for the conventional heat exchanger, this assumption is reasonable for a counter flow heat exchanger over a certain range of operating temperatures, the inclusion of constant effectiveness model in the optimization model would reduce the analysis to much simpler form; however, this needs to be checked. In parallel flow arrangement the sudden drop of overall efficiency at higher mean temperatures is due to higher thermal losses originated due to the higher mean plate temperature. Whereas in series flow arrangement, for the most part of the receiver tube the fluid is at lower temperatures, thus making the mean plate temperature to be relatively at a lower temperature.

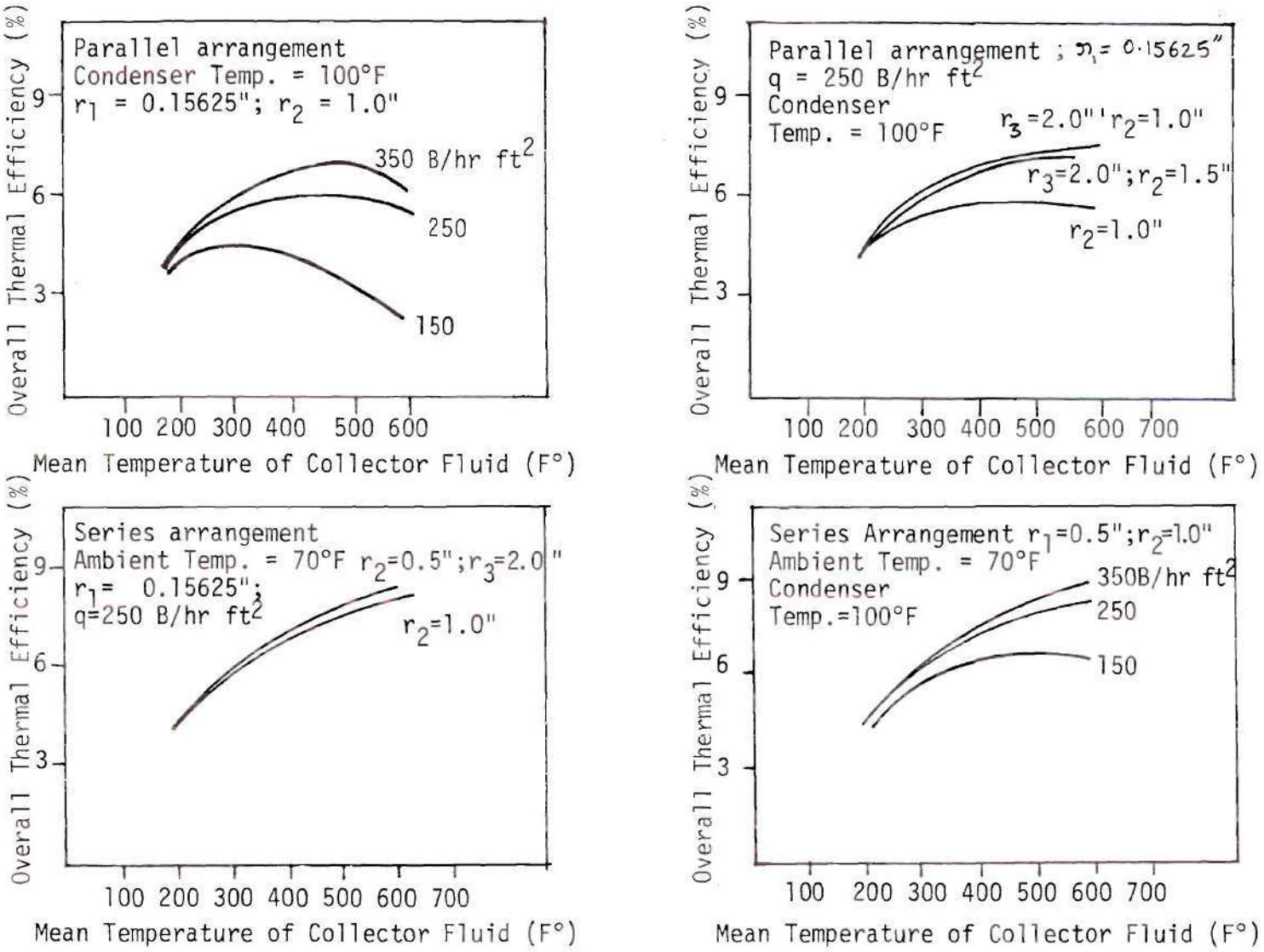

Figure 32. Effect of Variation of Receiver Efficiency with Fluid Flow Arrangement and Insulation Thickness

The flow rates in each receiver tube of series arrangement are higher than that in parallel arrangement, and this would increase the pumping power losses in series arrangement. Since the receiver fluid is liquid, this increase in pumping power losses is out-weighed by increase in the receiver efficiencies of the series arrangement. (Refer to Figures 26 and 32). The simple power plant without storage can also be used along with a multi-stage turbine to cope with variable solar intensity on the ground.

Section D. A Detailed System Optimization Procedure for Minimum Cost

The practical and realistic approach to analyze a solar system would be to evaluate the unit power cost. Evaluation of unit power cost demand the models of the components that constitute the system together with cost data of each component. The models of the concentrator and that of solar collector are already explained in the previous chapters. The models for the remaining components like storage tank and heat exchangers, etc., are already well established in solar energy literature. Since the fixed mirror concentrator is a relatively new concept, its cost has not been well established at the present time. Scientific-Atlanta, the company that designed and fabricated the present concentrator quoted an approximate cost of $15 per sq. ft. for a purchase order of 10,000 sq. ft. or greater collector area. The concentrator area also determines the size of the storage tank and consequently the amount of alternate fuel consumed to produce a given constant power. It is convenient, therefore, to express the cost of storage tank in terms of area of concentrator. Thus, finally the cost of unit power produced will depend basically on the concentrator area and the amount of auxiliary fuel consumed over a year.

In the present analysis, a solar/fossil power plant of 100 MW is considered and component equations are written and a procedure is outlined to optimize the solar concentrator system to produce a 100 MW power at the least cost. An extremely simple optimization analysis is carried out to determine the optimum concentrator area for the least cost per unit power produced. Figures 33, 34 and 35 schematically

represent the solar/Rankine power plant system and the corresponding T-S diagram. As complete properties of rankine fluid is not needed in this case unlike the previous optimization analysis in which Benzene is considered. Toluene (cp 25) is considered as a rankine fluid due to its favorable properties over Benzene as indicated in D. R. Miller's [31] report. Miller identified and thermodynamically characterized ten candidate fluids to be used in rankine cycle to convert a part of the solar energy into electrical power. He obtained rankine cycle efficiencies of each fluid for a given cyclic conditions. In his analysis Benzene produce slightly better rankine efficiency than Toluene, however considering the properties like, minimum flammability, toxicity and initial costs are concerned, he suggested Toluene to be the best candidate fluid. A further discussion on this subject is presented in chapter on recommendations. The following information is taken from reference [28].

"Toluene fluid expanding from 550°F to 296°F. (condensing at 150°F) with a flow rate of 3494 lbm/hr is capable of producing the electric power of 40 KW at an efficiency of 17.7 %." Based on this information, a flow rate of 8.752×10^6 lbm/hr of Rankine fluid is needed to produce 100 MW of electrical power. The temperature restrictions are as shown in Figure 35. The corresponding heat required from collector fluid is $Q_c = 1927.6826 \times 10^6$ BTU/hr. This requires a flow rate of collector fluid in the counterflow heat exchanger to be of the order of 13.89132×10^6 lbm/hr. The collector fluid enters the counter flow heat exchanger at 590°F and leaves at 340°F thus making the heat exchanger to be 85% effective.

The concentrator area and the size of storage tank and auxiliary heaters are so selected and arranged that a heat supply of Q_c = 1927.6826 x 10^6 BTU/hr is always maintained in the counterflow heat exchanger. Referring to Fig. 33, the temperatures T_4 and T_5 are always at 590°F and the value of T_2 depends upon available solar flux. T_2 can reach 590°F only at higher solar fluxes at a given flow rate. At lower flux levels T_2 can reach this temperature only when T_1 is close to 590°F for the same flow rate, this would mean higher mean temperature of collector fluid that makes receiver to have a negative thermal efficiency. Thus at a lower solar flux levels, the collector fluid at a flow rate of m_1 is directed to storage tank through the 3-way valve-2. Depending on the value of T_2, it may be possible for a part of m_1 to be mixed with m_2 to have the supply at point 5 at required conditions. That is only *a fraction of* m_1 *will* return to storage tank.

The variable speed pump controls the flow rate to maintain turbulent flow conditions which can be achieved with a flow rate of 0.5 gpm in each receiver tube. In case when this solar flux and the temperature T_1 are such that T_2 exceeds the maximum usable temperature of the collector fluid, then the variable speed pump would increase the flow rate to keep T_2 within the bonds.

Thus the collector system circuit may operate at different conditions (flow rate, solar flux) and modes depending on the solar flux and state of the system. The various possible modes are as shown in Appendix.

The component models of the system can be written as

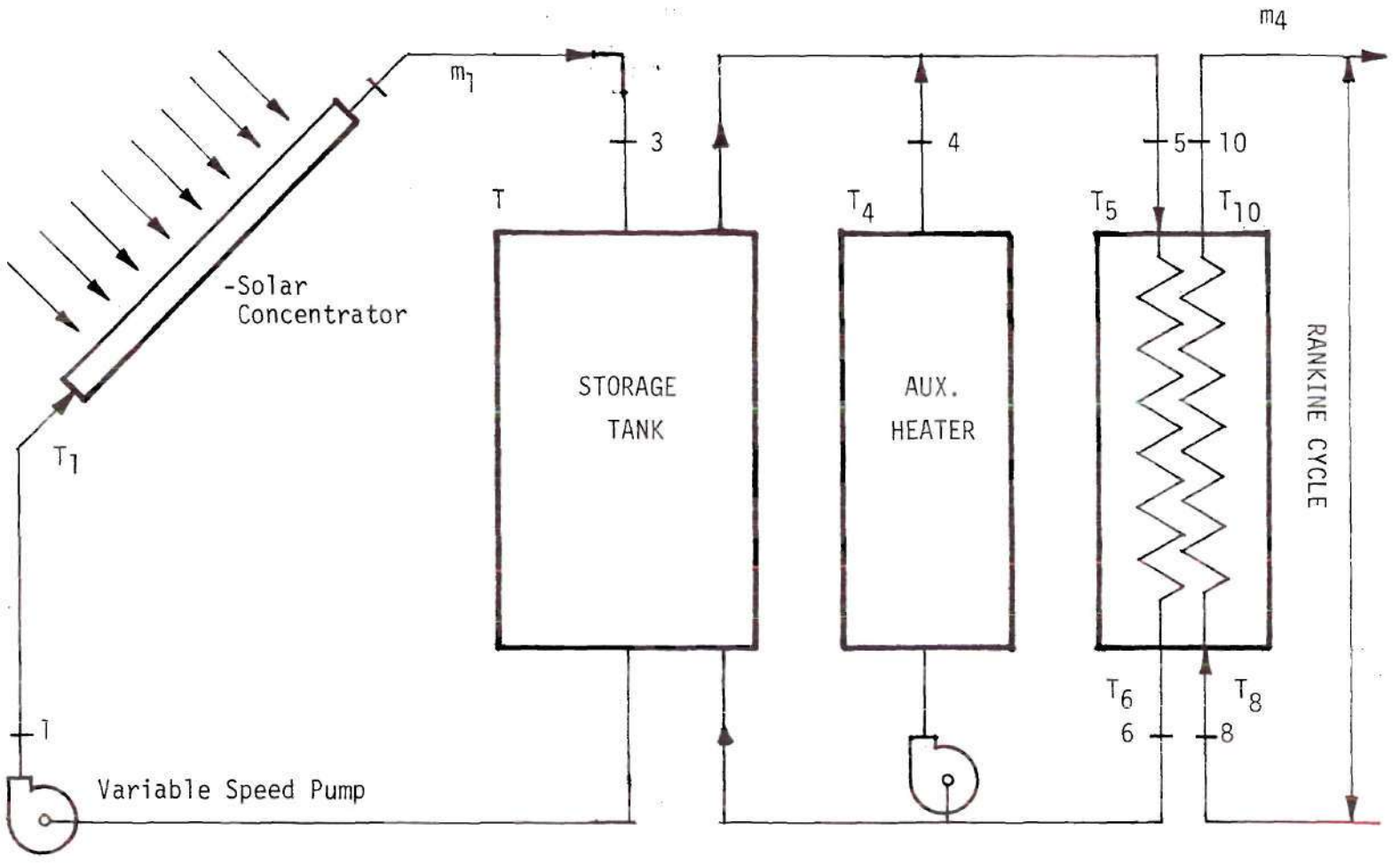

Figure 33. Solar Power Plant System

Established Design Conditions

Electrical Power output	100 MW
Rankine fluid: Toluene	
Rankine fluid flow rate	8.752×10^6 lbm/hr
Fluid Temperature entering turbine	550
Fluid temperature leaving turbine	375
Condenser temperature	$165^{\circ}F$
Heat required in preheater	1276.92×10^6 BTU/hr
Heat required in boiler	650.76×10^6 BTU/hr
Total heat required by rankine fluid	1927.68×10^6 BTU/hr
Regenerator efficiency	80%
Rankine Cycle efficiency	17.7%
Collector fluid: Therminol '66	
Collector fluid temperature entering heat exchanger	590
The collector fluid temperature leaving heat exchanger	340
Collector fluid flow rate	13.8913×10^6 lbm/hr

Refer Table 3 for: temperatures, pressures and entropy values at different state points of the rankine cycle.

Table 3. Properties of Rankine Fluid

State Point	Temperature F^o	Pressure Psia	Entropy BTU/16m-R^o
8	296	477	-0.255
9	550	465	-0.072
10	550	458	0.0229
11	375	3.73	0.047
12	211	3.617	-0.0352
13	165	3.33	-0.332
14	170	504	-0.329

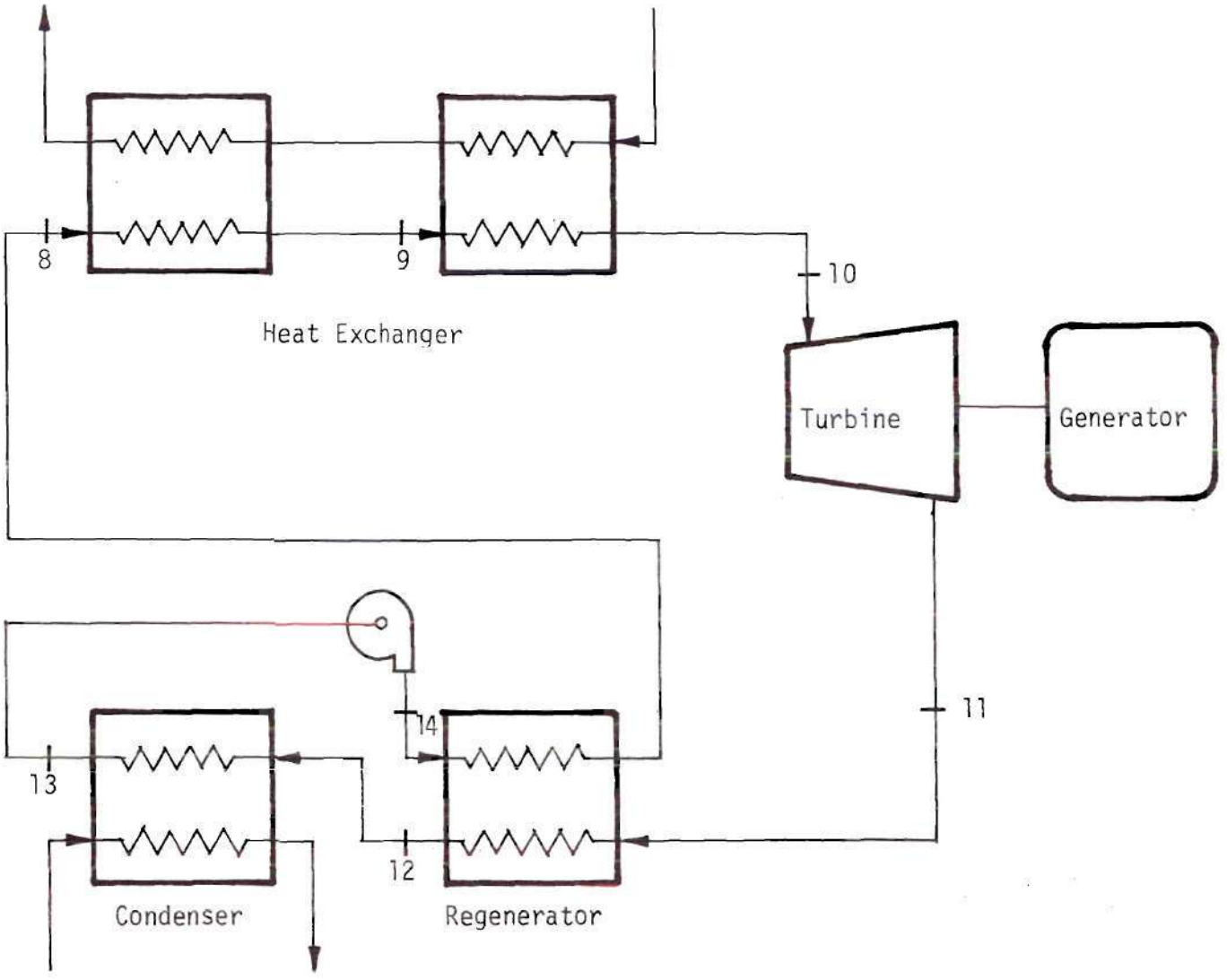

Figure 34. Rankine Cycle Power Plant

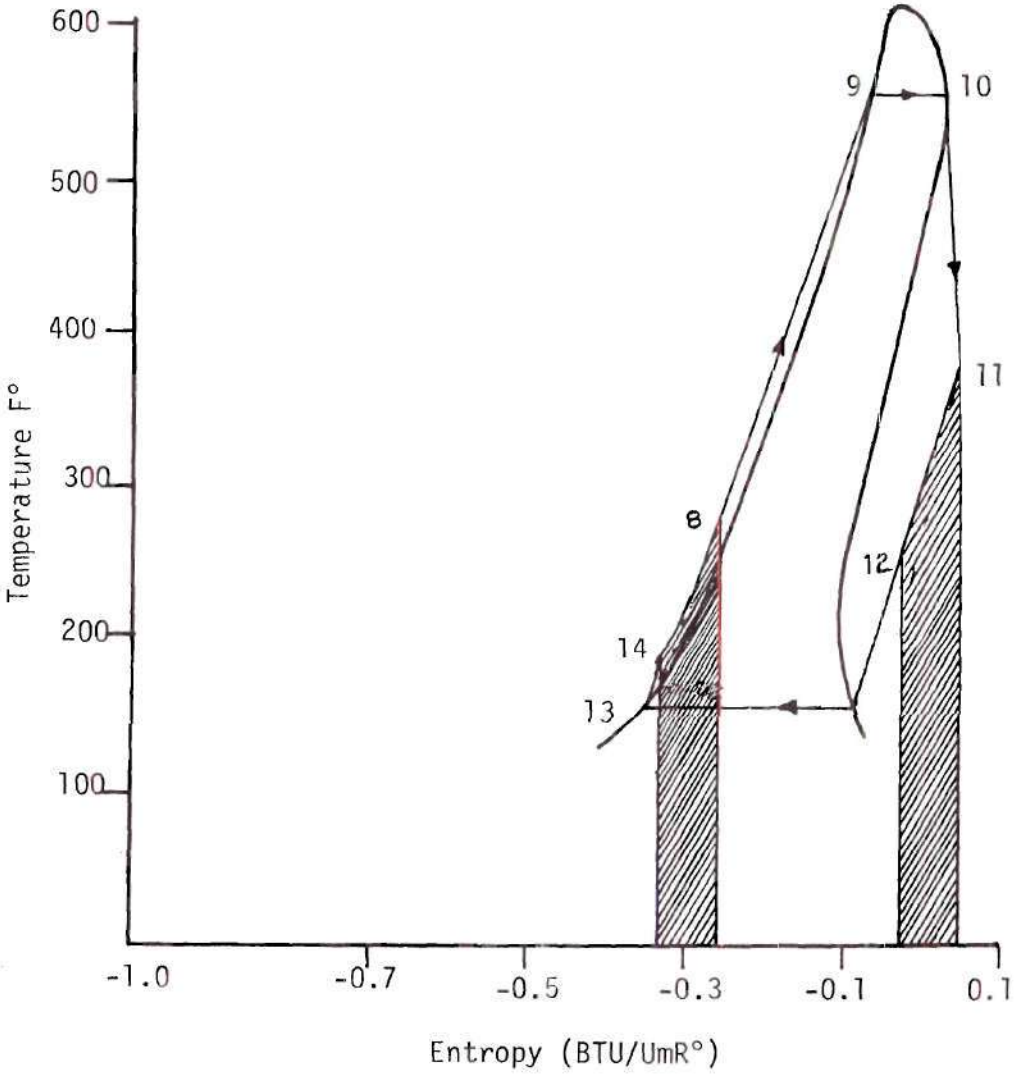

Figure 35. T-S Diagram of Rankine Cycle

$$Q_u = A_c \eta_c \eta_r q_{in} \cos \theta \eta_p \eta_L \quad (48)$$

η_c = concentrator efficiency, method of obtaining it at any hour is explained in previous chapters

η_L = factor that accounts for thermal losses from the piping and storage system

η_p = loss co-efficient due to the pipe fittings at the end of each receiver and it is found to be around = 0.94

q_{in} = normal solar insolation measured by pyroheliometer, usually the pyranometer data i.e., total solar flux data in a horizontal plane are available for a standard year

The approximate data for a beam component is obtained as follows:

$$I_{h,d} = 0.78 + 1.07 \alpha + 6.17 \text{ C C} \quad (49)$$

where $I_{h,d}$ diffuse component of solar radiation on horizontal plane.
The equivalent pyroheliometer reading would be

$$q = \frac{I_{h,d}}{\sin \alpha} = \frac{I_{hT} - I_{hd}}{\sin \alpha} \quad (50)$$

Thus beam component is determined in absence of pyroheliometer readings.

θ = is the solar incident angle, the method of computing it for any hour is outlined in previous chapters

A_c = concentrator aperture area, and

η_r = is the efficiency of the solar receiver.

$$\eta_r = a + b \{T_i + T_e)/2 - T_\infty\}/I$$

as outlined in Figure 28 where a and b are constants, T_i and T_e are entering and leaving temperatures of collector fluid.

$$Q_u = \dot{m} C_p (T_2 - T_1) \tag{51}$$

where m_i is the mass flow rate of collector fluid through solar receivers. In this system it is necessary to control the flow rate such that the temperature of the collector fluid leaving the receivers is equal to or less than the maximum useable temperature of the collector fluid (620°F). Thus, there is a need for a variable speed pump pushing the fluid through receiver of solar concentrator as shown in Figure 33. Hence m_i is dependent on T_i and solar insolation. The component model for storage tank is

$$(\dot{m}\ Cp)_s \frac{dTs}{dt} = Q_u - (UA)_s (T_s - T_r) - \dot{m} (p)_L (T_s - T_{L,r}) \tag{52}$$

where

T_s = storage temperature

$(Ua)_s$ = heat loss co-efficient of storage tank

The heat supplied by the auxiliary Q_A is given by

$$Q_A = (\dot{m}_2\ Cp)_A (T_5 - T_6) \tag{53}$$

$$\text{pumping losses in system} = P_w = (V \times \Delta P_c \times N)_c + (V \times \Delta P_h \times N)_h + (V \times \Delta P)_{rank} + (V \times \Delta P \times N)_f + (V \times \Delta P)_{HEx} + (V \times \Delta P)_{Cond} + (V \times \Delta P)_{Turb} + (V \times \Delta P)_{reg} \quad (54)$$

where

$(\Delta P)_c$ = pressure drop in one solar receiver as derived in previous chapters.

$(\Delta P)_{rank}$ = pressure drop in Rankine piping system

N = No. of receivers in the system

ΔP_h = pressure drop in the header pipes

ΔP_f = pressure drop in the pipe fittings

N_f = No. of pipe fittings

$(\Delta P)_{H-Ex}$ = pressure drop in heat exchangers

$(\Delta P)_{turb}$ = pressure drop in turbine

$(\Delta P)_{reg}$ = pressure drop in regenerator

Control strategy for the auxiliary heaters is well explained in the flow chart diagrams of the optimization procedure. The standard year solar data of the given location is taken from the nearby weather station, and system simulation is done for the standard year. The auxiliary energy consumed over a year is computed for a given solar concentrator area. The concentrator area is then optimized for the least unit power cost.

Determination of Collector Field Size

The collector field size can be as much as twice or thrice or even more than the area of solar concentrators. It is necessary to keep two adjacent rows of concentrators sufficiently apart to prevent the shadow of one row to fall on the adjacent one. A simple method of computing the collector field size (of square shape for maximum utilization land) is as follows:

$$\frac{D}{2} B_1 \; 2N = A_c$$

where

A_c = given concentrator area

B_1 = overall width of solar concentrator (7' 0")

N = number of rows of concentrator arrays

D = side length of the collector field

B_2 = width of the clearance between two rows of concentrators to prevent shadowing

$$(B_1 + B_2) \; 2N \; \frac{D}{2} = D^2$$

$$N = \sqrt{\frac{A_c}{B_1 \; (B_1 + B_2)}} \tag{55}$$

$$D = (B_1 + B_2) \; N \tag{56}$$

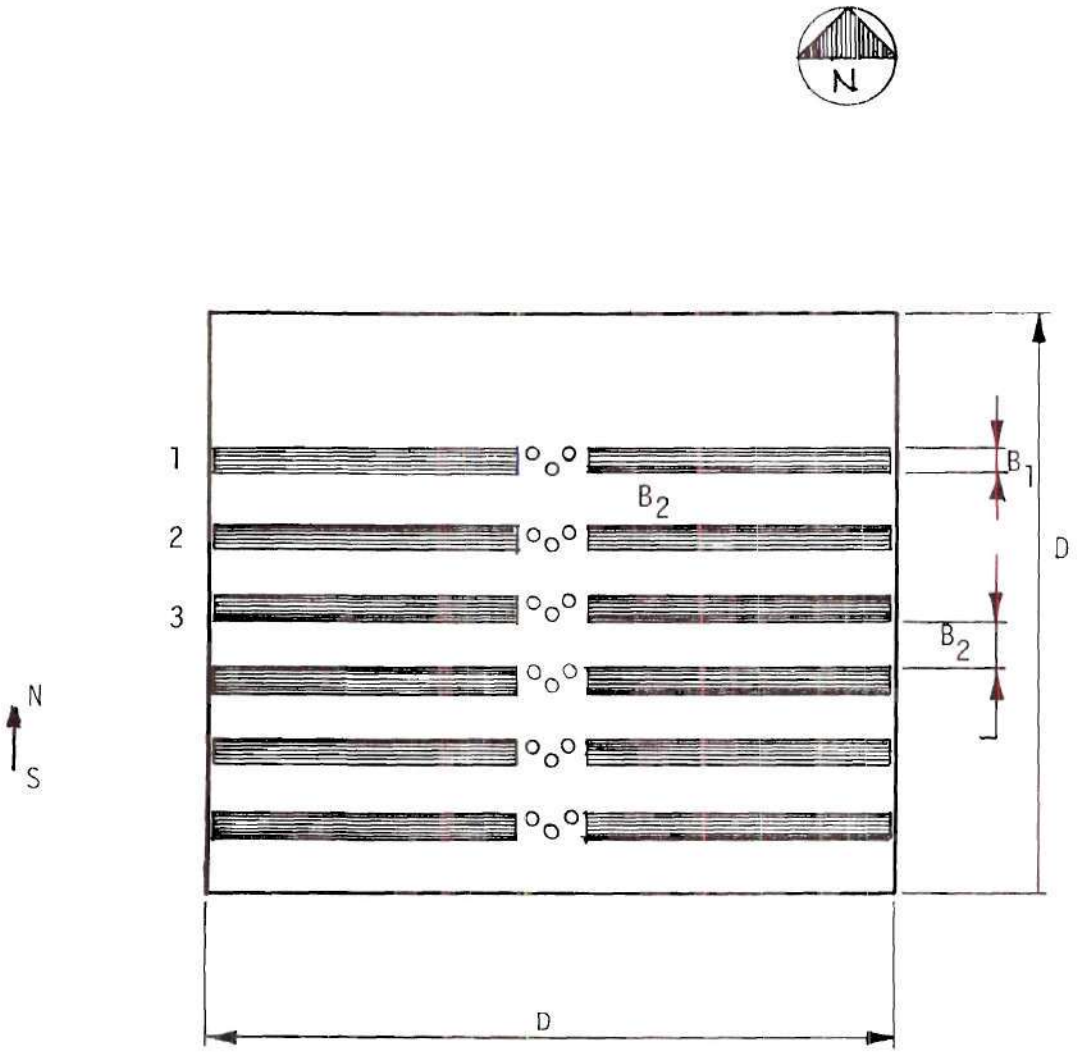

Figure 36. Concentrator Field Arrangement

The above equations determine approximately the size of the collector field and the number of rows of concentrator arrays. Thus for a given A_c, the economic analysis is carried out as follows.

Let

P = present value of capital

P_{ann} = annual cost of the capital

t = life of equipment

i_{ann} = interest rate

$$P_{ann} = P \frac{i_{ann} (1 + i_{ann})^t}{(1 + i_{ann})^t - 1} \tag{57}$$

$$P_{ann} = P \frac{0.08 (1 + 0.08)^{20}}{(1.08)^{20} - 1} = 0.10185P \tag{58}$$

for $t = 20$ years

and $i_{ann} = 8\%$

Now total annual cost of the entire solar concentrator system can be obtained as:

$$C_{T,a} = [(C_L + C_c + C'_{st}) A_c + C_E + C_{r,i}] I + Q_A C_F + P_w C_p + C_{mm} + C_{ml} \tag{59}$$

where

$I = \frac{i_{ann}(1 + i_{ann})^t}{(1 + i_{ann})^{t-1}}$ = the fraction of investment to be charged per year (interest and depreciation varies from place to

place)

P_w = annual power requirements of the solar energy systems

$$P_w = \Sigma \Delta P_i \times V_i \tag{60}$$

Where $\Delta P_i, V_i$ are the pressure drop and flow rates in each component of the system Viz. receivers, heat exchanger, pipings, etc.

C_p = the unit cost of power (varies from town to town and also over a year)

C_c = cost of concentrator per square foot

C_{mm} = the annual cost of maintainance of materials (it is unknown, no data available)

C'_{st} = cost of storage unit per square foot of concentrator area

C_{ml} = the annual cost of maintainance of labor

C_E = cost of the equipment, that includes pumps, valves, pipe headers, etc.

Q_a = auxiliary power consumed over a year

C_L = cost of land per square foot of concentrator area

$C_{r,i}$ = cost of Rankine power unit

In the above equation (59), the values of C_c, C_E, Q_a, and C_{mm} are directly related to the concentrator area A_c. Thus finally it can be concluded that $C_{T,a}$ largely dependent on the parameters A_c and Q_a. It can be expected that there exists an optimum value for A_c at which $C_{T,a}$ is minimum. A flow chart to determine these values of $C_{T,a}$ and A_c are shown in Appendix D.

Section E: A Simple Procedure for Optimization Calculations

The optimum concentrator area and the corresponding unit power cost of a 100 M.W. plant is determined by a very simple method as follows.

The solar radiation data is stoichaistic, therefore the predicting the performance of the power plant is always accompanied by some amount of deviation. For major cities of U.S., a standard year is defined such that the solar data of that year is expected to produce least deviation in designing the solar systems for the future solar data. Nevertheless, it is reasonable to expect that the deviation in estimating the available solar energy will not exceed 10% over a range of one year. As it is indicated in many texts and numerous papers [42], the standard year data is the best basis for design purposes.

As it is explained in previous section of this chapter that the total annual plant costs $C_{T,A}$ primarily dependent on concentrator cost, auxiliary fuel cost C_F and the concentrator area A_c. When C_c and C_F are dependent upon the concentrator area only then the extremum conditions exists for an optimum value of A_c at which $C_{T,A}$ will be minimum. As shown in reference [2] a graphical technique for the optimisation is a good choice and this technique is used here in this analysis. Finally a comparison is made between the cost of unit power at optimum conditions and the present selling cost of local power plant. For the sake of measuring the merits of concentrator in producing power over that of flat plate collector, this corresponding cost of unit power as produced by flat plat collector system is

evaluated and compared. However, flat plat collectors are economically found to be suitable for heating and cooling of buildings, thus an alternate form of comparing concentrators with flat plate collectors would be to obtain cost of the plant for meeting a given heating or cooling load.

The following assumptions are made in this simplified analysis to obtain the optimum concentrator area at which the total annual cost of power plant is minimum.

1. The solar energy is collected only during the period of four hours before and after solar noon on clear days. The energy collected before or after these hours are accounted for Thermal losses - from storage and other piping.
2. The receiver efficiency has a range of 57.5% to 65% the latter value applies around noon time. These efficiency values applies only for Therminol '66 fluid.
3. The conversion factor X_2 in equalion 61 on the edge losses of the concentrator on the 15th day of each month represents averages for that month; however these values are evaluated for a particular hour of the day as indicated by range of hour angle ω=0, 15, 30, 60 as shown in table 5 of the 15^{th} day of the month.
4. A very large thermal storage is implicit in the analysis and the energy is stored when the concentrator receiver system collects more energy than needed to produce 100 MW of electrical power (equivalent thermal energy required 1927

X 10^6 BTU/hr.). The stored energy is used during night time and cloudy days to supplement the auxiliary energy to meet the constant thermal energy requirements of 1927 X 10^6 BTU/hr.

5. The auxiliary energy heater or boiler has sufficient wide capacity range to meet the variable auxiliary energy requirements. It is capable of heating the collector fluid entering at temperatures of 340° to a temperature of 575° F.

6. The energy collected per a representative day of each month is computed from daily monthly average data for ±4hrs of solar data and when multiplied by number of days of that month given the energy collected for that month. The annual total solar energy collected is the sum of the energy collected per each month. The difference of annual total solar energy collected and the annual thermal energy requirement (16.88 X 10^{12} BTU/year to deliver 100 MW of electrical power) is assumed to be supplied by auxiliary energy source. This assumption makes thermal storage system to be implicit in the analysis and therefore stored energy do not appear in the calculations of energy interactions. Thus the assumption make this analysis very simple and compact with reasonable amount of uncertainties of the result. However, the amount of auxiliary energy consumed can be determined correctly (if not too erroneous) only when it is known at what temperature the energy is supplied.

7. In order to assure constant output of 100 MW the heat input to the Rankine Power Plant as well as the temperature ranges are fixed. Such an assumption can be accommodated with an infinitely variable speed pumps shown in Figure 33. In order to assure this assumption as the concentrator area increases the corresponding storage tank capacity need to be increased. The excess energy collected over that required by the power plant need to be stored over a narrow temperature range in order to validate the analysis. The reason being the invariant component efficiencies, frozen temperatures for the thermal cycle and constant power plant efficiency.
8. In this example of optimization pumping power required to push the fluid through the vast array of collector fluid, the annual maintainence cost C_{ℓ} and C_{st}^{1} are neglected.

The standard year beam component solar radiation data is not available for many locations. Based on total radiation data, the following equation is suggested for computing the approximate value of heat gained by the collector fluid of a solar concentrator.

$$q_u = I_{\text{Daily, Total}} \rho_c A_c \left\{ \sum_{\omega=0}^{75^\circ} 2 \, (x_i x_2 x_3 \eta_r) \, (1-x_4) \right\} \qquad (61)$$

where $x_1 = \dfrac{\text{hourly radiation on a horizontal plane surface}}{\text{daily radiation on a horizontal surface}}$

The conversion factor, $x_2 = \frac{\text{Cos}\Theta}{\text{Sin}\ \alpha}$

$x_3 = (1 - K_e)$ where K_e = edge loss factor

η_r = Thermal efficiency of receiver (assumed to range from 57.5% to 65%, See Table 5)

$x_4 = \frac{\text{Monthly average daily diffuse}}{\text{Monthly average daily total}}$

The values of x_1 and x_4 are obtained from references [42] and [43] respectively.

ω = is the hour angle as defined in Chapter VI.

Tables 4 and 5 are constructed from the daily total solar radiation data. From equation (61), the monthly average daily heat gained can be computed for each month. Figure 37 shows the yearly variation of overall collection efficiency, which is the ratio of heat gained by the fluid to the energy falling on the concentrator. From Figure 37, the annual heat gained by the fluid per square foot of concentrator is found to be

$$q_{u,\ \text{annual}} = 0.163 \times 10^6 \text{ BTU/year, sq. ft.}$$

Assuming the thermal losses from the storage tank and others to be negligible, the annual solar energy collected from a concentrator of Area A_c is given by

$$Q_{S,T} = 0.163 \times 10^6\ A_c \qquad (62)$$

Table 4. Solar Radiation Data for Atlanta for a Standard Year 1964

Day of The Year	Day Length Hours	Declination	Beam Radiation Total Radiation $(1-x_4)$	Monthly Average Daily* Total Radiation BTU/Day,ft^2
1-15	9.8	-21.27	0.6	848
2-15	10-8	-13.29	0.6	1080.1
3-15	11.8	-2.82	0.65	1426.9
4-15	12.7	9.41	0.551	1807
5-15	13.8	18.8	0.561	2018.1
6-15	14-4	23.3	0.70	2102.6
7-15	14.2	2152	0.545	2002.9
8-.5	13.2	13.78	0.559	1898.2
9-15	12.2	2.22	0.515	1519.2
10-15	11.0	-9.6	0.543	1290.8
11-15	10.0	-19.15	0.51	997.8
12-15	9.5	-23.37	0.474	7516

*On a horizontal surface.

Table 5. Distribution of Solar Energy During the Day and the Corresponding Edge Losses and Inclination Factor.

	W = 15° Nr = 65%			W=30° Nr = 80%		
Day	x_1	x_2	x_3	x_1	x_2	x_3
1-15	0.155	1.64	0.89	0.13	1.707	0.87
2-15	0.148	1.431	0.925	0.122	1.463	0.92
3-15	0.14	1.26	0.98	0.12	1.25	0.98
4-15	0.13	1.08	0.99	0.113	1.06	0.99
5-15	0.12	0.97	0.93	0.11	0.95	0.92
6-15	0.117	0.93	0.88	0.11	0.90	0.88
7-15	0.118	0.94	0.88	0.11	0.92	0.87
8-15	0.128	1.03	0.92	0.111	1.01	0.90
9-15	0.132	1.17	0.98	0.112	1.17	0.98
10-15	0.145	1.36	0.99	0.12	1.38	0.99
11-15	0.152	1.57	0.95	0.13	1.63	0.94
12-15	0.162	1.70	0.91	0.13	1.79	0.88

Table 5. Distribution of Solar Energy During the Day and the Corresponding Edge Losses and Inclination Factor. (Continued)

	$W = 45^{o}$ Nr = 58%			$W = 60^{o}$ Nr = 57.5%		
Day	x_1	x_2	x_3	x_1	x_2	x_3
1-15	0.09	1.89	0.78	0.04	2.47	0.72
2-15	0.09	1.54	0.86	0.05	1.75	0.82
3-15	0.09	1.26	0.97	0.06	1.28	0.96
4-15	0.091	1.04	0.98	0.06	0.98	0.97
5-15	0.09	0.91	0.88	0.07	0.83	0.86
6-15	0.09	0.86	0.87	0.07	0.76	0.86
7-15	0.07	0.88	0.87	0.07	0.79	0.87
8-15	0.09	0.98	0.86	0.07	0.91	0.83
9-15	0.09	1.16	0.96	0.06	1.14	0.93
10-15	0.09	1.43	0.98	0.05	1.55	0.98
11-15	0.09	1.78	0.9	0.042	2.2	0.85
12-15	0.09	2.01	0.82	0.04	2.8	0.72

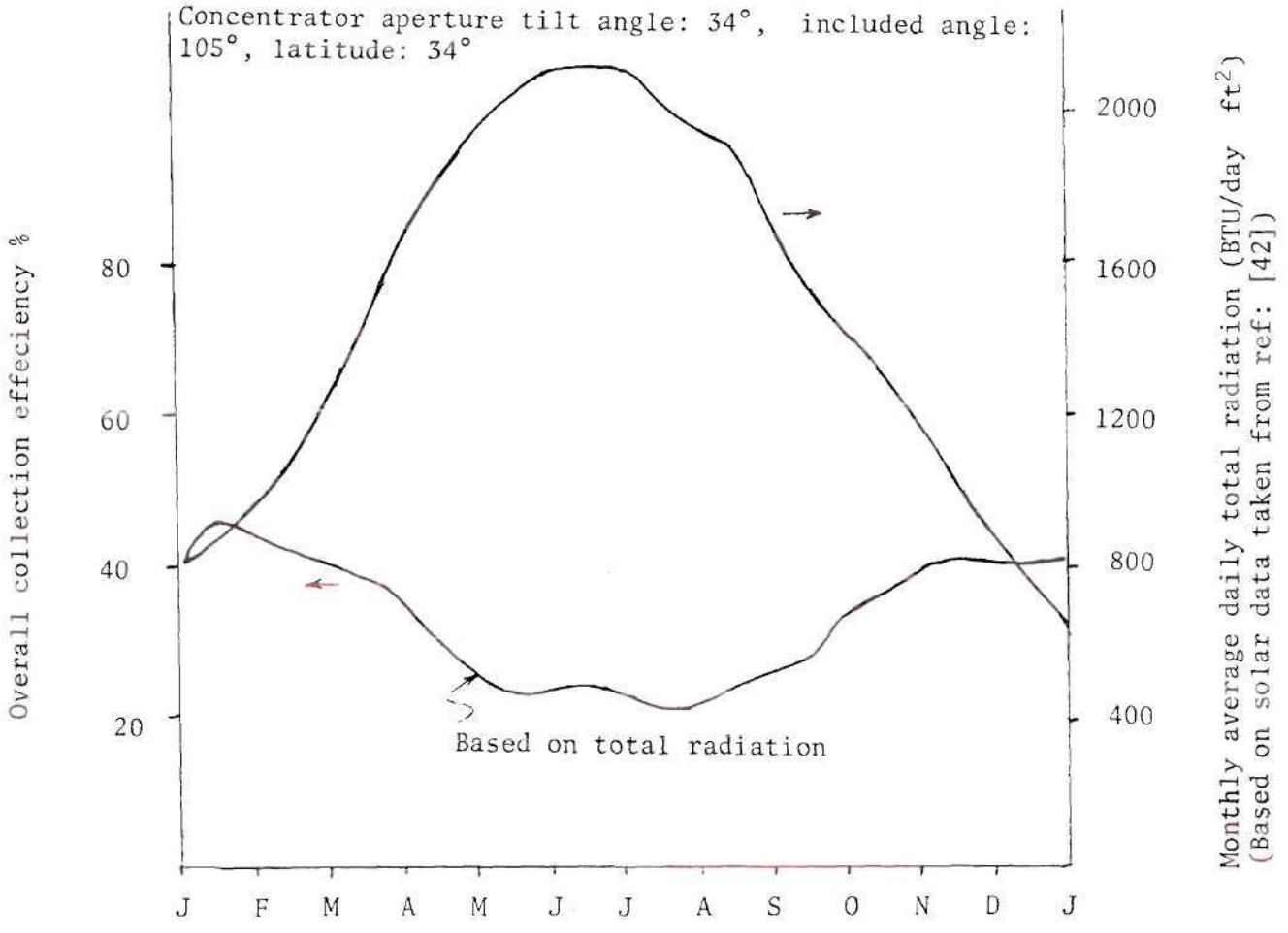

Figure 37. Yearly Performance of Fixed Mirror Concentrator Receiver System

The annual thermal energy needed to produce 100 MW of electrical power is $Q_{Tot} = 1688.65 \times 10^{10}$ BTU/year

Therefore auxiliary energy needed $Q_{A,T} = Q_{Tot} - Q_{S,T}$

$$Q_{A,T} = 1688.65 \times 10^{10} - 0.163 \times 10^{6} A_c \qquad (63)$$

Neglecting the annual cost of maintainance, labor, pumping power and cost of storage per unit concentrator area, the total annual cost of the solar power plant is computed from equation (59) which simplifies to

$$C_{T,a} = [C_c A_c + C_E + C_{r,i}] I + Q_{A,T} C_F \qquad (64)$$

Assuming interest rate of the capital investment to be 8% and life of solar equipment to be 20 years would make I = 0.10185 (65)

Let $\left(C_E + C_{r,i}\right) = \$ 10 \times 10^{6}$ (from refs. 44 & 45)

From equations (63), (64) and (65)

$$C_{T,a} = 0.10185 \, (C_c A_c + 10 \times 10^{6}) + (1688.65 \times 10^{10} - 0.163 \times 10^{6} A_c) \, C_F \qquad (66)$$

Equation (66) indicates that the total annual cost of the solar-power plant system is primarily dependent on area and cost of solar concentrator and also the unit cost of the auxiliary fuel.

The above equation can be written in a general form as

$$C_{T,a} = a_1 (C_c A_c + a_2) + (a_3 - a_4 A_c) C_F \qquad (67)$$

It is to be noted that extremum values for $C_{T,a}$ exists only when right hand side of equation (67) is non-linear in A_c, thus requiring C_c or/and C_F to be functions of A_C.

Physical Significance of the Constants

a_2 and a_3 are representative of capital cost of the plant and are dependent on the capacity of the plant, a_4 is a measure of fraction of load carried by solar energy and is dependent upon the type of concentrator, receiver and the latitude of the location, therefore for a given type of concentrator-receiver system it depends only on the latitude of location. Thus, $C_{T,a}$ can generally by expressed as a function of

$$C_{t,a} = f\ (C_c,\ A_c,\ C_F, \phi\ ) \qquad (68)$$

where ϕ = latitude of the location.

Thus equation (66), (67) or (68) can be treated as an objective function of the optimization problem. Keeping in view the required conditions for optimum concentrator area, two sets of C_F & C_c values (schedules A & B) are assumed based on the approximate data given in references [2] and [45].

Table 6 shows the summary of values of $C_{T,a}$ for two different sets of C_F and C_c values. The graphs in Figure 38 represents the results of this simple optimization technique.

Figure 39, shows relative proportions of monthly components of solar energy and auxiliary energy for the optimum collector are of 152 million square feet shown in Figure 38. It is necessary to carefully consider assuptions made in this P.T.O. optimization before a critical

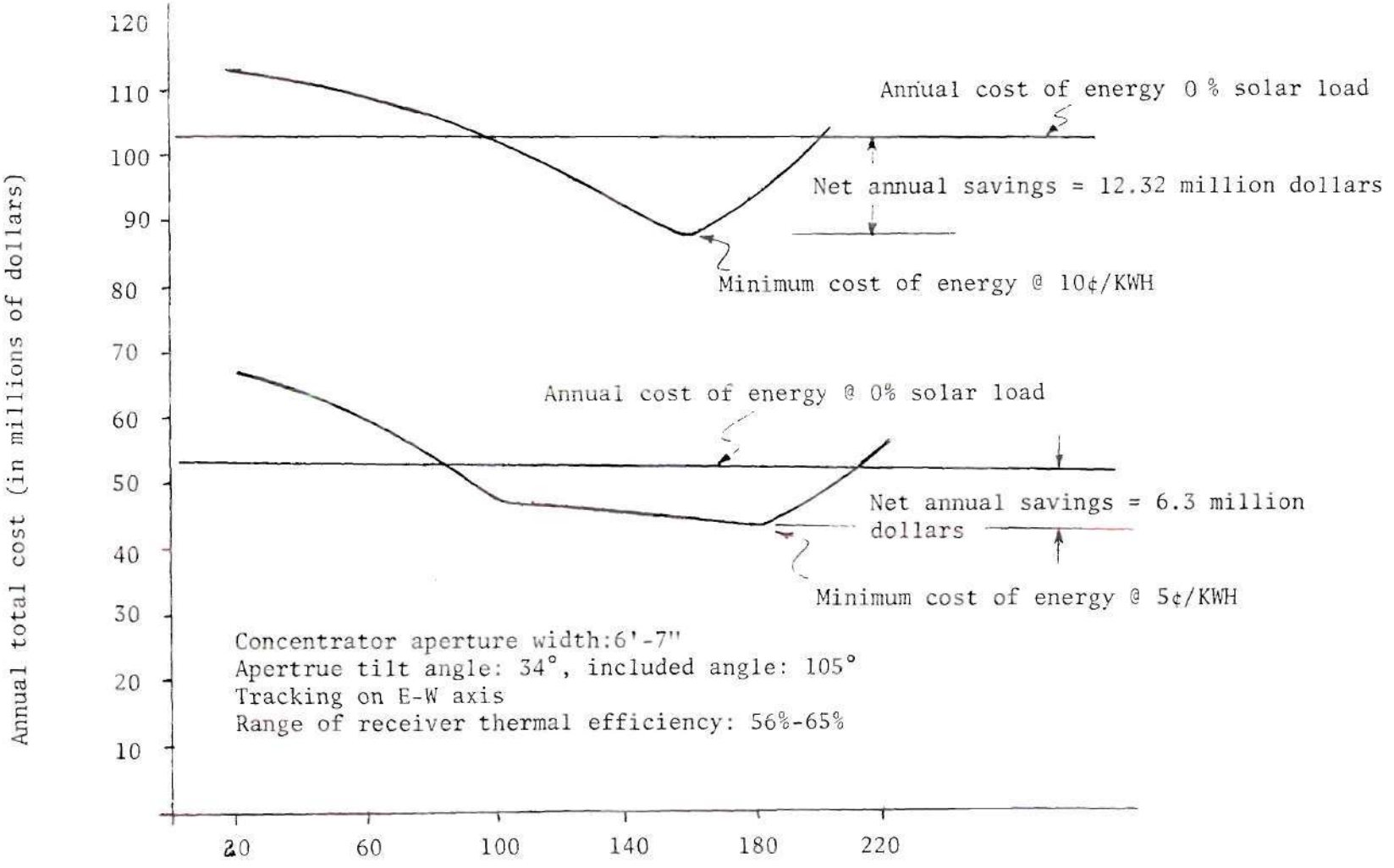

Figure 38. Optimum Concentrator Area of Solar Power Plant in Million Square Feet.

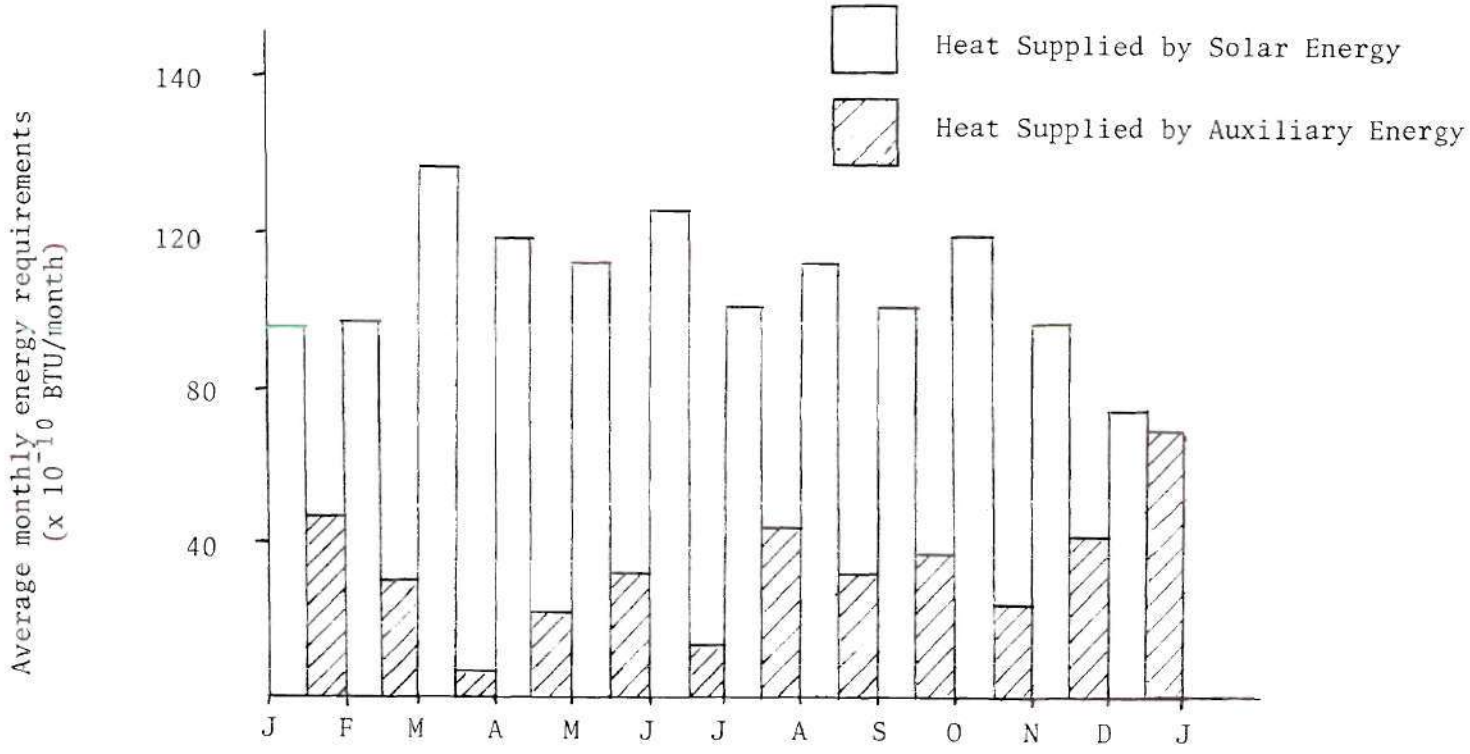

Figure 39. Average Monthly Solar and Auxiliary Energy Requirements (at Optimum Concentrator Area)

review of Figure 39 can be made. The data in Figure 39 is for Atlanta, Georgia and for the Solar data of 1964, considered as standard year. The variations in Solar component in part reflects the losses associated with this type of segmented concentrator. The thermal analysis is based on Steady State which is difficult to achieve considering the stochastic nature of the Solar input and the large thermal inertia associated with collector and power plant fluid.

CHAPTER VII

DISCUSSIONS

The most expensive component of the solar power plant system of capacity more than 1000 KW is the solar concentrator and also the largest amount of energy losses occur in concentrator nearly as much as 20% to 40% of incident solar flux.

Considering the global picture of the energy in the collector system as shown in Fig. 40, the solar insolation can be broken down into the following categories.

1. Concentrator losses
    a. Edge losses
    b. Imperfection losses
    c. Reflection losses
2. Thermal losses of the receivers
    a. Transmission losses
    b. Conductive and radiative losses
3. Thermal losses from the piping system (if any)
4. Pumping power losses
5. Mechanical shaft power (if Rankine cycle is coupled)

The potential for partially reducing the concentrator losses lies in eliminating the imperfection losses that is done by aligning perfectly the mirror slats and other mechanisms true to their angular configuration. Reflective losses can be minimized with new and better quality inexpensive materials. Research in this area must be undertaken

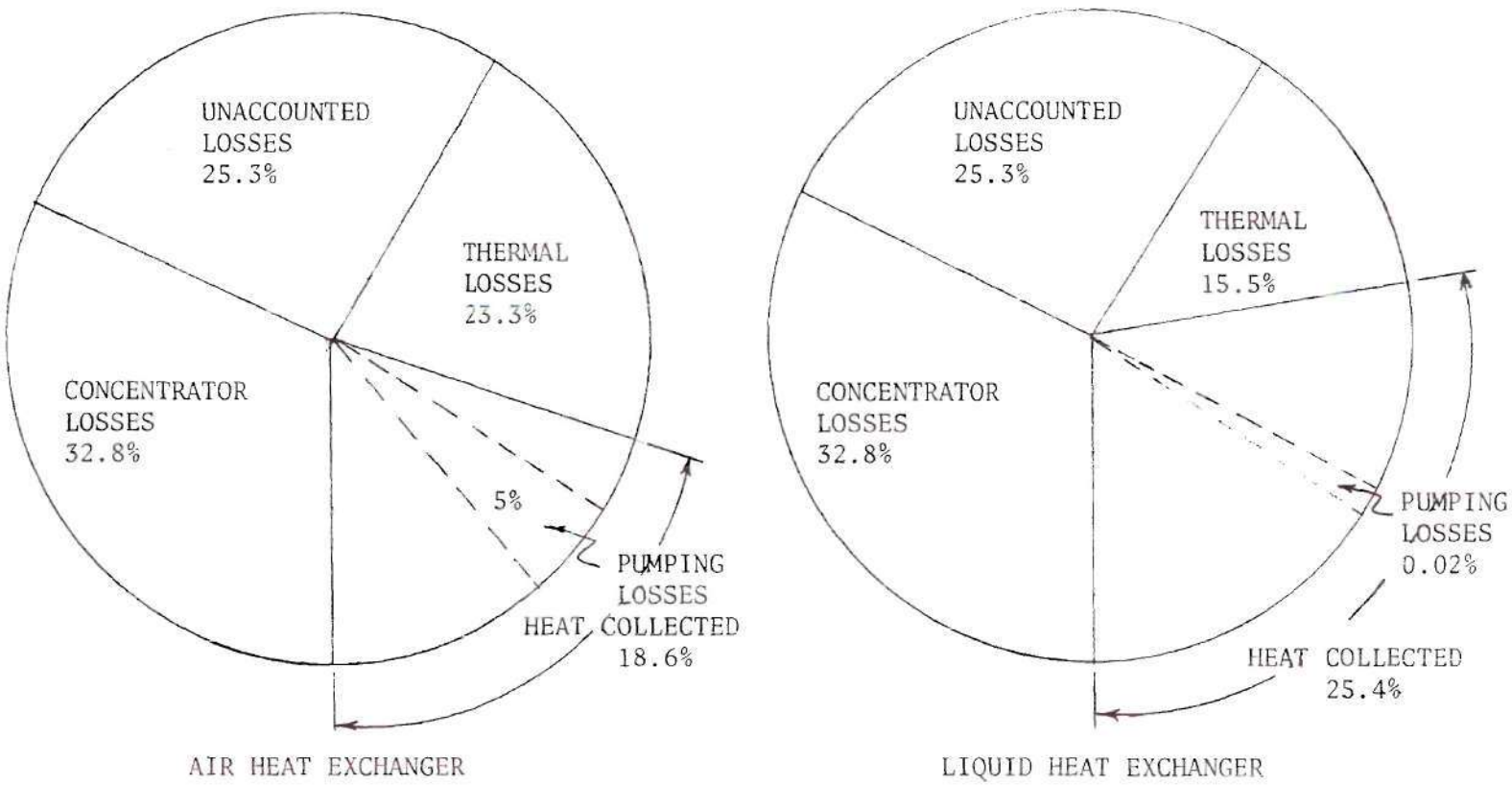

Figure 40. Thermal Performance of Heat Exchangers

and success in this area will have a remarkable and profound effect on the future of solar concentrators. Edge losses, which do not exceed 10% of the incident flux are inevitable with the fixed faceted mirror concentrator. The edge losses are the solar flux falling in the region b-c-d of Figure 42a and region g-h and m-n in Figure 42b. The variation of the edge losses for a concentrator of 105° included angle is shown in Figure 13. It is to be noted that edge losses at and around noon time are much less compared to the early or late hours from noon time. Receivers may be designed and constructed to be used with fixed mirror concentrator for different applications of the system.

The air heat exchangers are made of inexpensive materials and can be built easily. The experimentally measured collection efficiencies varied from 15% to 30%. The frictional losses ranged from 10% to 25% of heat collected. Conservatively speaking, one unit of mechanical energy is worth about 4 to 5 units of thermal energy. The experimentally measured pressure drop is only that of heat exchangers and it does not include the pressure drops occurring in the remaining portions of the piping systems, the valves and the other hydraulic bends, etc., used for transporting the fluid. The total pressure drop in the entire system and the consequent frictional power losses would be much bigger than the solar energy collected (measured in mechanical power units) in the air heat exchangers. The air heat exchanger may collect solar energy after compensating for the frictional power losses by employing the following measures.

1. Reducing the piping and fitting configuration to the bare minimum required.

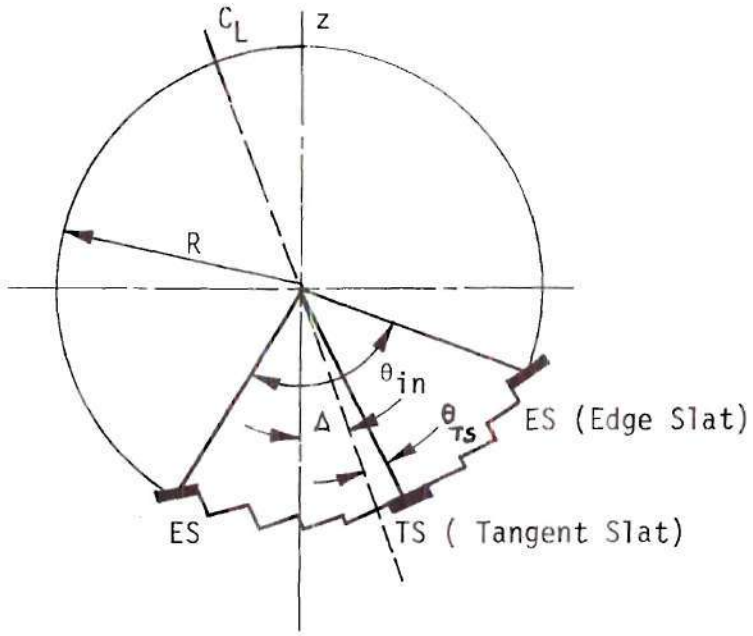

Figure 41. Labeling of Geometry of a FMC

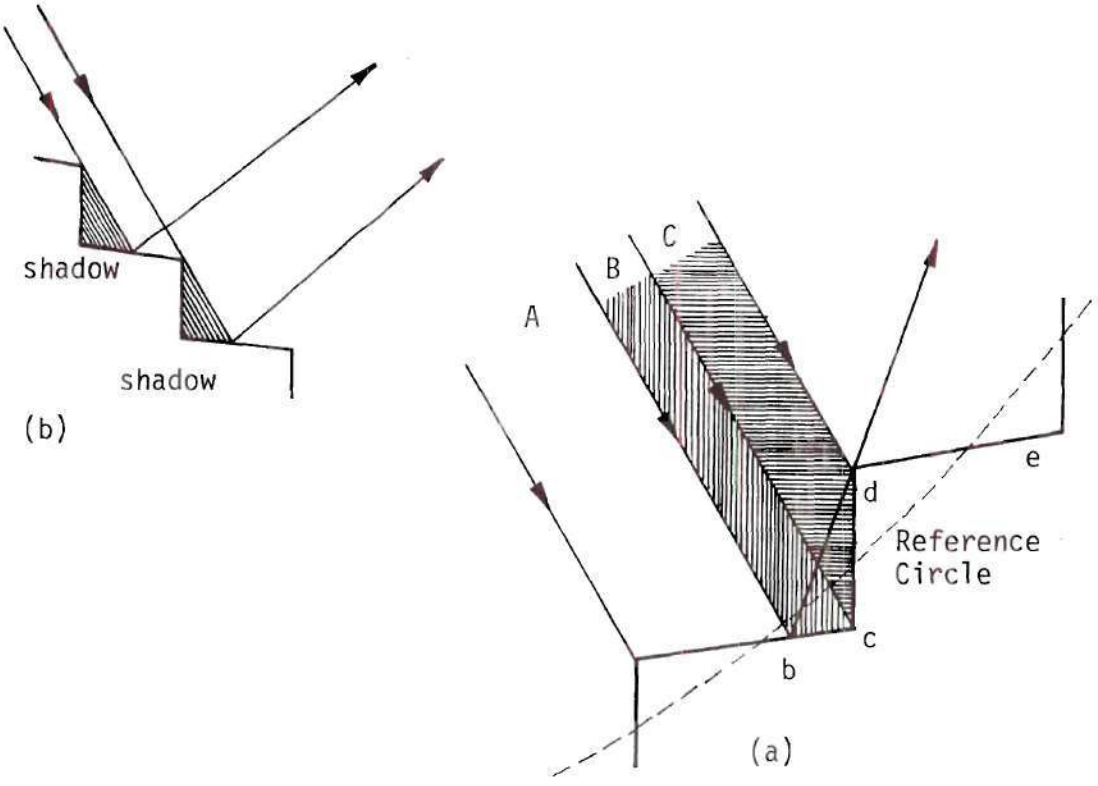

Figure 42. Edge Losses and Shadowing.

2. Improving the design of air heat exchangers with better quality insulation and applying black chrome coating to the receiver surface.
3. Finally, improving the concentrator efficiency.

Nevertheless, the air heat exchangers are inferior to the liquid heat exchangers in extracting heat. A comparison of thermal performance of air and liquid receivers are shown in Figure 40 and Table 6. They are based on experimental data taken on air-heat exchanger on March 10, 1976, @ 2:30 p.m.

In the thermal analysis of Corning Glass receivers, only the molecular heat conduction and radiation processes are assumed to exit due to near vacuum conditions within the glass envelope. The analytical computation of the molecular heat conduction for the exact geometric configuration as shown in Fig. 5 is very complicated, as such a simpler model of flat plate configuration as shown in Fig. 21 is assumed to simplify the analysis to great extent. Axial conduction is neglected as it is negligible compared to that in transverse direction. Another important assumption made in thermal analysis of receiver is that of steady state conditions. In reality these conditions exists for only a short period of time may be of the order of 15 min. to an hour. Naturally as it is expected, the smaller the interval, better would be prediction of results. The heat transfer fluid most commonly used for concentrator receivers is Therminol 66 due to its favorable properties. The dynamic viscosity of this fluid is highly sensitive to the temperature, (it varies from 67.8 at 100°F to 0.82 lb/hr ft at 600°F) because of which thermal analysis is carried out on differential fluid elements and properties are evaluated by

Table 6. Summary of Optimization Calculations

A_c $x10^{-6}$ sq.ft.	C_c $ per 2 ft.	C_F $ per 10^6 BTU	Q S,T $x10^{-12}$ BTU	Q A,T $x10^{-12}$ BTU	% Solar	C S,T $x10^{-6}$ $	C A,T $x10^{-6}$ $	C T,a $x10^{-6}$ $	Min Unit Power Cost ¢/Kwh
SCHEDULE 'A'									
20	10	6	1.63	15.26	10	21.39	91.56	113.00	
60	0	6	4.88	12.01	29	37.7	72.06	110.00	
100	5	6	8.14	8.75	48	51.94	52.5	104	
160	4	6	13.02	3.87	77	66.20	23.22	89	10.0
180	4	9	14.67	2.22	87	74.35	19.99	94.40	
200	4	30	16.30	0.59	97	82.50	17.7	100.2	
SCHEDULE 'B'									
20	10	3	1.63	15.26	10	21.4	45.76	67.18	
60	4	3	4.88	12.01	29	25.46	36.00	61.46	
100	2	3	8.14	8.75	48	21.40	26.25	47.65	
160	2	3	13.02	3.87	77	33.60	11.61	45.20	5.0
180	2	3	14.67	2.22	87	37.7	6.66	44.36	
200	2	10	16.30	0.59	97	41.80	11.80	47.7	

Table 7. Comparison of Air and Liquid Receivers

	Air Heat Exchanger* Experimental Data	Liquid Heat Exchanger** Theoretical Prediction
Heat Flux: BTU/hr	12847	12847
Concentrator efficiency	67.2%	67.2%
Ambient Temp: F°	70	70
Inlet fluid temp: F°	317	317
Glass temp: F°	325	149
Mean plate temp: F°	387	375
Flow rate: lbm/min	6.6(127 cfm)	3.8(0.07 cfm)
Dia. of tube: inch	3.0	0.3125
Temp rise: F°	25.2	48.0
Heat Flux available at focal plane	8633	8633
Thermal losses: BTU/hr	2985	1992
Unaccounted losses: BTU/hr	3253	3253
Heat gained: BTU/hr	2395	3388
Collection eff: %	18.6	26.4

* Experimental data taken on March 10, 1976 @ 2:30 p.m. (refer Fig. 6 of Appendix A) concentrator efficiency at this time $\eta_c = P_c (1 - K_c) = 0.672$.

** Computed by the extrapolation of computer results and also can be obtained through Figures 24, 25 and 27.

iterative procedure for each element at the local fluid temperature.

The rankine space power plant without storage is a specialized plant that requires a constant solar input power from the collector fluid; in turn this requires that the concentrator be oriented toward the sun constantly, at a fixed angle. This plant would obviously produce a constant power; however, a similar plant can operate on the ground where the cumulonimbus clouds are not very active and the change in intensity of sunshine is not large for a long period of time. Different rankine fluids are suggested for different maximum temperatures of rankine cycles. Freon gasses are used for temperatures up to $300^{o}F$. For temperatures over $500^{o}F$, benzene and toluene are most commonly used. At any given maximum temperature of a rankine cycle, both the fluids have approximately the same rankine efficiency, but considering the other properties like flammability, toxicity and corrosion, toluene is often singled out to be the best fluid for solar energy applications.

The section C of the Chapter VI dealt with optimization of power plant (without storage) to obtain maximum shaft power for a given solar intensity. The turbine shaft power dependent upon the maximum temperature of rankine fluid which in turn depends on the exit collector fluid temperature or the mean collector fluid temperature. The receiver efficiency varies with mean collector fluid temperature, having low values at higher mean collector fluid temperatures. Thus, there exists an optimum mean collector fluid temperature at which the shaft power of the turbine or the overall thermal efficiency of the plant is maximum. Mean collector fluid temperature can be varied either with mass flow rate of the collector fluid or that of rankine fluid for a given solar

intensity. Since the receiver efficiency assumes an asymptotic value around 0.5 gpm, the collector fluid flow rate is fixed at that condition, thus enabling the rankine fluid flow rate to control the mean collector fluid temperature and in turn controlling the overall thermal efficiency. A mathematical expression for shaft power is obtained in terms of rankine fluid flow rate and this expression is differentiated for obtaining maximum power. The effect of receiver arrangement and insulation thicknesses or header pipes are also considered in this section.

Section D and E of Chapter VI dealt mainly in evaluating the optimum concentrator area at which annual cost of power plant is minimum. The simple procedure described in section E differs from that of Section D, in the method of computing the auxiliary energy supplied.

In short the procedures outlined in section D and E are similar, they are different only by the time interval considered between each data point. It is pointed out that the power plant annual cost or cost of unit power produced primarily depends upon the unit cost of concentrator C_c, auxiliary energy, cost C_F, and the concentrator area A_c. It is required that the C_F and C_C are to be functions of A_c for existence of extreme conditions. Based on appropriate cost data two schedule of costs are assumed and optimum concentrator area is evaluated. At this optimum configuration, the unit cost of the power produced is determined for each schedule of costs.

CHAPTER VIII

CONCLUSIONS AND RECOMMENDATIONS

As far as extraction of heat energy and the power requirements of the collector fluid to overcome the friction are concerned, the receivers using liquid are always superior to air heat exchangers. This fact is evident from Figures 26 and 40. The theoretical results obtained in graphical form in Figures 24 through 28 for receivers using liquid (Therminol 66) are in good agreement with those in reference [16]. Similar trend results are obtained for receivers of parabolic concentrators. These receivers are in the shape of a circular cylinder enclosed in transparent concentric cylinder. Ortabasi [35] performed indoor tests to determine the effect of vacuum on the performance of a tubular flat plate collectors which is exactly similar in shape as the one considered in the present analysis. The values, he obtained for overall heat transfer co-efficients of the black coated plate are within 10% of those predicted by the present analysis.

The collection efficiency of the concentrator, defined as the ratio of heat gained by the collector fluid to the solar energy falling on the concentrator varied from 32% to 48%. All of the graphical results shown in Figures 24 through 28 are obtained based on this assumption that the concentrator has an efficiency of 60%. The concentrator located at the Georgia Institute of Technology, Atlanta assumes this value on January 15 and July 15 at an hour before or after solar noon.

Conclusions

Concentrator receiver systems are generally used for power plant applications because of high temperatures of the collector fluid obtainable at high concentrations. Liquids whose vapor pressures are not excessive at high temperatures should be used. At low pressures the receivers can be designed and built of light weight, thereby consuming less power for their rotation along the reference circle during this day time. When air is used for high temperature industrial application, a careful study of pumping power requirements of the entire heat transfer loop should be made.

The thermal analysis of the liquid receivers have demonstrated that:

a) The thermal efficiency is not affected by flow rate in the operating range of 0.5 gpm to 5 gpm.

b) In the design range of flow rate, thermal efficiency increases about 5% with three fold increase in solar intensity varying from 60 to 180 BTU/hr ft^2 .

c) Property variations such as caused by operating temperature range causes small changes in thermal efficiency.

d) 10 to 1 increase in flow rate increases thermal efficiency by 2 to 3%.

e) Thermal efficiency is insensitive to the choice of fluid, but pumping power requirement is least with water. It is very large (astronomical!) with air, thus generally low air flow rates are preferred.

f) Thermal efficiency is unaffected by wind speed or ambient temperature due to large internal resistance offered by the near vacuum conditions.

g) Minimum width of absorber plate for the receiver should be 6" to take advantage of maximum efficiency for the care of slat width of 2.9".

h) Smaller diameter copper tube, less than 1/16" in diameter is preferred, as it takes advantage of better fin effectiveness and flow rate factor of the absorber plate. In the present design this value is 3/16" diameter.

i) Temperature rise in each receiver unit can be controlled by reducing flow rate with only 2 to 3% reduction in thermal efficiency.

The following conclusions are made from the analysis of optimization of space power plants with no storage having its concentrator fixed in geosynchronous orbit at a fixed orientation with sun.

a) The overall thermal efficiency of the concentrator-receiver rankine power plant is sensitive to the solar intensity. This sensitivity is more for parallel arrangement than for series. The efficiency doubles when the solar intensity changes from 150 to 350 BTU/hr. ft^2 at mean temperatures of collector fluid greater than 400°F.

b) The optimum mean collector fluid temperature for maximum power increases with solar intensity specially for parallel fluid flow arrangement from 300°F to 500°F when the intensity changes from 150 to 350 BTU/hr ft^2.

c) The effect of insulation thickness of header pipes on overall thermal efficiency is appreciable in parallel flow arrangement than in series flow arrangement.

d) The overall thermal efficiency of the power plant is always greater for series arrangement than for parallel flow arrangement for any given solar intensity or header piping insulation thickness.

e) For series arrangement, the overall thermal efficiency is slightly sensitive to mean temperature of collector fluid only at low solar intensity.

Rankine cycle efficiency defined as the ratio of electrical power produced over the heat supplied to the rankine fluid and is assumed to be 17.7% based on a rigorous study made by Miller [31]. Based on this value, the overall efficiency of the solar power plant converting available solar energy to electrical power ranges from 5.7% to 8.5%.

An extremely simple cost optimization analysis is performed in which the cost of land, labor and material maintainance are neglected. The capital cost of the pumps and rankine system components are assumed to be around 10 million dollars for a power plant of capacity 100 MW. Based on these assumptions, the optimum concentrator area is found to be 180 million square feet or 1.8 square feet per watt of electricity generation at which the cost of the unit power produced is minimum. The total cost of plant at optimum conditions is 370 million dollars. The corresponding cost of the power is 5¢/kwh compared to the present commercial generating cost of 2.8¢/kwh from Georgia Power

Company. The above optimum concentrator area of 180 million square feet supplies 87% of load from solar energy over a standard year. The solar energy thus collected saves annually 6.3 million dollars compared to a plant that is entirely operated by auxiliary energy. Similar results are obtained for a different set of cost values of concentrator and auxiliary fuel. These results are shown in Figure 38.

While the optimization method outlined in flow chart of Appendix considers the more detailed transients analysis of power plant of Figure 33; the procedure adopted in above optimization is similar but at a different time span between two data points. The above optimization for least unit power cost and the evaluation of corresponding concentration area is done by utilizing solar data for the standard year (1964 data for Atlanta) data.

The best type of flat plate collectors give an annual collection efficiency of the order of 40%. The maximum temperatures obtained from these collectors is around 200°F. The rankine efficiency at this temperature of a corresponding rankine cycle [20] is around 6.25%. This gives an overall efficiency of a flat plate collector system to be around 2.5%. The corresponding flat plate collector area required to supply 87% of the plant load is found to be [from Tables 4 and 5] 447 million square feet.

A flat plate collector system requires approximately two and one half times the corresponding area of concentrator system. The necessary additional storage, land, piping and plumbing requirements would make the flat plate collector power plant system unsuitable and uneconomical for power production.

Recommendations

Solar energy is an alternate energy source which is at a stage of infancy. It's ability to compete with other forms of energy depnds on its overall cost per unit of power developed. Since the capital installation costs of solar energy systems is large, the realistic and more precise approach to compare its viability requires quantitative evaluation of its performance over a long range (at least over a year). The continuous production of power require a thermal energy storage. The capacitance effects of storage influence the thermal losses. A sketch of a typical solar power plant system using thermal storage is shown in Figure 43. Transient thermal analysis of such a system require a complete weather data including the cloud cover factor over an extended period of time, 5-6 years. The weather data of a standard year can be used. In absence of beam radiation data, a relationship between beam and total radiation is needed. Treadwell [46] indicated that this particular problem is presently being studied at Sandia Labs.

Appropriate models for storage system can be coupled to the weather data and the previous steady state models for solar receivers and heat exchangers to evaluate long range performance of the solar power plant system. The latest cost data of each equipment and materials should be gathered and a complete economic viability of this system should be studied for the purpose of comparing its validity with other alternate sources of energy. The results as obtained should be compared with that obtained from the simplified optimization analysis.

The cost of solar powered energy is minimum when maximum shaft power is obtained for a given solar flux and installation cost, this in

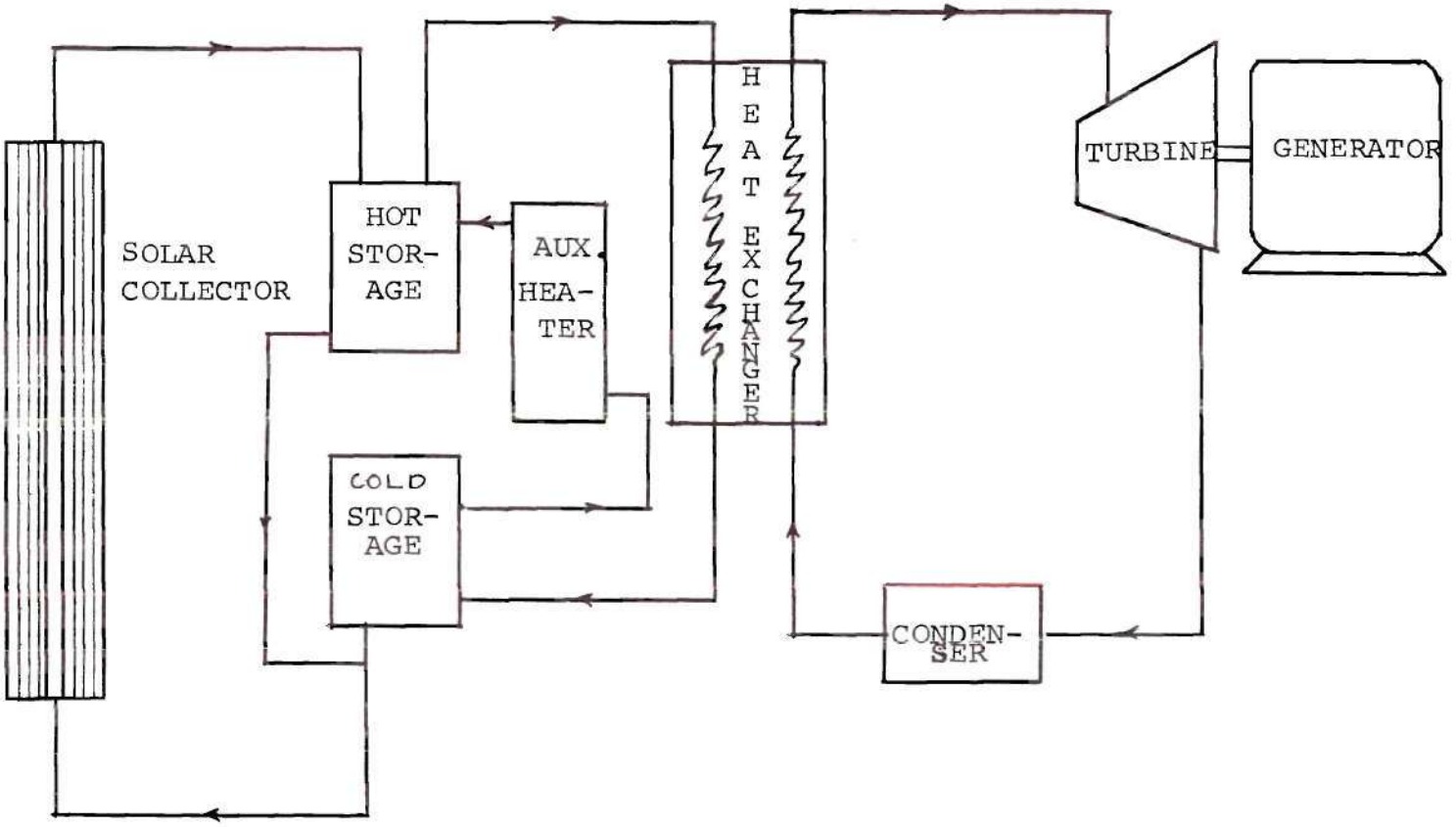

Figure 43. Schematic of Solar Power Plant System Considered for Optimization.

turn can be achieved only when solar collectors operate at the maximum collection efficiency. The following measures are recommended to enhance the receiver efficiency.

1. The solar collectors should be operated in series arrangement.
2. Insulation on half of the circumference of the glass envelope of the receiver is to be added.
3. Internal fins or twisted tapes may be provided inside the copper tubes to enhance the heat extraction.
4. Since the major fraction of losses are in the concentrator, research may be conducted to obtain cost effective high reflection glass mirrors.
5. A general program of investigation to replace the expensive materials with inexpensive ones may be initiated to bring down the unit cost of solar energy.

The above measures are expected to bring down the unit cost of solar energy to the minimum. In addition, a further concentration of solar flux may be obtained by placing a lens at the focal plane of the solar collectors. Additional concentrations are specially helpful at places where the solar insolation levels are very low.

In this thesis the major emphasis is given on the thermal analysis of the solar receivers and, therefore, experimental verification of the theoretical results should be initiated.

G. H. Eggers and J. L. Russell [36] indicated an economic approach to build these concentrators on concrete blocks. This approach should enhance their life and also will reduce the maintainance costs. No matter how the concentrator is constructed, it is recommended that the

experiments be conducted to determine precisely the concentrator efficiency at different solar angles above the southern horizon. D. B. McKay [37] showed a methodical approach for proper selection of the rankine fluids. Although Toluene is reelected for use in Rankine cycles, a systematic analysis for a proper choice of this fluid should be done. Finally, the fixed mirror concentrator should be compared with other competitive concentrators like vee-trough collectors by Seleuk [38], the concentrator based on an array of linear clipped V channels by Bynum, Donnell, and Bordoloi [39], and a planar, fresnel reflector, rotatable facet concentrator by Anderson, Jr. [40]. A long range cost effective analysis of these collectors to obtain a given amount of power should be done.

From the knowledge gained in this work and the literature survey made by the author found no particular fluid as yet chosen as the best for the Rankine cycle. Toluene has been mentioned quite often, but its validity as the best among the fluids has not been established on a rational basis. A good amount of research potential lies in the study of power fluids. Donald McKay [37] has outlined a systematic procedure to rate different fluids, probably this should form a foundation for a study of power fluids.

APPENDICES

APPENDIX A

AIR HEAT EXCHANGER

Preliminary experiments were conducted using air heat exchangers as shown in Figure 2 of Chapter IV. Thermocouples were installed on only one module of heat exchanger (8' - 0" length) as shown in Figure 3. The required instruments are 1) The potentimeter to measure thermocouples output, 2) the 20 channel switch, 3) the pyrohelimeters to measure the pressure drop and 4) a velometer to measure the velocities of air in the duct. Air flow meters could not be used as they create a large pressure drop across them. A schematic diagram of the experimental set up is as shown in Figure 1. The instrumentation needed for the experiments are shown in Figure 2. A butterfly valve is placed in the duct at a far distance from the entrance to the heat exchanger that controls the flow rate of air inside the duct. The wind velocity and its direction is also recorded by a separate instrument. The normal pyroheliometer and the HyCal Pyroheliometer (for measuring conccentrated solar flux) are connected to a two-channel recorder for continuous recording.

The incident solar flux on the solar concentrator is given by

$$q = q_{in} A_c \text{ Cos } \Theta$$

where A_c is the area of the concentrator

and Θ is the incident angle, the method of evaluating this angle is already explained in previous chapters and,

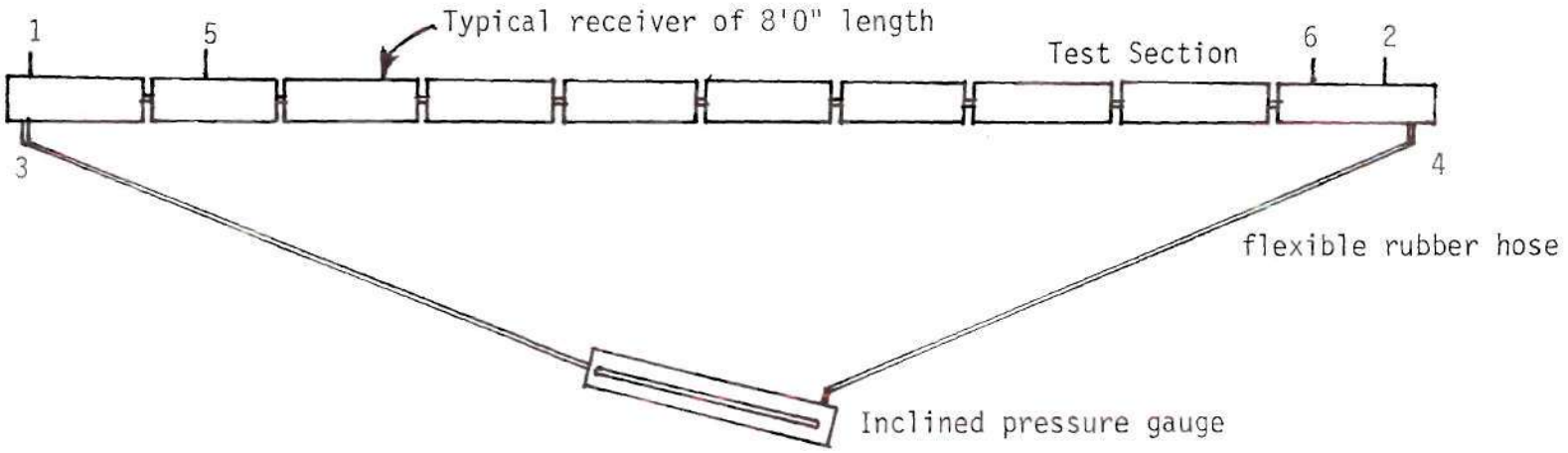

1,2. Thermocouples
3,4. Taps for measuring pressure drop
5,6. Taps for measuring mean velocity of air.

Figure 1. Air Heat Exchanger Experimental Arrangement

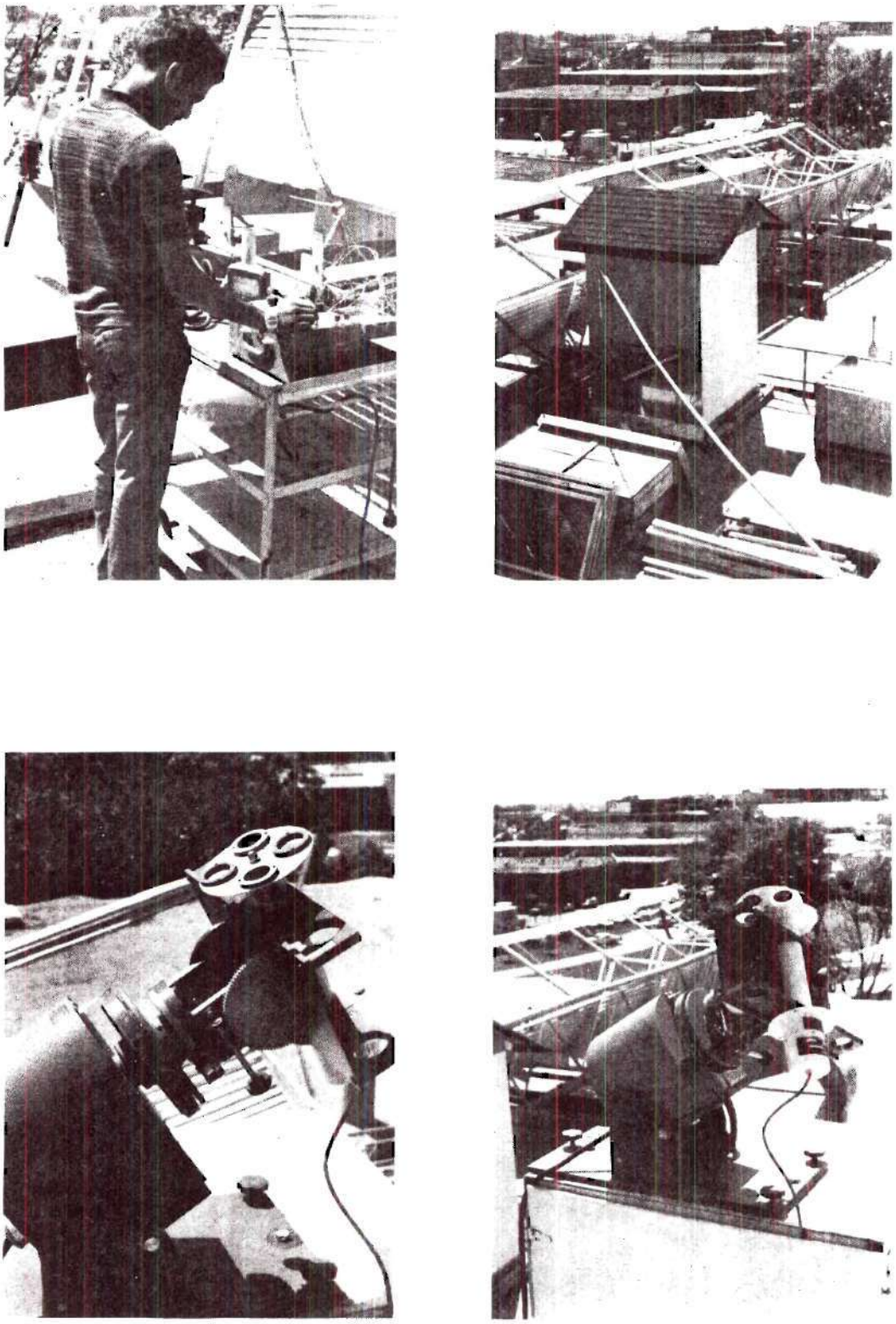

Figure 2. Instrumentation

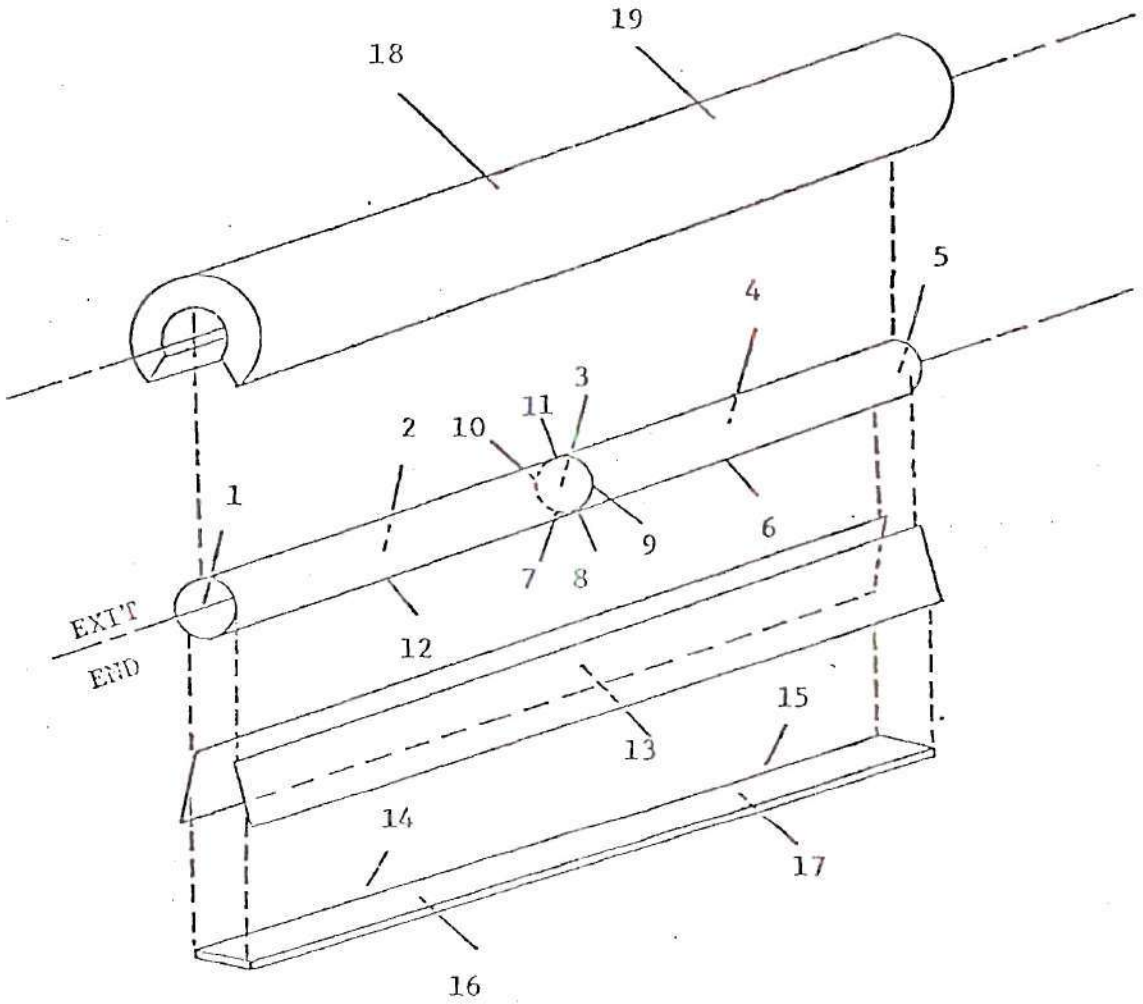

Figure 3. Location of Thermocouples

Table 1. Location of Thermocouples

Number	Location
1	center of air flow, at exit end of pipe
2	center of air flow, 2 feet from exit
3	center of air flow, center of pipe
4	center of air flow, 2 feet from entrance
5	center of air flow, at entrance end of pipe
6	center of blackened surface, 1 foot from entrance
7	center of blackened surface, center of pipe
8	45° around pipe from no. 7
9	90° around pipe from no. 7
10	135° around pipe from no. 7
11	180° around pipe from no. 7
12	center of blackened surface, 1 foot from exit
13	on terminal concentrator at center of pipe in stagnant air gap
14	center of stagnant air gap, 1.5 feet from exit
15	center of stagnant air gap, 1.5 feet from entrance
16	center of transparent cover, 2 feet from exit
17	center of transparent cover, 2 feet from entrance
18	center of cover back side, 1.5 feet from exit
19	center of cover back side, 1.5 feet from entrance
20	in ambient air

q_{in} is the solar flux as measured by the pyroheliometer.

The heat gained by the air is given by

$$q_u = \dot{m}\ Cp\ (T_{exit} - T_{in})$$

where $\dot{m}$ = mass flow rate of air and is given by

$$= 0.9 \times V_c \times \frac{\pi}{4} \times d^2 \times \rho_m \text{ (as it is a turbulent flow)}$$

where V_c = velocity of air at the center of the duct as measured by a velometer.

d = diameter of duct

and ρ_m = mean density of air = $\frac{V_{in} + V_{exit}}{2}$

The collection efficiency is then given by $\frac{q_u}{q}$. The frictional power losses are calculated from the expression:

$$W = \Delta P \times 0.9 \times V_c \times \frac{\pi}{4} \times d^2$$

The results of collection efficiency, frictional power losses (or pumping power) and plate temperature vs the flow rate are shown in Figures 4-8.

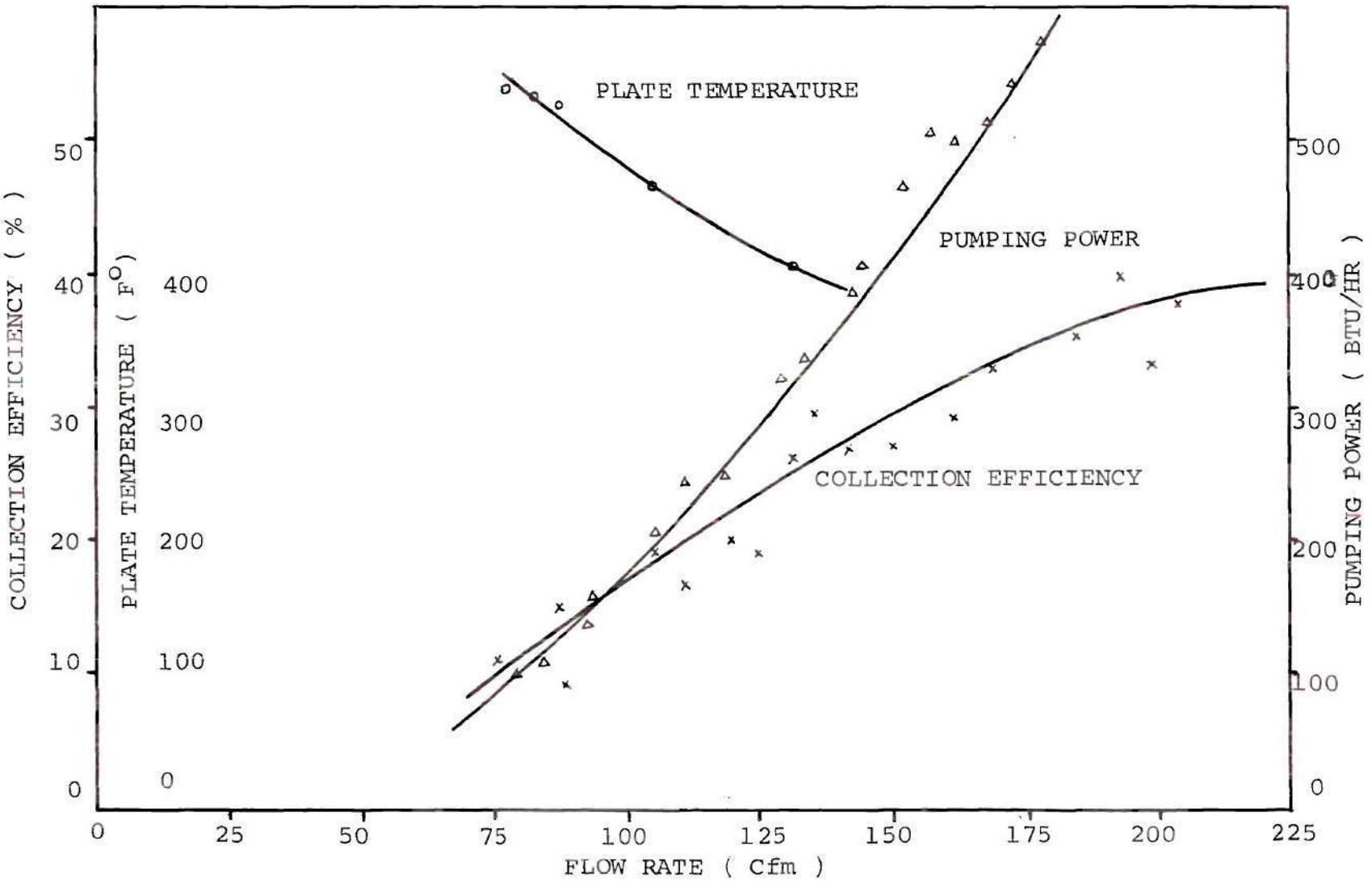

Figure 4. Performance Curves of Air-heat Exchanger.

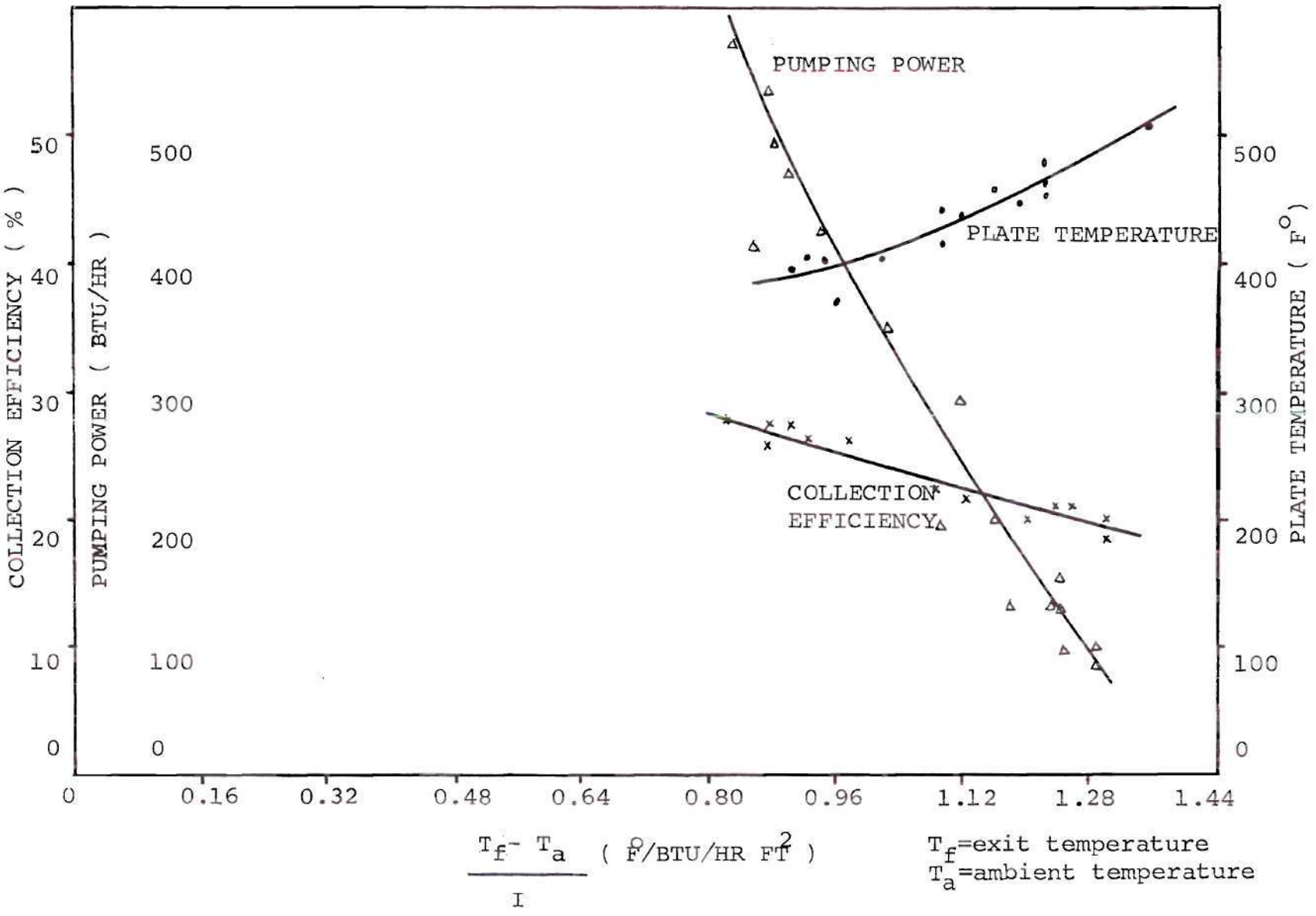

Figure 5. Experimental Data on Air-heat Exchanger.

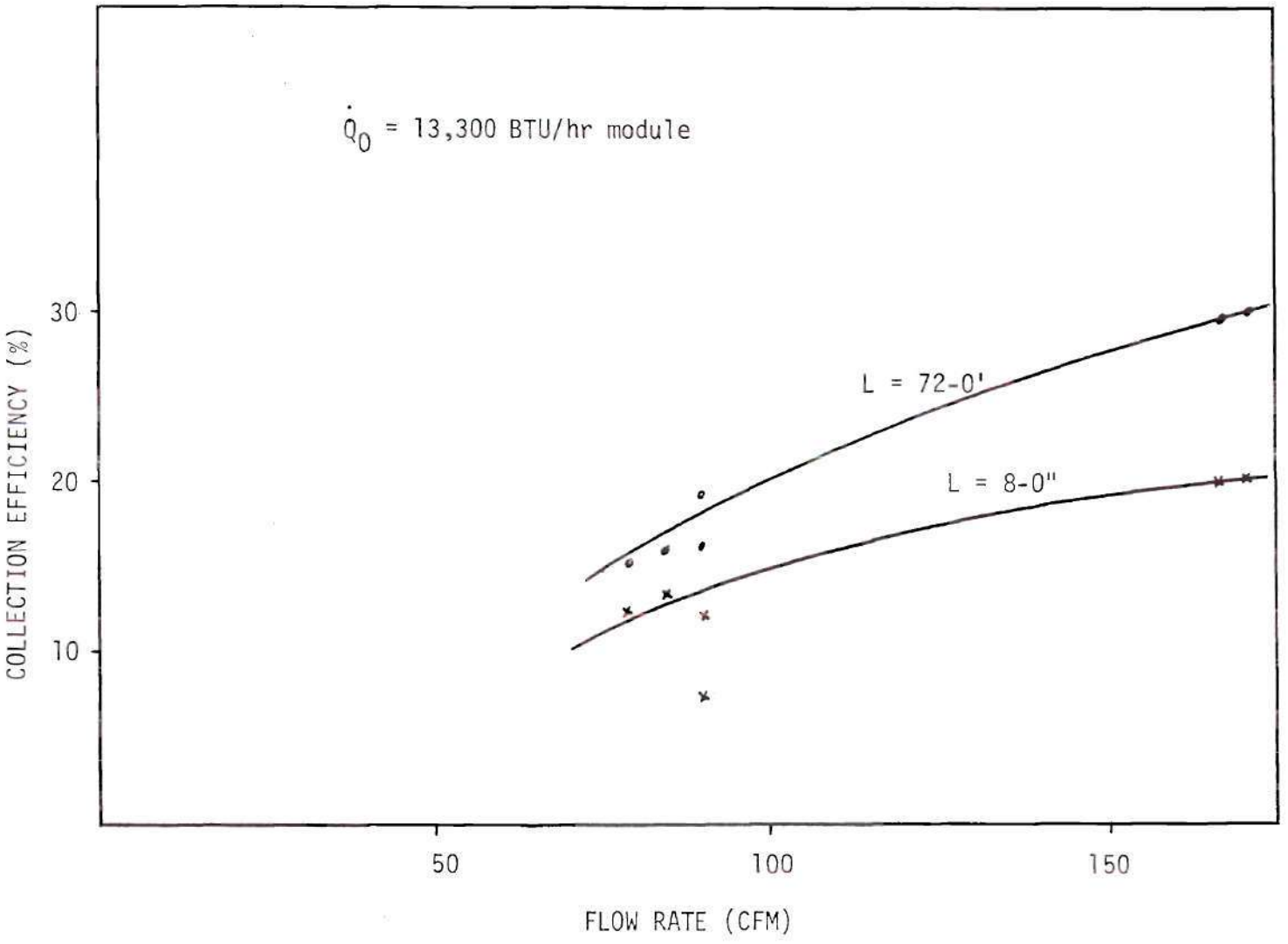

Figure 6. Comparison of Air-heat Exchangers of Different Lengths.

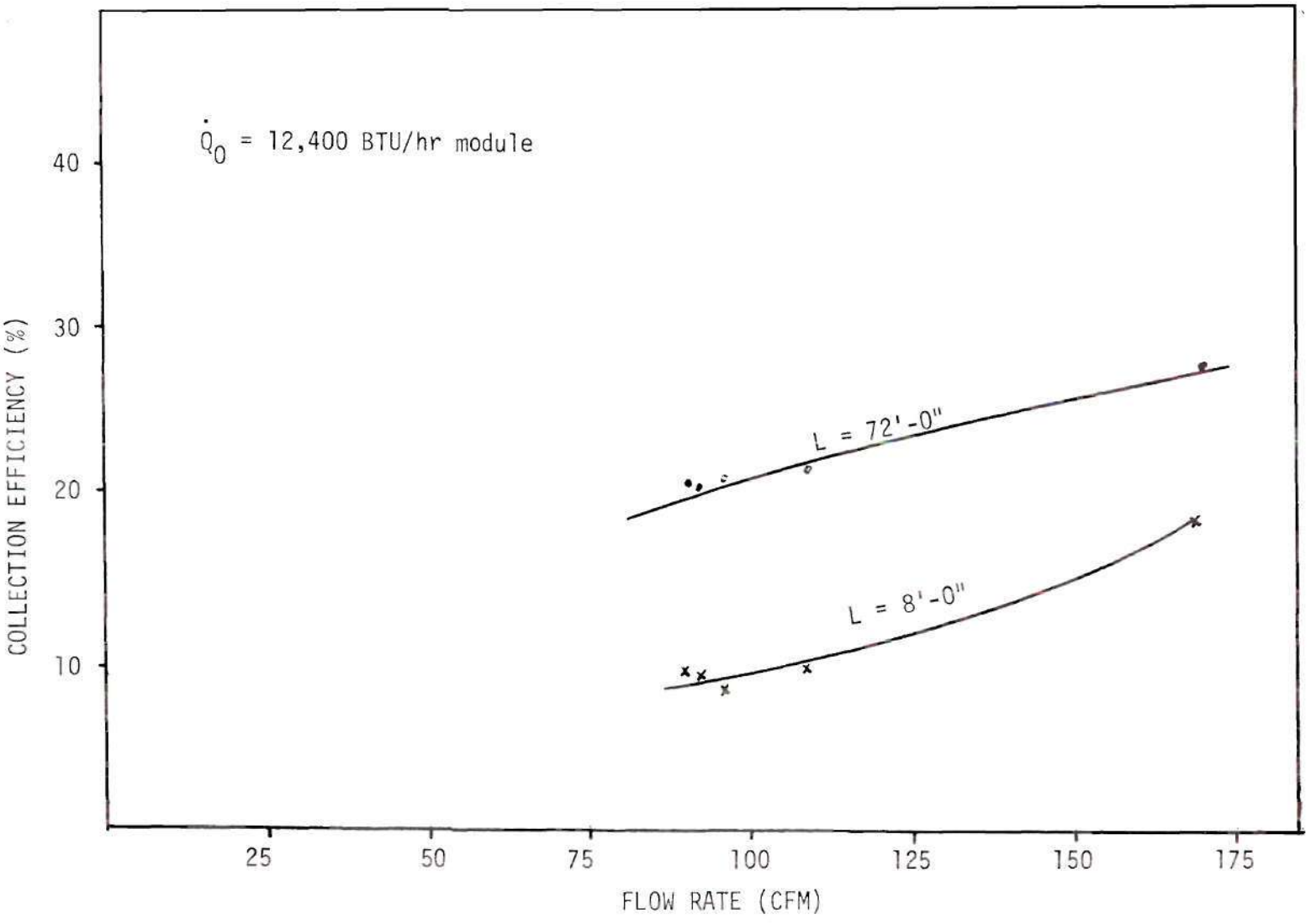

Figure 7. Comparison of Air-heat Exchangers of Different Lengths.

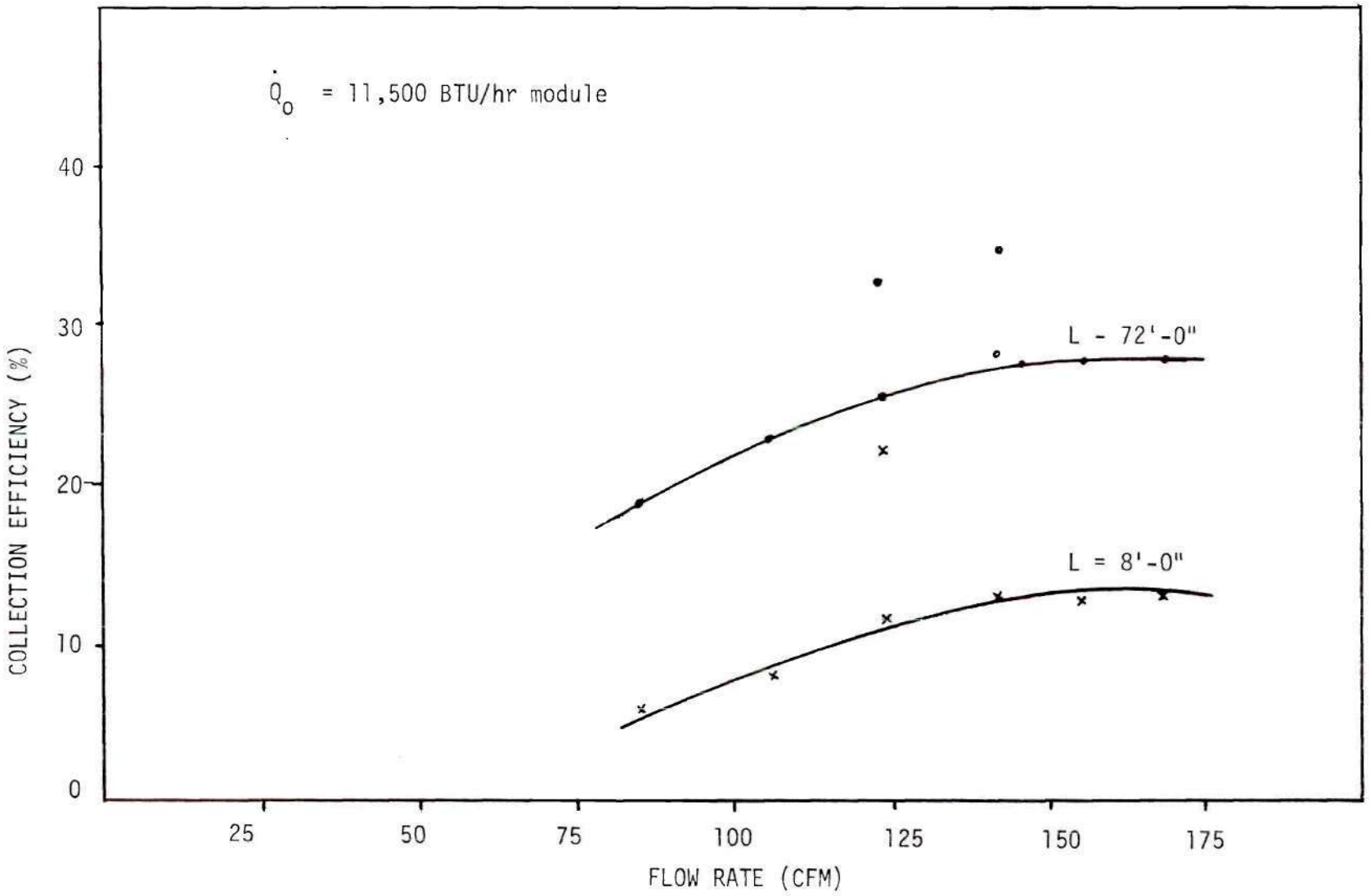

Figure 8. Comparison of Air-heat Exchangers of Different Lengths.

EXPERIMENTAL PROCEDURE

The blower is always started before the air heat exchanger is brought into focus. The automatic switch for the sun tracking mechanism is put on. The pyroheliometer is adjusted as follows:

1. connect the pyroheliometer to the power supply,
2. set the declination angle seal for that day's declination,
3. adjust the tube such that the white image falls on the black spot as shown on the disc of the pyroheliometer,
4. adjust and set the hour angle to the local time,
5. connect the output cords of the pyroheliometer to the chart recorder and the time of connection is recorded,

The wind velocity instrument is also switched on. The butterfly valve is adjusted and set at an initial position. The velocity of air at the center of the duct is measured at two different locations of the duct. One is near entrance and the other at the end of the heat exchanger. The flow rate is computed from the mean of these two velocities. The air leakage is minimized by applying the silicone glue at the duct joints. Thermocouples readings are recorded very rapidly for a particular flow rate. The time at which the thermocouple readings are taken, should be recorded to check later the corresponding incident solar flux from the pyroheliometer recording chart. The corresponding pressure drop across the heat exchanger is recorded for each flow rate position. This procedures is repeated for varying positions of flow rates. Care

is taken to see that the thermocouple readings are taken in shortest possible time. The thermocouple data should be discarded if a cloud casts a shadow on the concentrator during the time that data are taken.

APPENDIX B

THERMAL ANALYSIS OF RECEIVERS

Derivation for the Exit Fluid Temperature of the Receiver Fluid

The absorber plate of the receiver is further divided into 3 regimes as shown in Figure 1.

For region i = o

$$x \text{ varies from o to } \frac{w-d}{2}$$

The governing equation for heat conduction across the plate in x-direction is given by

$$\frac{\partial^2 \Psi_i}{\partial \xi_i^2} - n^2 \Psi_i = 0 \tag{1}$$

where

$$\Psi_i = \frac{T_i - T_a - (S/U_L)}{T_{bi} - T_a - (S/U_L)} \tag{2}$$

and

$$\xi_i = \frac{x - [(i-1)\, w + (w + D)/2]}{(w - D)} \tag{3}$$

i refers to the type of regime as shown in Figure 1

$$n^{\sim} = U_L\, (w - D)^{\sim}/k\delta$$

T_{bi} = Temperature of the tube surface of the absorber plate assumed uniform

For regime i = 0

The ξ_i varies from 1/2 to 1 corresponding to the variable x_i = 0 to $\frac{(w-d)}{2}$

Equation (1) is obtained through balance of energy on an element of the plate.

S = is the absorbed solar energy per unit area.

U_L = heat loss co-efficient of the absorber plate w.r.t. ambient temperature at T_a.

This heat loss co-efficient takes into account the heat conduction and radiational losses from absorber plate to the glass envelope and also the heat conduction and radiation losses from glass envelope to the environment. The corresponding thermal network for U_L is shown in Figure 2.

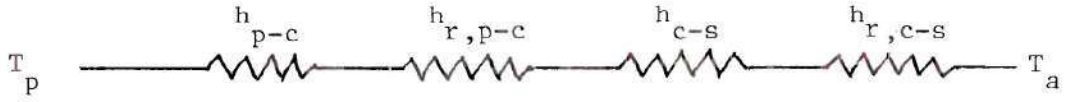

Figure 2. Thermal Resistance Circuit

$$U_L = \frac{2}{(h_{p-c} + h_{r,p-c})^{-1} + (h_{c-s} + h_{r,c-s})^{-1}} \qquad (4)$$

where h_{p-c} = heat loss co-efficient due to heat conduction for absorber plate to glass cover.

$h_{r,p-c}$ = heat loss co-efficient due to heat radiation from

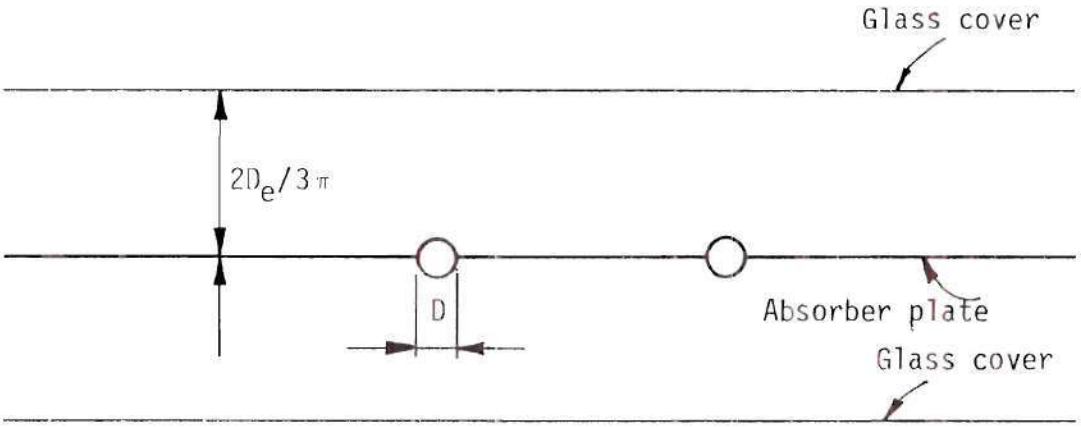

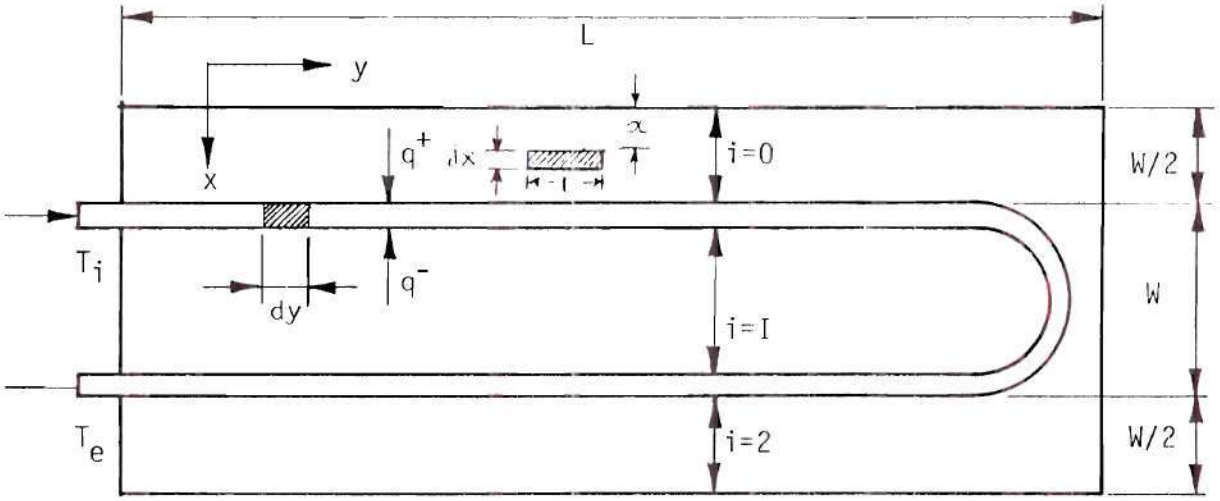

Thermal Analysis of Absorber Plate

absorber plate to glass cover.

h_{c-s} = heat loss co-efficient due to heat convection from the glass cover to the environment.

$h_{r,c-s}$ = heat loss co-efficient due to heat radiation from the glass cover to the environment.

The 2 in numerator of equation accounts for the heat losses on both sides of the absorber plate.

The general solution to equation (1) is written as

$$\Psi_i = C_1 \cos h\, n\, \xi_i + C_2 \sin h\, n\, \xi_i \tag{5}$$

The boundary conditions for regime i = 0 are

at $\xi_i = 1/2$ $\Psi_i = 1$ (6)

$\xi_i = 1/2$ $\frac{d\Psi_i}{d\xi_i} = 0$ (7)

$\xi_i = 1$ $\Psi_i = \frac{\Theta_{i+1}}{\Theta_1}$ (8)

where $\Theta_i = T_{bi} - T_a - (S/U_L)$

$$\frac{d\Psi_i}{d\xi_i} = nc_1 \sin h\, n\, \xi_i + n\, c_2 \cos h\, n\, \xi_i \tag{9}$$

From equations (6), (7) and (9) we get

$$\Psi_i = \cos h\, \frac{n}{2} \cos h\, n\, \xi_i - \sin h\, \frac{n}{2} \sin h\, n\, \xi_i \tag{10}$$

i.e.

$$T_{po}(x) = T_a + S/U_L + T_{ed} \{\cos h \frac{n}{2} \cos h\ n\ \xi_i - \sin h \frac{n}{2} \sin h\ n\ \xi_i\} \quad (11)$$

Equation (11) gives the temperature distribution of the plate in regime

$i = 0$

T_{ed} = is the left edge temperature at $x = 0$ or $\xi_i = 1/2$

The expression for T_{ed} is obtained later by using boundary condition (8) and the expression for Θ_2.

For region $i = 1$, range of $\xi_i = 0$ to 1

$$x \text{ varies from } \frac{w+D}{2} \text{ to } \frac{3w-D}{2}$$

The governing equation remains the same as in case of $i = 0$.

The general solution is again:

$$\Psi i = C_1 \cos h\ n\ \xi_i + C_2 \sin h\ n\ \xi_i \quad (12)$$

The boundary conditions are:

$$\text{at} \qquad \xi_i = 0\ ; \qquad \Psi_i = 1 \quad (13)$$

$$\xi_i = 1\ ; \qquad \Psi_i = \frac{\Theta_{i+1}}{\Theta_i} \quad (14)$$

From equations (12), (13) and (14), we get:

$$\Psi_i = \cos h\, n\, \xi_i + \frac{\left(\frac{\Theta_2}{\Theta_1} - \cos h\, n\right)}{\sin h\, n} \sin n\, \xi_i \qquad (15)$$

and $$T_{p1}(x) = T_a + \left(\frac{S}{U_L}\right) + \Theta_i \left\{\frac{(\Theta_2/\Theta_1) - \cos h\, n}{\sin h\, n}\right\} \sin h\, n\, \xi_i \qquad (16)$$

Equation (16) gives the expression for temperature distribution of the absorber plate in regime i = 1 in terms of θ_2 , the plate temperature over the second tube surface assumed uniform. The expression for θ_2 is obtained as follows:

For region i = 2,

x varies from $\frac{3w+D}{2}$ to 2w and

ξ_i corresponds 0 to 1/2.

The governing equation is same as equation 1.

The boundary conditions are:

at $\xi_i = 0$; $\Psi_i = 1$ (17)

$\xi_i = 1/2$; $\frac{d\Psi_i}{d\xi_i} = 0$ (18)

Solving equation (1), (17), and (18) we get the solution as:

$$\Psi_i = \cos h\, n\, \xi_i - \tan h\, \frac{n}{2} \sin h\, n\, \xi_i$$

$$T_{p2}(x) = T_a + \left(\frac{S}{U_L}\right) + \Theta_2 \left(\cos h\, n\, \xi_i - \tan h\, \frac{n}{2} \sin h\, n\, \xi_i\right) \qquad (19)$$

Equation (19) gives the temperature distribution of the absorber plate in region i = 2.

The equations (11), (16) and (19) gives the temperature distribution of absorber plate from x = 0 to x = 2w. But these equations involve Θ_1 and Θ_2, the uniform temperatures of the absorber plate over tube 1 and 2 respectively. These variables are unknown, as they are related to heat transfer taking place within these tubes.

Useful Energy Gain to Heat Transfer Fluid

Referring to Figure 1:

$$q_1^+ = - \frac{k\delta\Theta_o}{(w-D)} \left.\frac{d\Psi_o}{d\xi_o}\right|_{\xi_o = 1} \tag{20}$$

$$\bar{q}_1 = + \frac{k\delta\Theta_1}{w-D} \left.\frac{d\Psi_1}{d\xi_1}\right|_{\xi_1=0} \tag{21}$$

Total heat flow rate per unit length entering the base of segment i, q_i is given by

$$q_i = q_i^+ + \bar{q}_i \tag{22}$$

From equation (20), (21) and (22) we get

$$q_1 = K \{[\Theta_2 - 2\Theta_1 \cos h\, n + K\, \Theta_1]\} \tag{23}$$

Now applying the heat balance on this tube surface,

$$q_{ui} = q_i - D\ U_L\ \Theta_i \tag{24}$$

i.e. $$q_{ul} = q_1 - D\ U_L\ \Theta_1 \tag{25}$$

but $$\Theta_i = \Theta_{fi} + R\ q_{ui} \tag{26}$$

where $$R = 1/h_f A_t$$

where $$\Theta_{fi} = T_{fi} - T_a - (S/U_L)$$

T_{fi} = Fluid temperature in segment i

From equations (23), (25) and (26) we get

$$q_{ui} = KA\ [\{1 - KR\ (1 + \gamma)\}\ \{(1 + \gamma)\ \Theta_{f1} + \Theta_{f2}\} + KR\ \{\Theta_{f1} + \Theta_{f2}\ (1 + \gamma)\}] \tag{27}$$

where $$A = \frac{1}{1 + K\tilde{R}\tilde{\gamma}\ (\gamma + 2) - 2\ KR\ (1 + \gamma)} \tag{28}$$

and $$\gamma = -2 \cos h\ n - (D\ U_L/K) \tag{29}$$

Similarly $$q_{u_2} = KA\ [\{KR\ \{(1 + \gamma)\ \Theta_{f1} + \Theta_{f2}\} + \{(1 + \gamma)\ \Theta_{f2} + \Theta_{f1}\}\ \{1 - KR\ (1 + \gamma)\}] \tag{30}$$

After simplifications we get

$$q_{u1} = KA\ [\theta_{f2} + \theta_{f1}\ (1 + \gamma)\ (1 - 2\ KR\ \gamma)] \tag{31}$$

$$q_{u2} = KA\ [\theta_{f1} + \{\theta_{f2}(1 + \gamma) - 2\ KR\ \gamma\ (1 - \gamma)\}] \tag{32}$$

From equations (26), (31) and (32) we get

$$\theta_1 = T_{b1} - T_a - \frac{S}{U_L} = \theta_{f1} + R\ KA\ [\theta_{f2} + \theta_{f1}(1 + \gamma)\ (1 - 2\ KR\ \gamma)] \tag{33}$$

$$\theta_2 = T_{b2} - T_a - \frac{S}{U_L} = \theta_{f2} + R\ KA\ [\theta_{f1} + \theta_{f2}(1 + \gamma)\ (1 - 2)KR\ \gamma)] \tag{34}$$

Fluid Temperature Variation

The governing equation for the heat transfer of fluid is given by

$$\frac{d\Phi_i}{d\eta} + (-1)^i \frac{L}{\dot{m}C_p}\, q_{ui} = 0 \tag{35}$$

where $$\Phi_i = \frac{\theta_{fi}}{\theta_{f1}} \Big|_{\eta = 0}$$

and $$\eta = \frac{y}{L}$$

Let $$a = \frac{-KL}{\dot{m}Cp}$$

$$b = KR\ (1 + \gamma) - 1$$

Then from equations (31), (32) and (35) we have

$$\frac{d\Phi_1}{d\eta} = a\ [\{b\ (1 + \gamma)\ \Phi_1\} - KR(\Phi_1 + \Phi_2(1 + \gamma)\}] \tag{36}$$

$$\frac{d\Phi_2}{d\eta} = ab\ (1 + \gamma)\ \Phi_1 + ab\ \Phi_2 - a\ kR\ \Phi_1 - a\ kR\ \Phi_2(1 + \gamma) \tag{37}$$

Solving two simultaneous differential equations (36) and (37) we have

$$\Phi_1 = \ell_1 e^{\lambda_1 \eta} + \ell_2 e^{\lambda_2 \eta} \tag{38}$$

$$\Phi_2 = \ell_1[(\beta_1 + \lambda_1)/\beta_2]\ e^{\lambda_1 \eta} + \ell_2[(\beta_1 + \lambda_2)/\beta_2]\ e^{\lambda_2 \eta} \tag{39}$$

where

$$\lambda_1 = (\beta_1^{\sim} - \beta_2^{\sim})^{0.5}$$

$$\lambda_2 = -\lambda_1$$

$$\ell_2 = (\beta_1 + \lambda_1 - \beta_2)/[(\beta_2 - \beta_1 + \lambda_1)e^{-2\lambda_1} + (\beta_1 + \lambda_1 - \beta_2)]$$

$$\ell_1 = 1 - \ell_2$$

and $$\beta_1 = \frac{LK}{\dot{m}Cp}\ \frac{[KR(1 + \gamma)^{\sim} - 1 - \gamma - KR]}{[[KR\ (1 + \gamma) - 1]^{\sim} - (KR)^{\sim}]}$$

$$\beta_2 = \frac{LK}{\dot{m}Cp}\ \frac{1}{\{[KR\ (1 + \gamma) - 1]^{\sim} - (KR)^{\sim}\}}$$

and $$K = \frac{K_T \, \delta\eta}{(w-D) \sin h \, n}$$

K_T = Thermal conductivity of absorber plate

Thus the exit temperature T_e, of the fluid is given by

$$\Phi_2 \Big|_{\eta = 0} = \frac{\Theta_{f2}}{\Theta_{f1}} \Bigg|_{\eta = 0} = (T_e - T_a - (S/U_L)/\{T_i - T_a - (S/U_L)\}$$

i.e. $$T_e = T_a + (S/U_L) + (T_1 - T_a - S/U_L) \, \Phi_2 \Big|_{\eta = 0}$$

Where Φ_2 can be computed from equation (39).

APPENDIX C

DETERMINATION OF MASS FLOW RATE OF RANKINE FLUID "W/O STORAGE"

Parallel Arrangement

The following five balance equations can be written for a system shown in Figure 21:

$$\dot{m}_1 c_1 (T_1 - T_i) = U_L \left(\frac{T_i + T_1}{2} - T_a \right) \quad (1)$$

$$\dot{m}_1 c_1 (T_e - T_i) = Q \eta_t \quad (2)$$

$$\dot{m}_1 c_1 (T_e - T_3) = U_L \left(\frac{T_e + T_3}{2} - T_a \right) \quad (3)$$

$$\dot{m}_1 c_1 (T_c - T_2) = \dot{m}_2 (h_4 - h_4 1) = \varepsilon_2 \dot{m}_1 c_1 (T_3 - T_4) \quad (4)$$

$$\dot{m}_1 c_1 (T_2 - T_1) = \dot{m}_2 c_2 (T_4 - T_c) = \varepsilon_1 \dot{m}_2 c_2 (T_2 - T_c) \quad (5)$$

When c_1 and c_2 are mean specific heats of fluids.

Let $\dot{m}_1 c_1 = x_1$ and $\dot{m}_2 c_2 = x_2$

Equation 1 can be written as

$$T_1 = a T_i - b$$

where

$$a = \frac{\dot{m}_1 c_1 + \frac{U\ell}{2}}{\dot{m}_1 c_1 - \frac{U\ell}{2}}$$

and

$$b = \frac{U_\ell T_a}{\dot{m}_1 c_1 - \frac{U\ell}{2}}$$

Equation (2) can be written as

$$T_i = T_e - \frac{a\eta_T}{x_1} \tag{8}$$

Where η_T = Thermal efficiency of the receiver

Equation (3) can be written as

$$T_e = a\, T_3 - b \tag{9}$$

From equation (7), (8) and (9) we have

$$T_1 = a \sim T_3 - \frac{aQ\eta_T}{x_1} - ab - b \tag{10}$$

Equation (4) can be written as

$$T_3 - \varepsilon_2\, T_3 = T_2 - \varepsilon_2\, T_4' \tag{11}$$

and equation (5) can be rewritten as

$$x_1\,(T_2 - T_1) = \varepsilon_1\, x_2\, T_2 - \varepsilon_1\, x_2\, T_c$$

$$(x_1 - \varepsilon_1\, x_2)\, T_2 = x_1\, T_1 - \varepsilon_1\, x_2\, T_c$$

$$T_2 = \frac{x_1\, T_1 - \varepsilon_1\, x_2\, T_c}{x_1 - \varepsilon_1\, x_2} \tag{12}$$

From equations (11) and L12)

$$T_3 - \varepsilon_2 T_3 = \frac{x_1 T_1 - \varepsilon_1 x_2 T_c}{x_1 - \varepsilon_1 x_2} - \varepsilon_2 T_4' \tag{13}$$

On substituting the equation (10) for T_1 in equation (13)

$$(x_1 - \varepsilon_1 x_2)(1 - \varepsilon_2) T_3 = x_1 (\tilde{A} T_3 - \frac{aQ\eta_T}{x_1} - ab - b) - \varepsilon_1 x_2 T_c - \varepsilon_2 T_4, (x_1 - \varepsilon_1 x_2)$$

$$T_3 = \frac{-aQ\eta_T - abx_1 - bx_1 - \varepsilon_1 x_2 T_c - \varepsilon_2 T_4, (x_1 - \varepsilon_1 x_2)}{\{(x_1 - \varepsilon_1 x_2)(1 - \varepsilon_2) - x_1 a\}} \tag{14}$$

Writing the balance equation for the whole heat exchanger

$$\dot{m}_2 (h_4 - h_c) = x_1 (T_3 - T_1) \tag{15}$$

From equations (10) and (15)

$$\dot{m}_2 (h_4 - h_c) = x_1 \left\{ (1 - \tilde{a}) T_3 + \frac{aQ\eta_T}{x_1} + ab + b \right\}$$

$$\dot{m}_2 (h_4 - h_c) = x_1 \left\{ (1 - \tilde{a}) f(x_2) + \frac{aQ\eta_T}{x_1} + ab + b \right\} \tag{16}$$

when $f(x_2) = T_3$ = as given by equation (14) (17)

Let $A = (1 - a)(aW + a b x_1 + b x_1 + \varepsilon_2 T_4, x_2)$ (18)

$$B = \frac{aQ\eta_T}{x_1} + ab + b \tag{19}$$

From equations (16), (17), (18) and (19)

$$\dot{m}_2 (h_4 - h_c) = \left[x_1 A + x_1 B (x_1 (a\sim - 1) + x_1 \varepsilon_2 + \varepsilon_1 x_2 (1 - \varepsilon_2) + \frac{x_2 \left\{ x_1 (1 - a\sim) \varepsilon_1 T_c^{-} - \varepsilon_1 \varepsilon_2 T_4' \right\}}{\left\{ x_1 (a^{\sim} - 1) + x_1 \varepsilon_2 + \varepsilon_1 x_2 (1 - \varepsilon_2) \right\}} \right] \quad (20)$$

$$C = x_1 B \left\{ x_1 (a^{\sim} - 1) + x_1 \varepsilon_2 \right\} \quad (21)$$

From equations (20) and (21)

$$\dot{m}_2 \left\{ \varepsilon_1 C_2)h_4 - h_c) (1 - \varepsilon_2) \right\} + \dot{m}_2 \left[(h_4 - h_c) \left\{ x_1 (a\sim - 1) + x_1 \varepsilon_2 \right\} - x_1 \varepsilon_1 C_2 B (1 - \varepsilon_2) + C_2 \varepsilon_1 \varepsilon_2 T_4' - x_1 (1 - a\sim) \varepsilon_1 C_2 T_c \right] - x_1 A - C = 0 \quad (22)$$

$$\dot{m}_2 = \frac{\sqrt{-\beta} \pm \sqrt{\beta^{\sim} - 4 D E}}{2D} \quad (23)$$

where $D = \varepsilon_1 C_2 (h_4 - h_c) (1 - \varepsilon_2)$

$$\beta = \left[(h_4 - h_c) \{ x_1 (a^{\sim} - 1) + x_1 \varepsilon_2 - x_1 \varepsilon_1 C_2 B (1 - \varepsilon_2) + C_2 \varepsilon_1 \varepsilon_2 T_4' - x_1 (1 - a^{\sim}) \varepsilon_1 C_2 T_c \right] \quad (25)$$

$$E = - (x_1 A + C) \quad (26)$$

Special Case

$\varepsilon_2 = 1.0$ then

$$\dot{m}_2 = \frac{\tilde{x_1}\ (1 - \tilde{a})\ T_4, + \tilde{x_1}\ \{-\frac{aQ\eta_T}{x_1} + ab + b\}}{\tilde{a}\ (h_4 - h_c)\ x_1 - x_1\ (1 - \tilde{a})\ \varepsilon_1\ \bar{C}_2\ T_c + C_2\varepsilon_1 T_4} \qquad (26)$$

When $T_4 = T_4'$ = Highest temperature of the Rankine fluid

T_c = Lowest temperature of the Rankine fluid

$\dot{m}_1$ = Flow rate of the receiver/collector fluid

Q = Heat flux on the receiver

η_T = Thermal efficiency of the receiver

For the given above variables, the flow rate of the Rankine fluid can be determined from the equation (26).

The above derivation for m_2 is for the parallel arrangement of the solar collector/receivers. A similar approach of analysis can be made for series arrangement of collectors as follows:

Series Arrangement

When the receivers are connected in series, the balance equations remain same as equations (1) through (5) except equation (2) which modified to include the individual efficiencies of receivers. Equation (2) can be rewritten for this case as

$$T_i = T_e - \frac{Q}{X}\ (\eta_1 + \eta_2 + \eta_3 + \ldots \eta_{10})$$

$$T_i = T_e - \frac{Q\eta}{x_1}$$

where $$\eta = 10 \times \bar{\eta}$$

$$\bar{\eta} = (\eta_1 + \eta_2 + \eta_3 + \ldots . \eta_{10})/10$$

and Q = Heat flux falling on one receiver unit.

Proceeding in similar lines, the expressions for m_2. The flow rate of rankine fluid can be obtained for a special case of $E_2 = 1.0$ as

$$\dot{m}_2 = \frac{\tilde{x_1} T_4 (1 - a) + (b \tilde{x_1} + a x_1 Q \bar{\eta}}{x_1 a (h_4 - h_c) + x_1 (1 - a) c_1 C_2 (T_4 - T_c)}$$

APPENDIX D

FREE CONVECTION EFFECTS

It is indicated in reference [41] that for a system of parallel plates the free convection effects are negligible when the Raleigh No. is less than 1700.

Raleigh No. = Grashoff's No. x Prandtle No.

$$\text{Ra No.} = \frac{\beta\, g\, (T_w - T_e)\, L^3\, P^{\sim}\, C_p}{K\, \mu}$$

Where $\beta = \frac{1}{\nu} \left(\frac{\partial \nu}{\partial T}\right)_p$

At low pressure air can be treated as an ideal gas $P\nu = RT$

$$P = \rho\, R\, T$$

$$\beta = \frac{1}{\nu} \left(\frac{R}{P}\right) = \frac{R}{P\nu} = \frac{1}{T}$$

$$\text{Ra No} = \frac{g \left(T_\omega - T_e\right) L^3\, \rho^2\, Cp}{T\, K\, \mu}$$

where $T = (T_w + T_e)/2$

T_w = Plate wall temperature

T_e = glass envelope temperature

Assuming $T_w = 450°F$

and $T_e = 150°F$

then $T = 300°F$

After balancing the units, the expression for Ra. No. becomes

$$\text{Ra. No.} = \frac{1.1592 \times 10^{5} \, (T_{\omega} - T_{e}) \, L^{3} \, \rho^{2} \, C_{p}}{(T_{\omega} + T_{e}) \qquad \kappa \, \mu}$$

But $\rho = \frac{P}{RT}$

Substituting the values of properties at = 300°F into the above equation, the P_c, critical pressure below which the free convection effects are negligible is found to be

$P_c = 43.896$ psf

or $P_c = 0.30476$ psi

or $P_c = 15.75$ Torres.

However, in the analysis the pressure inside the receiver tube was assumed to be

$P = 0.0021168$ psf

This much pressure is much smaller than the critical pressure and hence the assumption that the free convection is negligible is justified.

APPENDIX E - FLOW CHART OF THE COMPUTER PROGRAM FOR THE THERMAL ANALYSIS OF RECEIVERS

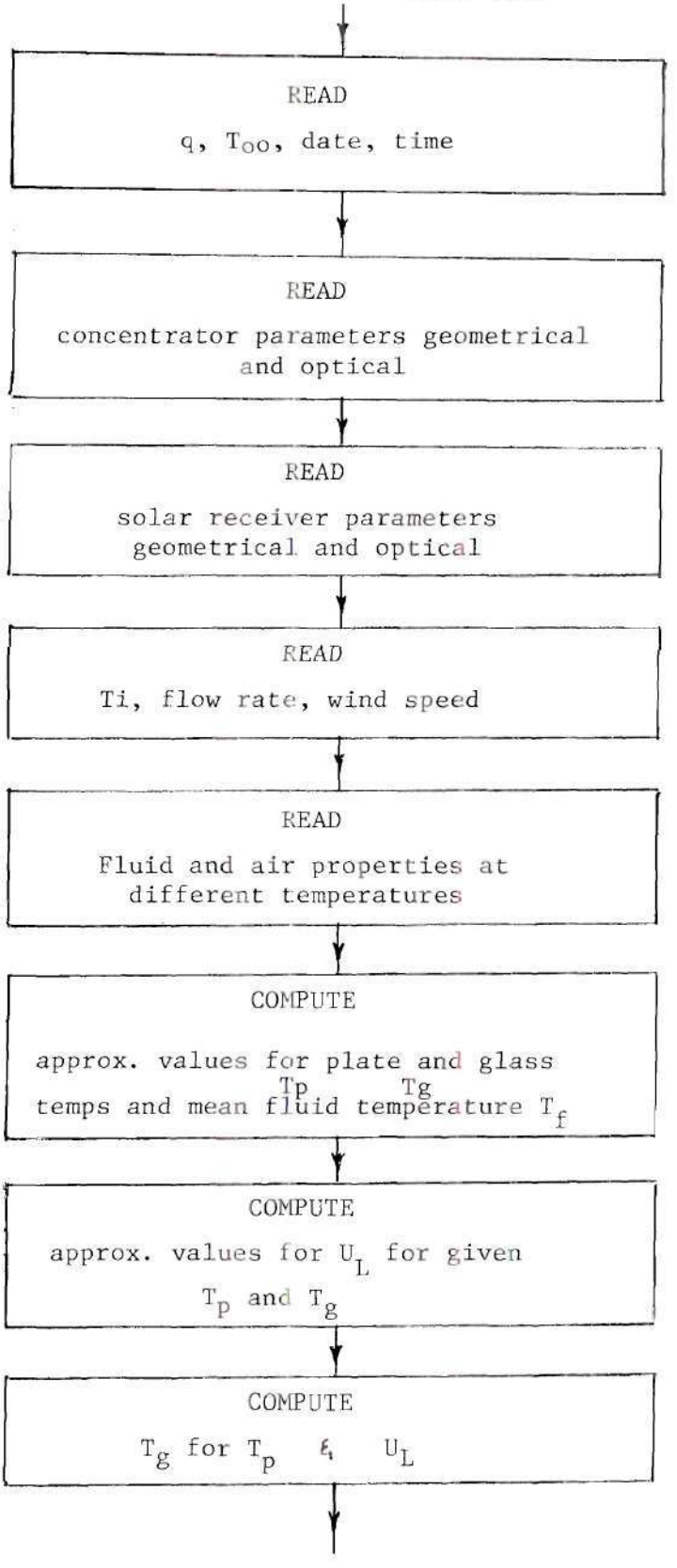

(continued on next page)

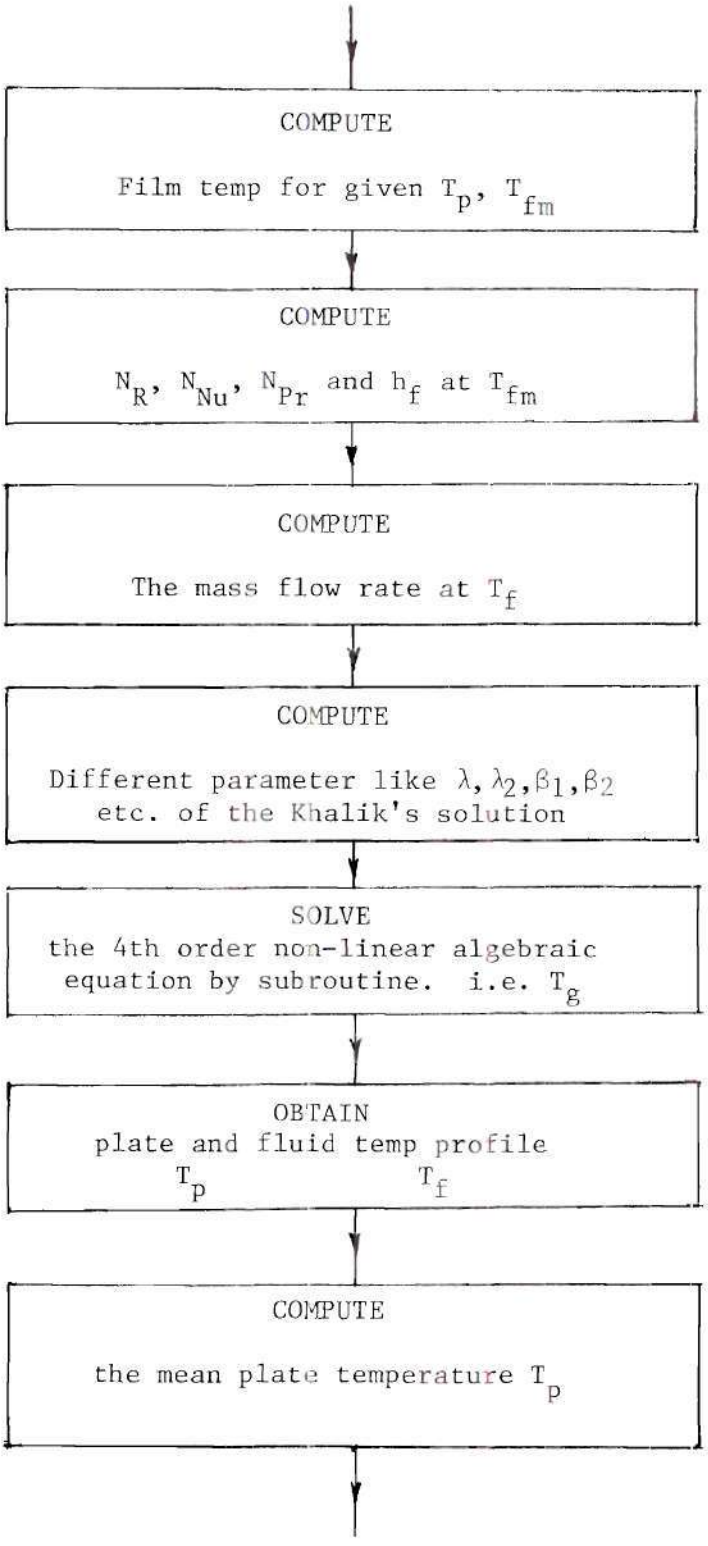

(Continued on next page)

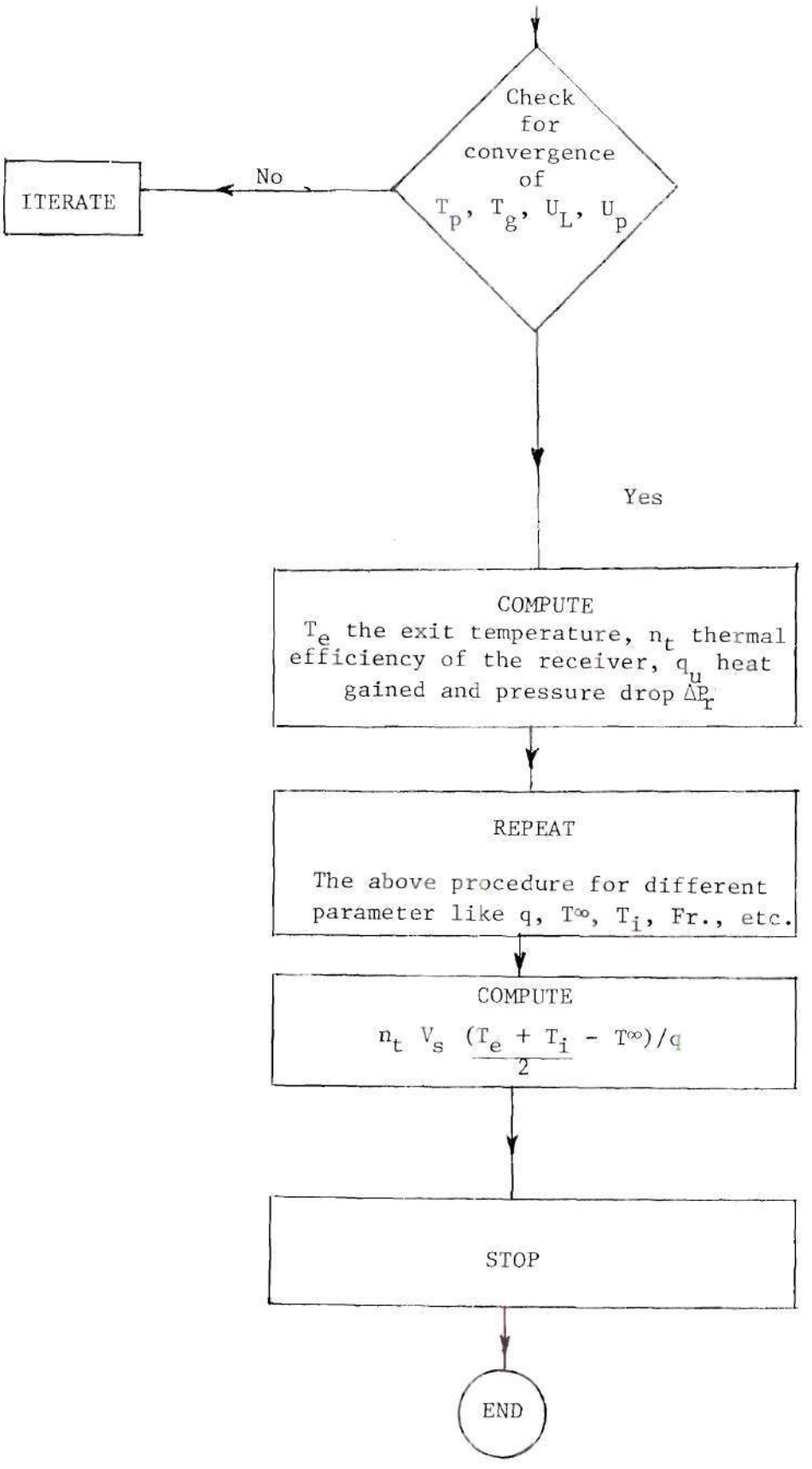
Check for convergence of T_p, T_g, U_L, U_p
No
ITERATE
Yes
COMPUTE T_e the exit temperature, n_t thermal efficiency of the receiver, q_u heat gained and pressure drop ΔP_r
REPEAT
The above procedure for different parameter like q, T^∞, T_i, Fr., etc.
COMPUTE
$n_t \ V_s \ \frac{(T_e + T_i}{2} - T^\infty)/q$
STOP
END

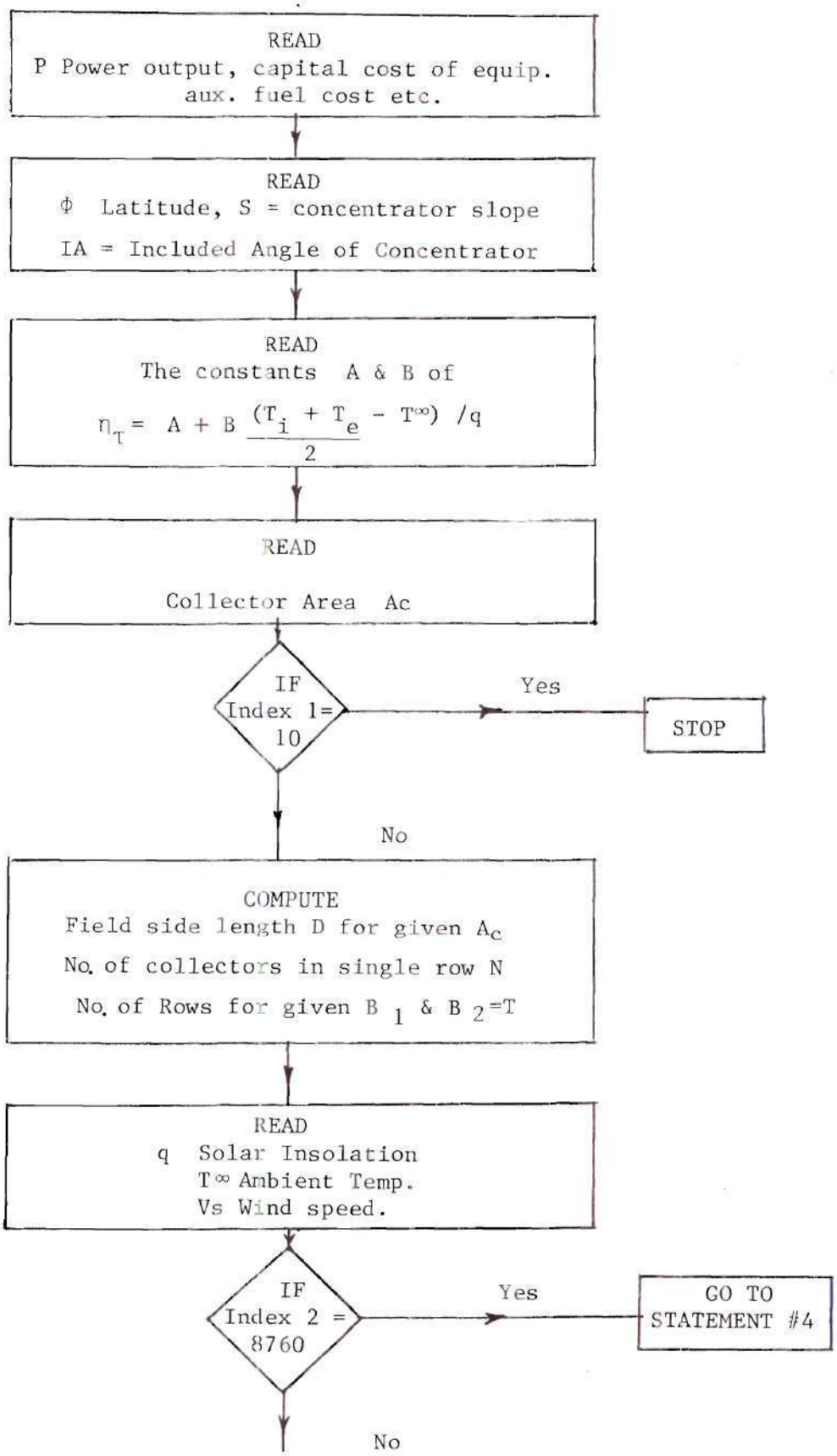

(Continued on next page)

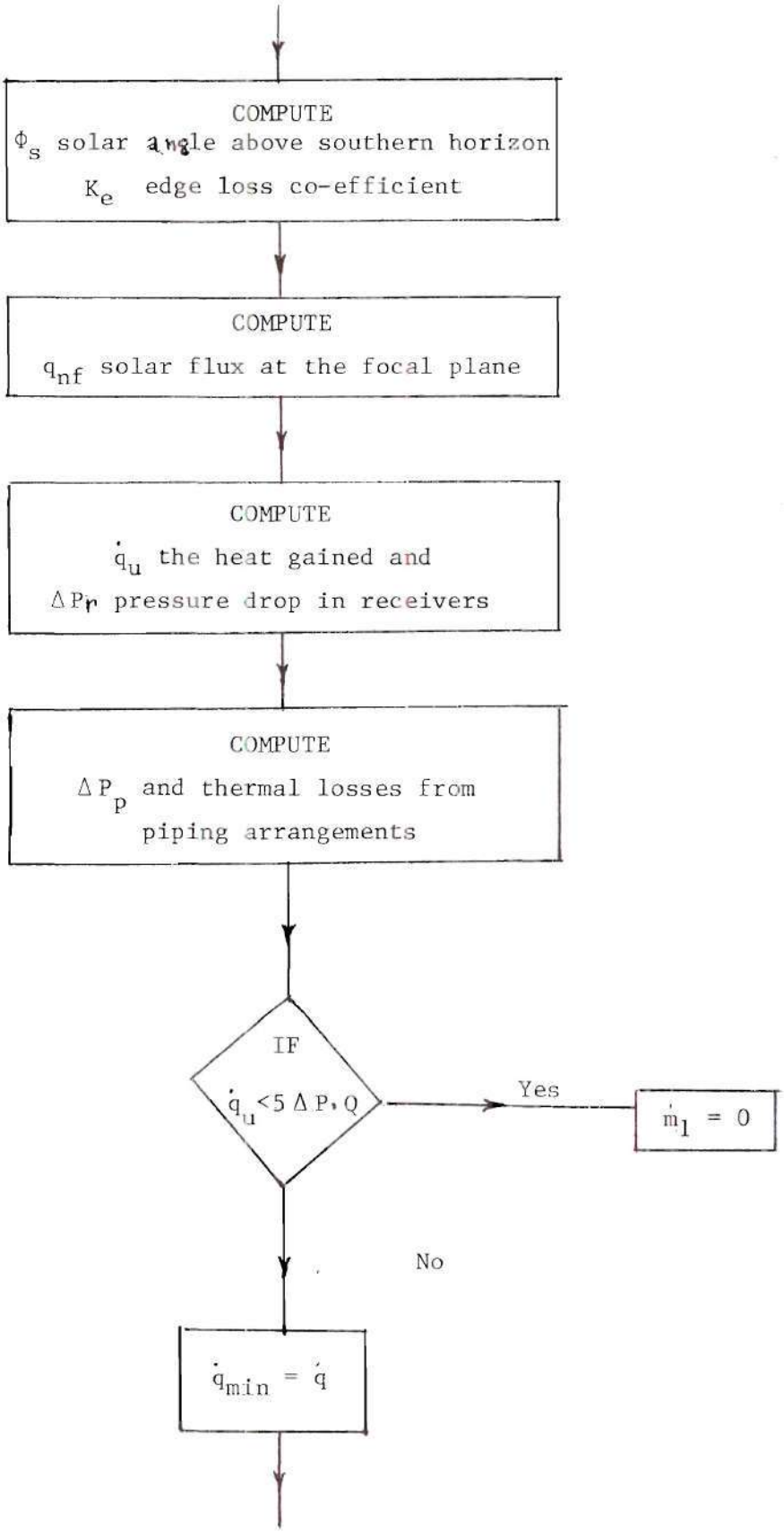

(Continued on next page)

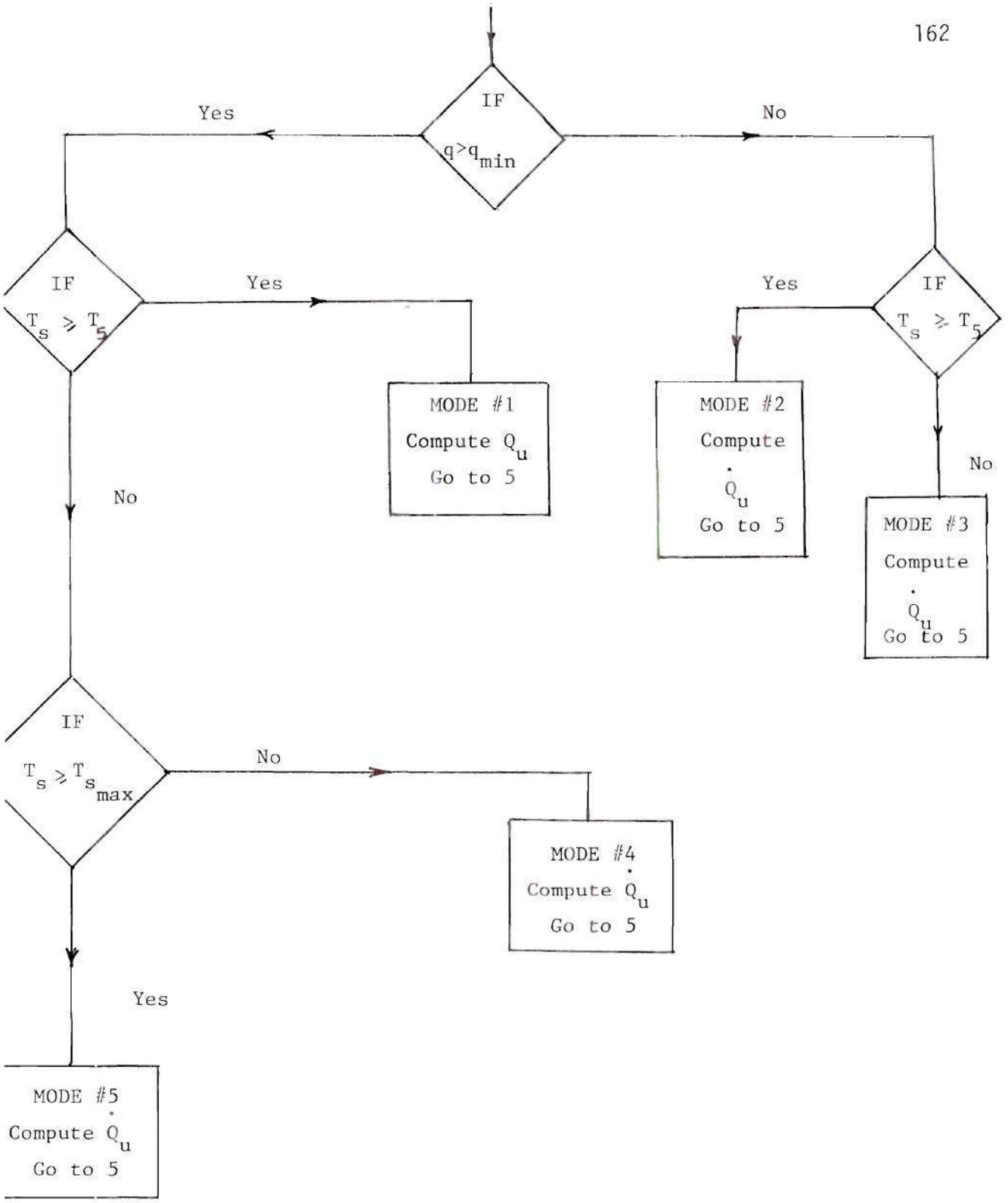

(See the figures following flow-charts for explanation of different modes.)

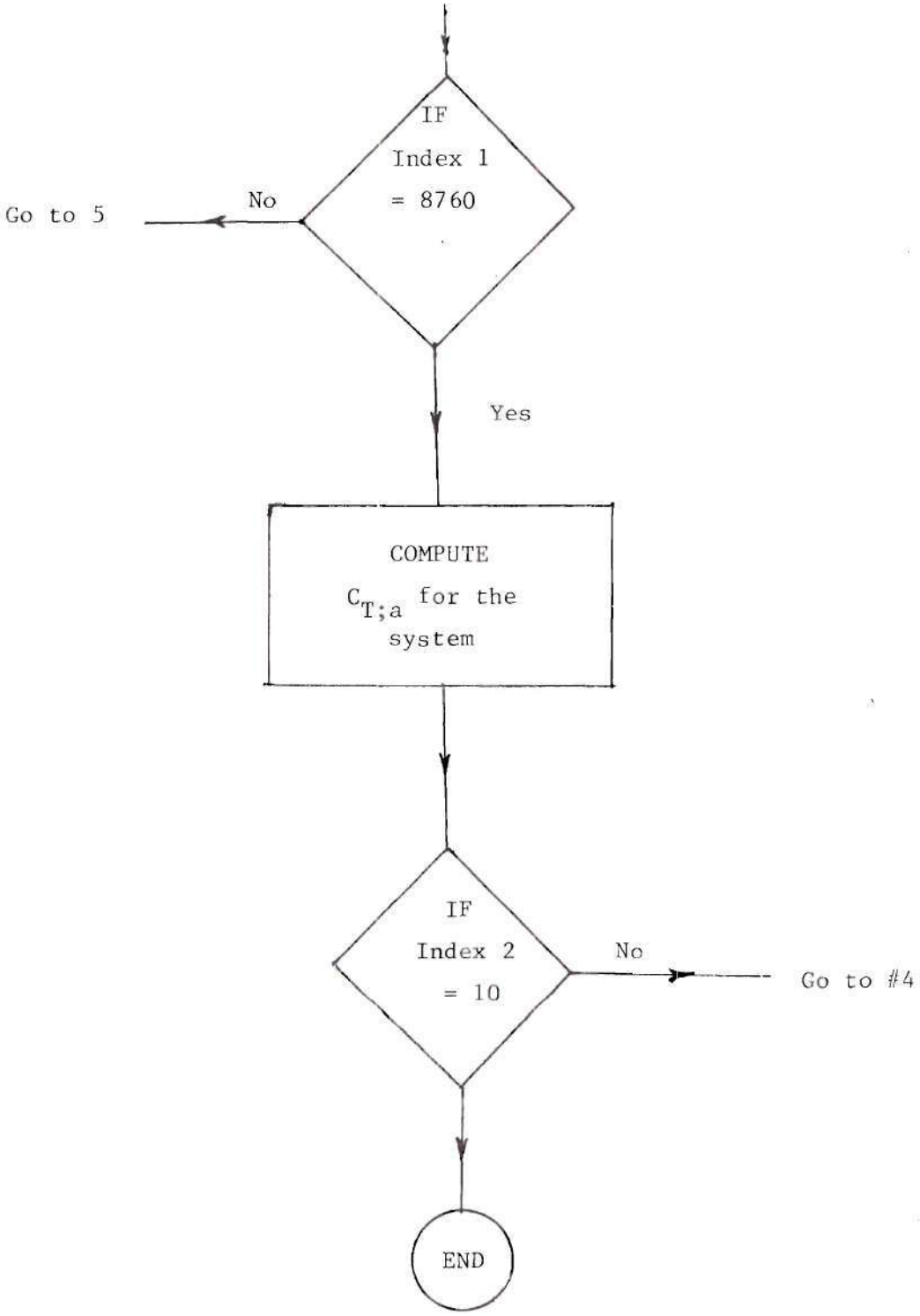
IF
Index 1
= 8760
No
Go to 5
Yes
COMPUTE
$C_{T;a}$ for the
system
IF
Index 2
= 10
No
Go to #4
END

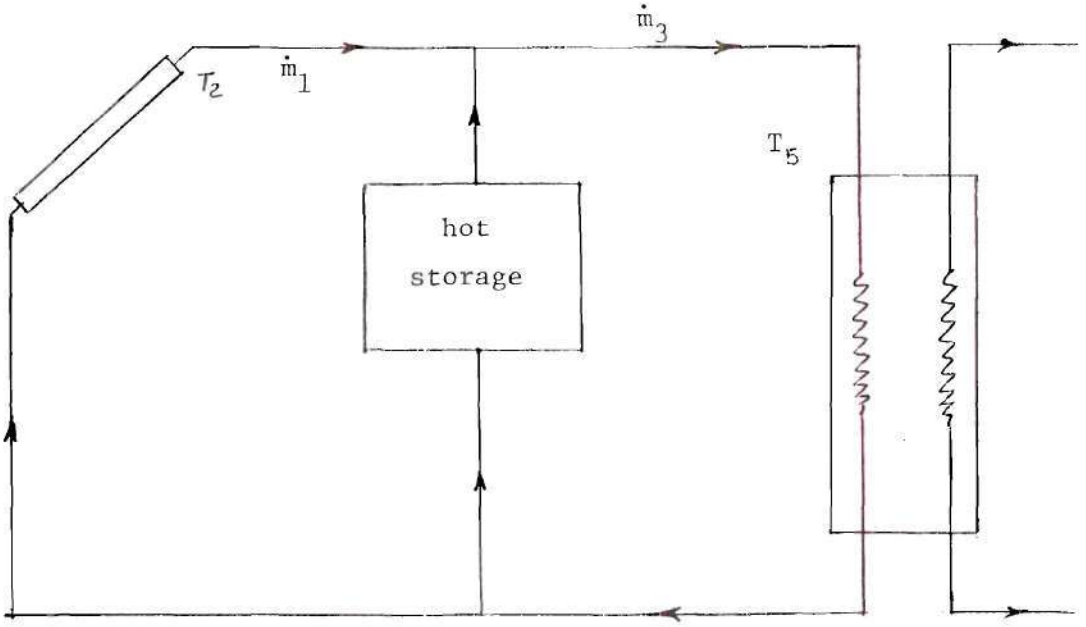

MODE: 1

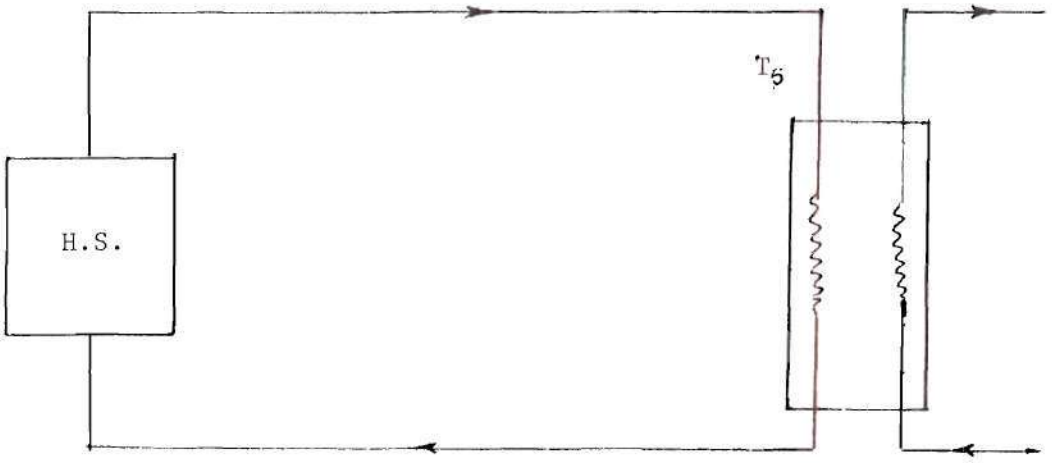

MODE: 2 & 6

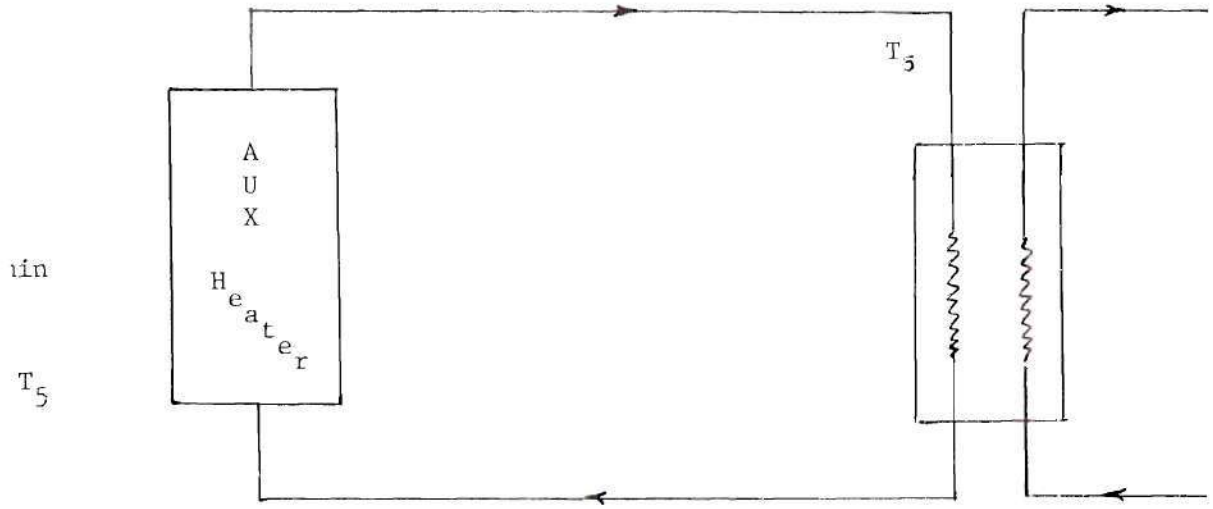

MODE #3

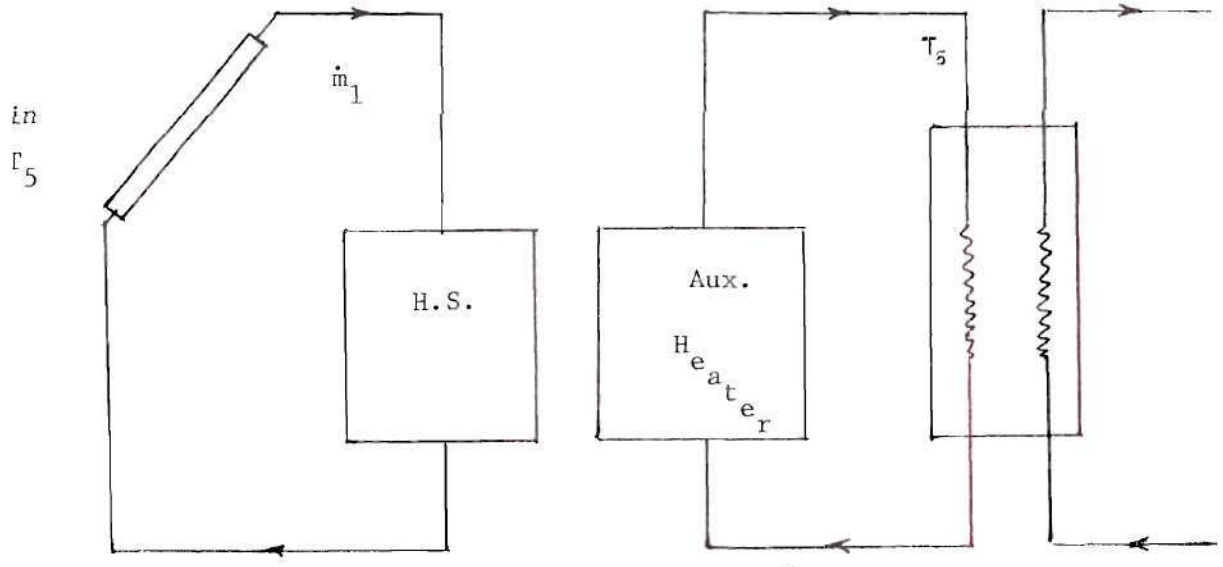

MODE #4

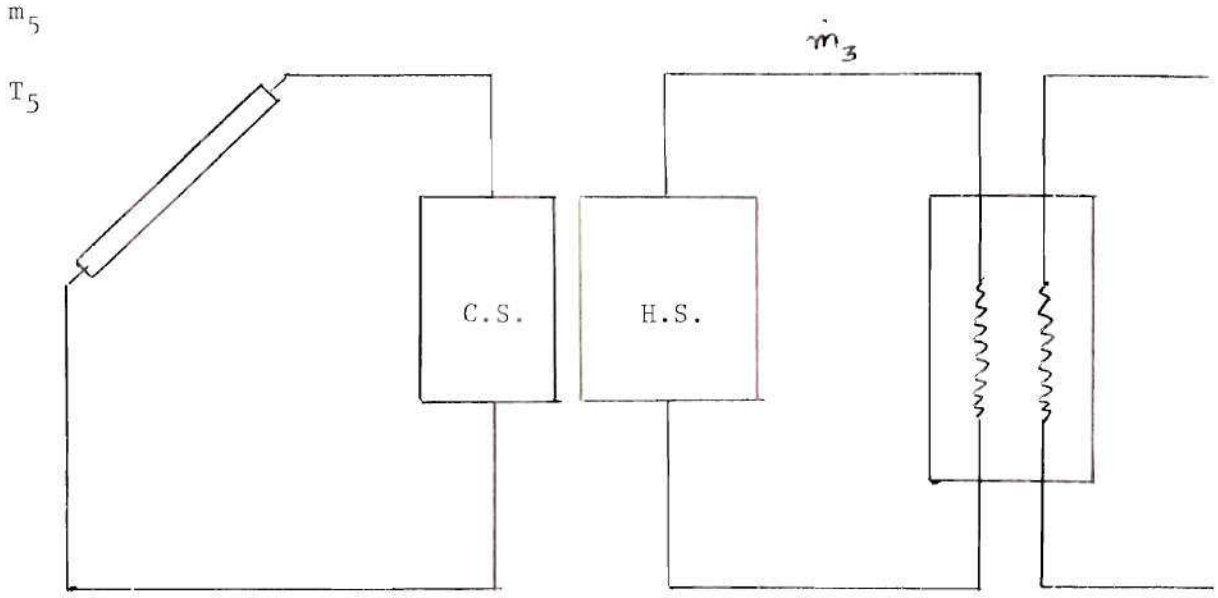

MODE #5

```
PROGRAM MAIN      73/74   OPT=1                    FTN 4.6+428      76/12/06. 16.12.10

      1           PROGRAM MAIN(INPUT,OUTPUT,TAPE5=INPUT,TAPE6=OUTPUT)
                  DIMENSION T(25),TF1(25),THC(7),VIS(7),DEN(7),CP(7),ATHC(7),AVIS(7)
                 1,ADEN(7),ACP(7),TEM(7),      PH(12),TF2(25),EWR(7),WT(5),CTP(3,3)
                 1,DIS(3),A(5),B(4),DR(4),Z(4),GLT(25),HPR(100),UTL(100),TC(100)
      5           REAL KT,L,KN,MI,N,KT,L1,LP ,N1,N2,N3
                  COMPLEX Z
                1 FORMAT(5F10.4)
                  READ (5,1) KT,WI,D,TMC,L
                  READ (5,1) RC,IS,O,TFT,ER
     10           READ(5,3)ABF,REFS,REFL,RERS,RERL,TRAE,EME,EMR,ABR
                3 FORMAT(9F7.4)
                  READ(5,4)(CP(I),I=1,7)
                4 FORMAT(7F10.4)
                  READ(5,4)(VIS(I),I=1,7)
     15           READ(5,4)(THC(I),I=1,7)
                  READ(5,4)(DEN(I),I=1,7)
                  READ(5,4)(TEM(I),I=1,7)
                  READ(5,4)(AVIS(I),I=1,7)
     20           READ(5,4)(ACP(I),I=1,7)
                  READ(5,4)(ATHC(I),I=1,7)
                  READ(5,4)(ADEN(I),I=1,7)
                  READ(5,1)(WT(I),I=1,5)
                  READ(5,4) (EWR(I),I=1,7)
                  NK=1
     25           TF1=1000.
                  DO 555 NK=1,2
                  WEWT(NK)
                  WIN=0
                  WEWT*0.27894*0.6
     30           AC=7.*WI
                  S=W*TRAE*ABR/AC
                  DO 555 KK=1,7
                  ER=EWR(KK)
                  API=3.14159*D*D/4.
     35           ALPA=0.9
                  GAMA=1.4
                  W=(WI-(2.*D))/2.
                  DTS(3)=(W-D)/2.
                  DTS(2)=W-D
     40           DTS(1)=(W-D)/2.
                  F=0.2
                  DIF=0./12.
                  AC=3.14159*DIF*L
                  TA=(0.02413*DIF)/2.
     45           RADF=(1./EMR)+(1./EME)-1.
                  P=0.002168
                  AR=AC
                  DO 5 J=1,7
                  IF (TF1.LT.TEM(J+1)) GO TO 6
     50         5 CONTINUE
                6 CPI=((CP(J+1)-CP(J))/100.)*(TF1-TEM(J))+CP(J)
                  DENT=(((DEN(J+1)-DEN(J))/100.)*(TF1-TEM(J)))+DEN(J)
                  ERP=ER*0.1337*DENT*60.
                  F1=TF1+((0.5*U)/(ERP*CPI))
     55           T(1)=TF1+(U/(ERP*CPI))+5.
                  MI=T(1)
              126 IF(I).IS+100.
```

```
                CT=TC(1)
                GTT(1)=CT
     60         DO 101 T=1,10
                IMP1=0.
                IMP2=0.
                IRM=0.
                QL=0.
     65         DS=-0.05
                HPR(1)=0.
                UTL(1)=0.
                AMDA=(8.64E-7)*(MT+CT)/(2.*P)
                C1=(2.-ALPA)*2.*GAMA*AMDA/(ALPA*(1.+GAMA)*TA)
     70         FT1=(MT+CT)/2.
                DO 161 J=1,7
                IF(FT1.LT.TEM(J+1)) GO TO 162
            161 CONTINUE
            162 ACPT=(((ACP(J+1)-ACP(J))/100.)*(FT1-TEM(J)))+ACP(J)
     75         AVIST=(((AVIS(J+1)-AVIS(J))/100.)*(FT1-TEM(J)))+AVIS(J)
                ATHCT=(((ATHC(J+1)-ATHC(J))/100.)*(FT1-TEM(J)))+ATHC(J)
                PNA=ACPT*AVIST/ATHCT
                C1=C1/PNA
                C2=(2.*C1)/(1.+(2.*C1))
     80         HPC=ATHCT*(1.-C2)/TA
                HRPC=(0.1714E-8)*((MT*MT )+(CT*CT))*(MT+CT)/RADF
                HRCS=EMF*(0.1714E-8)*((CT*CT)+(TS*TS))*(CT+TS)
                UT=1./((1./(HPC+HRPC))+(1./(HC+HRCS)))
                UT=2.*UT
     85         M=1
                UTL(M+1)=UT
                UT1=UTL(M)
                UT2=UTL(M+1)
                HPR(M+1)=HPC+HRPC
     90         HP1=HPR(M)
                HP2=HPR(M+1)
                TC(I+1)=MT-(UT*(MT-TS)/(HPC+HRPC))
                CT=TC(I+1)
            152 FT=(MT+FLT)/2.
     95     119 FORMAT(10X,*GLASS TEMP BY CT/MT/UL =*,F10.4)
                PRINT 119,CT
             16 DO 7 J=1,7
                IF (FT.LT.TEM(J+1)) GO TO 8
              7 CONTINUE
    100       8 CPT=(((CP(J+1)-CP(J))/100.)*(FT-TEM(J)))+CP(J)
                VTST=(((VIS(J+1)-VIS(J))/100.)*(FT-TEM(J)))+VTS(J)
                THCT=(((THC(J+1)-THC(J))/100.)*(FT-TEM(J)))+THC(J)
                DENT=(((DEN(J+1)-DEN(J))/100.)*(FT-TEM(J)))+DEN(J)
                RN=(((FP*60.*0.1337)/AFT)*D  *DENT)/VTST
    105         PN=CPT*VIST/THCT
                IF(PN.GT.2100.) GO TO 702
                NN=0.360
                GO TO 701
            702 NN=0.027*(RN**0.8)*(PN**0.333333)
    110     701 HF=NN*THCT/D
                R=1./(HF*3.14159*D)
                N=SQRT(UL*(W-D)*(W-D)/(KT*TMC))
                SHN=(EXP(N)-EXP(-N))/2.
                KT=(KT*TMC*N)/((W-D)*SHN)
```

```
      CPN=(EXP(N)+EXP(-N))/2.
      Y=(-2.*CPN)-(D*UL/KI)
      DO 71 J=1,7
      IF (FLT.LT.TEM(J+1)) GO TO 72
   71 CONTINUE
   72 CPT=(((CP(J+1)-CP(J))/100.)*(FLT-TEM(J)))+CP(J)
      DENT=(((DEN(J+1)-DEN(J))/100.)*(FLT-TEM(J)))+DEN(J)
      VIST=(((VIS(J+1)-VIS(J))/100.)*(FLT-TEM(J)))+VIS(J)
      RN=(((FR*60.*0.1337)/AFT)*D*DENT)/VIST
      FRP=FR*0.1337*DENT*60.
      CPM=FRP*CPT
      B3=KI*R
      B4=B3*(1.+Y)
      B5=((B4-1.)*(B4-1.))-(B3*B3)
      B1=1.*KI*(((B4*(1.+Y))-1.-Y-B3)/(B5*CPM)
      B2=1.*KI/(B5*CPM)
      Y1=SQRT((B1*B1)-(B2*B2))
      Y2=-Y1
      B6=Y1+B1-B2
      B7=EXP(-2.*Y1)
      L2=B6/(((B2-B1+Y1)*B7)+B6)
      L1=1.-L2
      BB=(1.+(((2.*L2*Y1)-B1-Y1)/B2))/UL
      TI=TFT
      TO=TI+((S-(UL*(TI-TS)))*BB)
      PH1=(L1*EXP(Y1))+(L2*EXP(Y2))
      PH2=PH1
      TF10=TO-TI-TS-(S/UL)
      TF1O=PH1*TF10
      TF20=TF10
      QU=CPM*(TO-TFT)
      F1=(0.1714E-8)*FME*AG
      F2=MC*AG
      F3=(Q*ARR*TRAF)-QU
      F4=(F1*(TS**4.))+(F2*TS)+F3
      A(1)=F1
      A(2)=0.
      A(3)=0.
      A(4)=F2
      A(5)=-F4
      NDEG=4
      CALL ZRPOLY (A,NDEG,Z,IER)
      DO 47 KR=1,4
      B(KR)=REAL(Z)
   47 DR(KR)=AIMAG(Z)
      DO 60 KR=1,4
      IF(DR(KR))60,61,60
   61 KM=KR
      ROOT=B(KM)
      IF(ROOT) 60,60,65
   60 CONTINUE
  191 FORMAT(///,5X,*NO SOLUTION EXISTS*,///)
      PRINT 191
      GO TO 158
   65 GT=ROOT
      GTT(I+1)=GT
      DO 755 NR=1,10
```

```
      D3=D3+0.1
      D1=EXP(D3*Y1)
      D2=EXP(D3*Y2)
  175 PH13=(L1*D1)+(L2*D2)
      PH23=(L1*((B1+Y1)/B2)*D1)+(L2*((B1+Y2)/B2)*D2)
      TF13=PH13*TF10
      TF23=PH23*TF20
      A1=1./(1.+(KI*R*R*Y*(Y+2.))-(2.*KI*R*(1.+Y)))
  180 A2=1.+Y-(2.*KI*R*Y)-(KI*R*Y*Y)
      A3=R*KI*A1
      S1=TF13+(A3*(TF23+(TF13*A2)))
      S2=TF23+(A3*(TF13+(TF23*A2)))
      S3=(W-D)/2.
  185 N1=SQRT(OL/(KI*TMC))
      S33=(W-D)*N1
      P1=S33/2.
      P3=TANH(P1)/N1
      S4=TS+(S/UL)
  190 S55=(EXP(S33)-EXP(-S33))/2.
      S5=(EXP(S3)-EXP(-S3))/2.
      S66=(EXP(S3)+EXP(-S3))/2.
      S6=(EXP(S33)+EXP(-S33))/2.
      P2=(S2-(S1*S66))/S55
  195 S7=S5/S6
      S8=(S66-1.)
      V=N/2.
      AR=SINH(V)
      AR1=COSH(V)
  200 AR2=TANH(V)
      AR3=(AR-AR1)/AR2
      AR4=AR1-AR
      TE=S1/((AR1*CHN)-(AR*SHN))
      AR5=((S2/S1)-CHN)/SHN
  205 X1=S4+(2.*TE*((AR1*SHN)-(AR*CHN))/N)
      X2=S4+(S1*(SHN+(AR5*(CHN-1.)))/N)
      X3=S4+(2.*S2*AR2/N)
      Z1=S1+TS+(S/UL)
      Z2=S2+TS+(S/UL)
  210 X1=X1*(W-D)/2.
      X2=X2*(W-D)
      X3=X3*(W-D)/2.
      G6=TS*(W-D)
      G7=G6/2.
  215 G8=0.1*UL*L
      G1=(X1-G7)*G8
      G2=(Z1-TS)*D*G8
      G3=(X2-G6)*G8
      G4=(Z2-TS)*D*G8
  220 G5=(X3-G7)*G8
  755 UL=UL+G1+G2+G3+G4+G5
      IT(I+1)=(OL/(UL*AC1))+TS
      DO 374 MM=1,2
      Y4=-0.05
  225 DO 374 MN=1,10
      Y4=Y4+0.1
      Y3=EXP(Y4*Y1)
      Y5=EXP(Y4*Y2)
```

```
      PROGRAM MAIN       73/74   OPT=1                    FTN 4.6+428       76/12/06. 16.17.10

                        IF(MM.EQ.2) GO TO 375
  230                   PH(MN)=(L1*Y3)+(L2*Y5)
                        TF1(MN)=PH(MN)*TF10
                        TF1(MN)=TF1(MN)+S0
                        TMF1=TMF1+TF1(MN)
                        GO TO 374
  235             375   PH(MN)=(L1*((B1+Y1)/B2)*Y3)+(L2*((B1+Y2)/B2)*Y5)
                        TF2(MN)=PH(MN)*TF10
                        TF2(MN)=TF2(MN)+S0
                        TMF2=TMF2+TF2(MN)
                  374   CONTINUE
  240                   TMF=(TMF1+TMF2)/20.
                        FLT=TMF
                        IF(ABS(TC(I+1)-TC(I)).GE.2.) GO TO 101
                        IF(ABS(UT2-UT1).GT.0.05) GO TO 101
                        IF(ABS(HP2-HP1).GT.0.05) GO TO 101
  245                   IF(ABS(T(I+1)-T(I)).LE.5.) GO TO 55
                        CT=(F*TC(I))+((1.-F)*TC(I+1))
                        MT=(T(I)*F)+((1.-F)*T(I+1))
                  101   CONTINUE
                  156   FORMAT(///,5X,*PLATE TEMP DO NOT CONVERGE*,I5,///)
  250                   PRINT 156,I
                   78   FORMAT(///,5X,*MT=*,E14.7,///)
                        PRINT 78,MT
                        GO TO 158
                   55   PRINT 455,FWR(KN),QT(NK)
  255              455   FORMAT(////,5X,*FLOW RATE=*,F10.2,*GPM*,10X,*HEAT FLUX =*,F10.2,//
                       1///)
                        X=((0.5*(TFT+T0))-TS)/QIN
                        QU=GPM*(TO-TFT)
                        EFF=QU/Q
  260                   PRINT 411,X,EFF
                  411   FORMAT(5X,*X=*,F10.4,10X,*EFFICIENCY=*,F10.4)
                   31   FORMAT(5X,*RN=*,E10.4,5X,*PN=*,E10.4,5X,*NN=*,E10.4,5X,*HF=*,F10.4
                       1)
                        PRINT 31,RN,PN,NN,HF
  265              409   FORMAT(10X,4(10X,E14.7))
                        PRINT 409,CPI,VTST,THCT,DFNT
                        PRINT 22,MT,CT
                    22  FORMAT(5X,*MEAN TEMPERATURE OF PLATE=*,E10.4,10X,*GLASS TEMP=*,F10
                       1.4)
  270              171   FORMAT(5X,*EFFICIENCY=*,E14.7,10X,*HEAT GAINED=*,E14.7)
                        PRINT 171, EFF,QU
                        PRINT 23, TO
                    23  FORMAT(5X,*EXIT FLUID TEMP=*,E10.4)
                        QLP=(MT-TS)*UL*AC
  275                   CT1=CT/100.
                        TS1=TS/100.
                        QLG=((((CT1**4.)-(TS1**4.))*0.86)+(HC*(CT-TS)))*AG
                        PRINT 271,QLP,QLG
                        QLK=QL+QU
  280                   QLK=QLK/(Q*ABSRATRAE)
                  501   FORMAT(10X,*CHEK WITH QL*, F10.3)
                        PRINT 501,QLK
                  271   FORMAT(5X,*QLP=*,E14.7,10X,*QLG=*,E14.7)
                        QPC=(QU+QLP)/(ABR*TRAF*Q)
  285                   QGC=(QU+QLG)/(ABR*TRAF*Q)
```

```
      PRINT 272,NPC,QGC
   88 FORMAT(5X,*GLASS TEMP=*,E14.4,10X,*UL=*,E14.4)
      PRINT 88,C1,UL
  272 FORMAT(5X,*CHECKING WITH PLATE LOSS=*,F10.4,10X,*CHECKING WITH GLA
     1SS LOSS=*,F10.4)
      PRINT 376,(TF1(MN),MN=1,5)
      PRINT 376,(TF1(MN),MN=6,10)
      PRINT 376,(TF2(MN),MN=1,5)
      PRINT 376,(TF2(MN),MN=6,10)
  376 FORMAT(5X,5(10X,F10.4))
      PRINT 378,IMF
  378 FORMAT(5X,*INTEGRATED MEAN TEMP OF FLUID=*,F10.4)
      UM=(FR*0.1337)/(60.*AF1)
      IF(RN.LT.2100) GO TO 541
      FF=0.316/(RN**0.25)
      GO TO 542
  541 FF=64./RN
  542 DP=(FF*L*DENI*UM*UM)/(D*32.1739)
      FPL=DP*FR*0.1337*60./778.
      PRINT 545,DP,FPL
  545 FORMAT(10X,*PRESSURE DROP=*,F12.5,10X,*FRICTIONAL POWER LOSS=*,F12
     1.5)
      DO 707 NT=1,9
      D3=NT
      D1=EXP(0.1*D3*Y1)
      D2=EXP(0.1*D3*Y2)
      PH13=(L1*D1)+(L2*D2)
      PH23=(L1*((B1+Y1)/B2)*D1)+(L2*((B1+Y2)/B2)*D2)
      TF13=PH13*TF10
      TF23=PH23*TF20
      A1=1./(1.+(KI*KI*R*R*Y*(Y+2.))-(2.*KI*R*(1.+Y)))
      A2=1.+Y-(2.*KI*R*Y)-(KI*R*Y*Y)
      A3=R*KI*A1
      S1=TF13+(A3*(TF23+(TF13*A2)))
      S2=TF23+(A3*(TF13+(TF23*A2)))
      DO 511 LL=1,3
      DO 511 LN=1,3
      D9=LN
      D4=DIS(LL)*0.25*D9
      IF(LL.EQ.2) GO TO 512
      IF(LL.EQ.3) GO TO 513
      XV=D4
      CY=(XV+W-((W+D)/2.))/(W-D)
      CY=CY*N
      CSY=SINH(CY)
      CCY=COSH(CY)
      CTP(LL,LN)=S4+(TE*((AB1*CCY)-(AB*CSY)))
      GO TO 511
  512 XV=D4+((W+D)/2.)
      CY=(XV-((W+D)/2.))/(W-D)
      CY=CY*N
      CCY=COSH(CY)
      CSY=SINH(CY)
      CTP(LL,LN)=S4+(S1*(CCY+(AB5*CSY)))
      GO TO 511
  513 XV=D4+(((3.*W)+D)/2.)
      CY=(XV-W-((W+D)/2.))/(W-D)
```

```
      PROGRAM MAIN       73/74  OPT=1                    FTN 4.6+428      76/12/06. 16.12.10

                         CY=CY*N
                         CCY=COSH(CY)
  345                    CSY=SINH(CY)
                         CTP(I,N)=S4+(S2*(CCY-(AB2*CSY)))
                  511    CONTINUE
                  515    FORMAT(9(5X,F9.3))
                         TFL=TF+S4
  350                    Z1=S1+S4
                         Z2=S2+S4
                         PRINT 777,TFL,Z1,Z2
                  707    PRINT 515, ((CTP(I,J),I=1,3),J=1,3)
                  777    FORMAT(10X,3(10X,F10.3))
  355                    XTI=(TFT-TS)/DIN
                  705    FORMAT(10X,*FLOW RATE IN POUNDS PER HOUR=*,F10.3,10X,*XTI=*,F10.4)
                         PRINT 705,FRP,XTI
                  555    CONTINUE
                  158    STOP
  360                    END


        SYMBOLIC REFERENCE MAP (R=1)

ENTRY POINTS
  4114  MAIN

VARIABLES     SN  TYPE          RELOCATION
  7046  A         REAL      ARRAY
  6321  AB        REAL
  6510  AB1       REAL
  6512  AB3       REAL
  6515  AB5       REAL
  6733  ACP       REAL      ARRAY
  6724  ADEN      REAL      ARRAY
  6346  AG        REAL
  6365  AMDA      REAL
  6372  ATHCI     REAL
  6371  AVIST     REAL
  6466  A2        REAL
  7053  B         REAL      ARRAY
  6426  B2        REAL
  6423  B4        REAL
  6431  B6        REAL
  6433  B8        REAL
  6417  CHN       REAL
  6421  CPM       REAL
  6564  CSY       REAL
  7032  CTP       REAL      ARRAY
  6563  CY        REAL
  6374  C2        REAL
  6670  DEN       REAL      ARRAY
  6345  DIE       REAL
  6553  DP        REAL
  6457  D1        REAL
  6364  D3        REAL
  6507  AB        REAL
  6351  AB2       REAL
  6511  AB2       REAL
  6513  AB4       REAL
  6555  AC        REAL
  6370  ACPT      REAL
  6340  AFT       REAL
  6341  ALPA      REAL
  6706  ATHC      REAL      ARRAY
  6715  AVIS      REAL      ARRAY
  6465  A1        REAL
  6467  A3        REAL
  6425  B1        REAL
  6422  B3        REAL
  6424  B5        REAL
  6432  B7        REAL
  6565  CCY       REAL
  6677  CP        REAL      ARRAY
  6353  CPT       REAL
  6357  CT        REAL
  6543  CTI       REAL
  6366  C1        REAL
  6312  D         REAL
  6354  DENT      REAL
  7043  DIS       REAL      ARRAY
  7057  DR        REAL      ARRAY
  6460  D2        REAL
  6561  D4        REAL
```

BIBLIOGRAPHY

1. Progress Report No. 1, NSF Grant GI-43936, Georgia Institute of Technology, September 1974.

2. Duffie, Beckman, Solar Energy and Thermal Processes, John Wiley & Sons, New York, 1974.

3. J. R. Williams, Solar Energy Technology and Applications, Ann Arbor Science Publishers, Inc., 1974.

4. Pamos Kokropolour, Ehab Salam and Farrington Daniesl, Solar Energy, 111-4, 19-23, December 1959.

5. McDonald, NASA Lewis Research Center Report, 1974.

6. W. F. Seifert, L. L. Jackson, C. E. Sech, "Design and Operational Consideration for High Temperature Organic Heat Transfer System," AIChE, 1972 meeting.

7. W. M. Kays and A. L. London, "Compact Heat Exchangers," Second Edn. 1964, McGraw Hill, Inc.

8. A. P. Watkinson, D. L. Miletti and P. Tarasoff, "Turbulent Heat Transfer and Pressure Drop in Internally Finned Tubes," AI ChE Symposium Series 1973, No. 131, Vol. 69.

9. R. L. Webb and E. R. G. Eckert, "Application of Rough Surfaces to Heat Exchanger Design," Int. J. Heat and Mass Transfer, Vol. 15, pp. 1647-1658, 1972.

10. O. H. Klepper, "Heat Transfer Performance of Short Twisted Tapes," AI ChE Symposium Series 1973, No. 131, Vol. 69.

11. Mike McKee, M. S. Thesis, Georgia Institute of Technology, August 1975.

12. M. H. Cobble, Heat Exchanger for Solar Collectors, Vol. 7, No. 1, Solar Energy, 1963.

13. G. O. G. Lof, D. A. Fester and J. A. Duffie, "Energy Balances on a Parabolic Cylinder Solar Collector, January 1962, Journal of Engineering Power.

14. G. O. G. Lof, J. A. Duffie, "Optimization of Focusing Solar Collector Design," Journal of Engineering Power, July 1963.

15. Edward Lumsdaine, "Comparison of Solar Heat Exchanger," Mechanical and Aerospace Engineering Department, The University of Tennessee, Knoxville, Tenn. 37916, 1961.

16. D. O. Lee and W. P. Schimmel, Jr., "An Axial Temperature Differential Analysis of Linear Focused Collectors for Solar Power," Proceedings 9th Intersociety Energy Conversion Engineering Conference, p. 347-3533, San Francisco, Aug. 26-30, 1974.

17. Howard B. Palmer and Simion C. Kuo, "Solar Farms Utilizing Low-Pressure Closed-Cycle Gas Turbines," 9th Intersociety Energy Conversion Engineering Conference, San Francisco, Calif. Aug. 1974.

18. Richard D. Cummings, "Solar Power Collector Breadboard Test", NSF Report AER 74-00289, Itek 75-8250-1, Optical Systems Division, March 1975.

19. S. L. Sargent, W. P. Teagan, "Compression Refrigeration from a Solar Powered Organic Rankine - Cycle Engine," An ASME publication 73-WA/SA-8.

20. D. Prigmore and R. Barber, "Cooling with the Sun's Heat Design Considerations and Test Data for a Rankine Cycle Prototype," Solar Energy, Vol. 17, pp. 185-192, 1975

21. S. L. A. Khalik, "Heat Removal Factor for a Flat Plate Solar Collector with a Serpentine Tube," Solar Energy, Vol. 18, pp. 59-64, 1976.

22. G. O. G. Lot and R. A. Tyboul, paper presented at the International Solar Energy Society Congress, Paris (1973) "The Design and Cost of Optimised Systems for Cooling Dwellings by Solar Energy."

23. J. L. Russel, Jr., "Investigation of a Central Station Solar Power Plant," General Atomic Company, Report Guls-GA-A12759, August 30, 1973.

24. F. Benford and J. E. Bock, Trans. Am. Illum. Eng. Soc., 34, 200 (1939), "A Time Analysis of Sunshine."

25. P. I. Cooper, Solar Energy, 12, 3 (1969), "The Absorptance of Solar Radiation in Solar Stills."

26. J. L. Russel, Jr., E. P. DePlomb, and R. K. Bansal, "Principles of the Fixed Mirror Solar Concentrator," General Atomic Report No. GA-A12902, April 1974.

27. A. B. Meinel, and M. P. Meinel, Thermal Performance of a Linear Solar Collector, Winter Annual Meeting, ASME, November 26-30, 1972.

28. D. O. Lee, W. P. Schimmel, Jr., J. P. Abbin, Jr., "Sizing of Focussed Solar Collector Fields With Specified Collector Tube Inlet Temperature" Sandia Laboratories report SANDA 74-0295.

29. Edenburn, N. W., "Performance Analysis of a Cylindrical Parabolic Focussing Collector and Comparison with Experimental Results, "Solar Energy," Vol. 18, pp. 437-444, 1976.

30. D. R. Stull, E. F. Westrum, Jr., and G. G. Sinke, "The Chemical Thermocynamics of Organic Compounds," John Wiley and Sons, 1969. p. 56.

31. D. R. Miller, "Rankine Cycle Working Fluids for Solar-to-Electrical Energy Conversion," Monsanto Research Corporation, MCR-SL-399, Jan. 19, 1974.

32. J. P. Holman, Heat Transfer, McGraw Hill Book Co., 2nd Edn. 1968.

33. Frank Kreith, Principles of Heat Transfer, 3rd ed. 1973, International Textbook Co.

34. W. M. Kays, "Convective Heat and Mass Transfer," McGraw Hill Book Co., p. 174.

35. V. Ortabasi, "Indoor Test Methods to Determine the Effect of Vaccumn on the Performance of a Tubular Flat Plate Collector," 76-WA/Sol. 24.

36. G. H. Eggers and J. L. Russel, "The FMSC Collector Subsystem being reapplied for Sandia Laboratories' Total Energy System," Solar Cooling and Heating a National Forum, Dec. 13-5, 1976, Miami Beach, Florida.

37. D. B. McKay, "Design of Space Power Plants," Addison Windy Co.

38. M. K. Selcuk, "A Vacumn tube vee-trough Collector for Solar Heating and Air Conditioning Applications," Solar Cooling and Heating, a National Froum, Dec. 13-15, 1976, Miami Beach, Florida.

39. F. A. Bynum, R. L. Donnelly, K. C. Bardoloi, "A Solar Collector Based on an Array of Linear Clipped V-Channels," Solar Cooling and Heating, a National Froum, De.c 13-15, 1976, Miami Beach, Fla.

40. H. Anderson Jrs., "Discussion of a Planar, Fresnel Reflector Rotatable Facet Concentrator," Solar Cooling and Heating, a National Forum, De.c 13-15, 1976, Miami Beach, Florida.

41. E. R. G. Edkert, R. M. Drake, Jr., "Analysis of Heat and Mass Transfer," p. 536, McGraw Hill Book 1972.

42. B.Y.H. Liu and R. C. Jordan, Solar Energy, 7, 53 (1963), "The Long-Term Average Performance of Flat-Plate Solar Energy Collectors."

43. B.Y.H. Liu and R. C. Jordan, Solar Energy, 4, No. 3 (1960), "The Inter-relationship and Characteristic Distribution of Direct, Diffuse and Total Solar Radiation."

44. Marks, "Handbook of Mechanical Engineers," McGraw Hill Company, pp. 17-55, 1967.

45. F. Kreith and J. Kreider, "Solar Heating and Cooling," published by International Textbook Company.

46. G. W. Treadwell and L. E. Torkelson, Solar Total Energy Program, Semi-annual report, Sand 76-0205, June, 1976.

47. A. M. Lindsey, "Investigation of a Segmented Plane Solar Energy Concentrator". M. S. Thesis, School of Mechanical Engineering, Georgia Institute of Technology, August, 1974.

48. C. Guntner, "The Utilization of Solar Heat for Industrial Purposes by Means of a New Plane Mirror Reflector", Scientific American, Supplement Number 1586, May 26, 1906, pp. 25409-25412.

VITA

Prakash Rao Damshala was born to Mrs. Shankaramma and Babiah Damshala on May 15, 1946, in Hyderabad City, India. He graduated from high school in 1st class from Gosha Mahal High School of Hyderabad in 1963. After joining engineering college of Osmania University in 1964, he obtained his B. E. degree in Mechanical Engineering from Svi Venkateswara University in 1970 and later joined the University of Miami, Florida, for graduate studies in Mechanical Engineering. The title of his Master's thesis is "One Dimensional Wave Analysis of Human Head Helmet System During Impact." After he obtained the M. S. degree from the University of Miami in 1972, he joined Florida Memorial College as an Instructor and later in 1972 he worked for Ronel Corporation in Miami, Florida, as a Design Engineer. He joined the Georgia Institute of Technology, Atlanta, in 1973 for a Ph.D. program. During his Ph.D. program, he presented a paper on "Optimization of Heat Exchanger for Solar Concentrators" in a national forum of Solar Cooling and Heating, held in June, 1976 at Miami Beach, Florida. While he was at Georgia Tech he worked as a teaching assistant. In January, 1977, he joined the Department of Mechanical Engineering at New Mexico State University, Las Cruces, as a visiting faculty member. The title of his doctoral dissertation is "Thermal Analysis of Receivers for Solar Concentrators and an Optimization Procedure for Power Production".